CHAPTER 1

THE TECHNIQUE OF INDUCTIVELY COUPLED PLASMA MASS SPECTROMETRY

1.1 The inductively coupled plasma *[1]*

There is basically no difference between the characteristics of the inductively coupled plasma as used in ICP-MS and those of the plasma as used in the ICP-AES. Knowledge of the nature of the inductively coupled plasma is important to an understanding of the basis and characteristics of ICP-MS and therefore an outline is given below.

1.1.1 Torch and plasma [1]

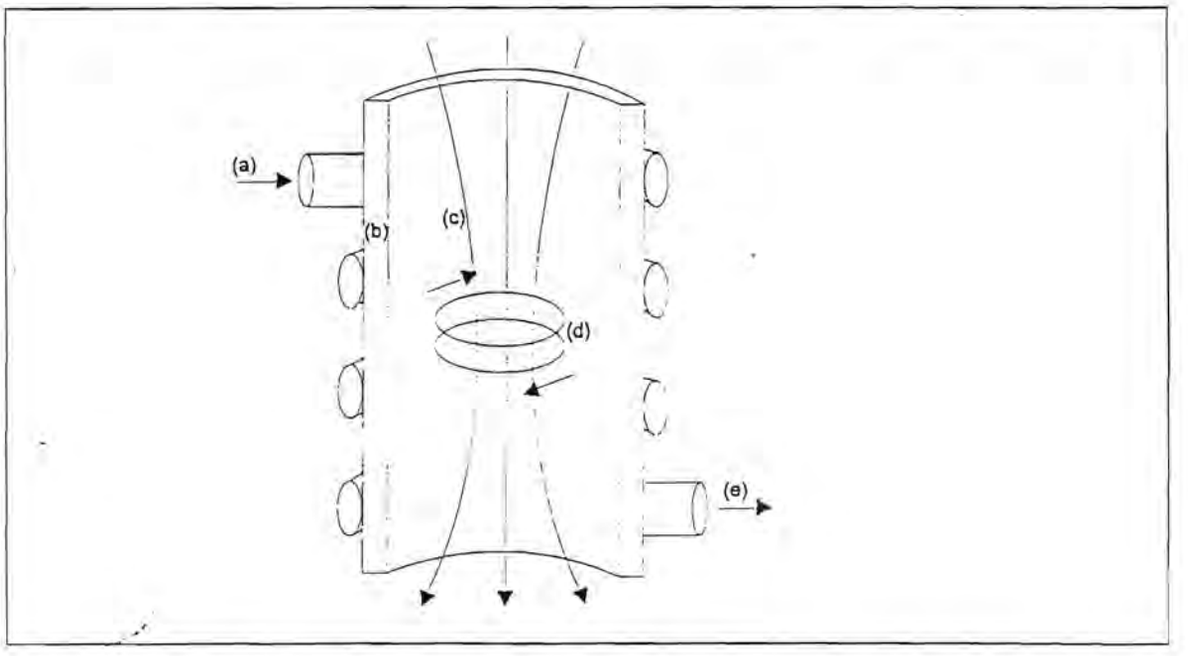

Figure 1.1: Operation of an inductively coupled plasma source. (a) Passing current through a coil (b) wrapped around a quartz tube (c) sets up a magnetic field, (d) which causes an eddy current of ions and electrons (e) whose motion generates intense heat in a continuously ionised flow of gas.

The inductively coupled plasma is an electrodeless discharge in a gas at atmospheric pressure, maintained by energy coupled to it from a radio frequency generator. This is achieved by a suitable coupling coil, which functions as the primary of a radio frequency transformer and the discharge itself acts as the secondary. The argon plasma is generated inside and at the open end of an assembly of quartz tubes known as the torch. The operation of an inductively coupled

plasma source is shown in figure 1.1 *[2]*. Minor changes have been made in the systems used for mass spectrometry – this includes the mounting of the torch with the axis horizontal which is done for convenience and some changes are made to the grounding point of the coupling (load) coil circuit to control the plasma electrical potential with respect to the mass spectrometer system which is grounded. The torch commonly used, based on the "Scott Fassel" design (see figure 1.2), has an outer tube of diameter 18 mm and the tube is about 100 mm long. Within this are two concentric tubes of 13 mm and 1.5 mm inner diameter which terminate short of the torch mouth. Each annular region formed by the tubes is supplied with gas by a side tube entering tangentially in such a way that it creates a vorticular flow. The center tube, through which the sample is introduced to the plasma, is brought out along the axis. The outer gas flow (termed the coolant flow) protects the tube walls and acts as the main plasma support and it is usually set between 10 and 15 $dm^3\ min^{-1}$. The main use of the second gas flow (termed the auxiliary flow), which is introduced to the inner annular space, is to ensure that the hot plasma is kept clear of the tip of the central capillary injector tube to prevent its being melted and its flow is usually set between 0 and 1.5 $dm^3\ min^{-1}$. The central gas flow (termed the injector, nebuliser or carrier flow) conveys the aerosol from the sample introduction system and is usually set at approximately 1 $dm^3\ min^{-1}$. This is sufficient, in the small diameter injector tube, to produce a high velocity jet of gas which then punches a cooler hole through the center of the plasma (termed the central or axial channel).

The load coil which consists of 2 - 4 turns of fine copper tube, cooled by a water or gas flow, is located with its outer turn a few millimeters below the mouth of the torch. The RF current which is supplied by the generator, produces a magnetic field which varies in time at the generator frequency (27 MHz), so that within the torch, the field lies along the axis. A spark from a Tesla coil initiates a discharge in a cold torch, thereby providing free electrons to couple with the magnetic field. Electrons in the plasma precess around the magnetic field lines in circular orbits and the electrical energy supplied to the coil is inverted into kinetic energy of electrons. At atmospheric pressure a free electron moves approximately 10^{-3} mm before it collides with an argon atom, to which its energy is transferred, thereby heating the plasma and forming a bright discharge. The skin effect which occurs in RF induction heating ensures that most of the energy is coupled into the outer or induction region of the plasma. The cool injector gas flow, which carries most of the sample aerosol, punches a channel through the center of the plasma so that little appears in the outer annular part of the plasma. Radiation and conduction from the annulus are mainly responsible for the heating of the gas in the center channel and

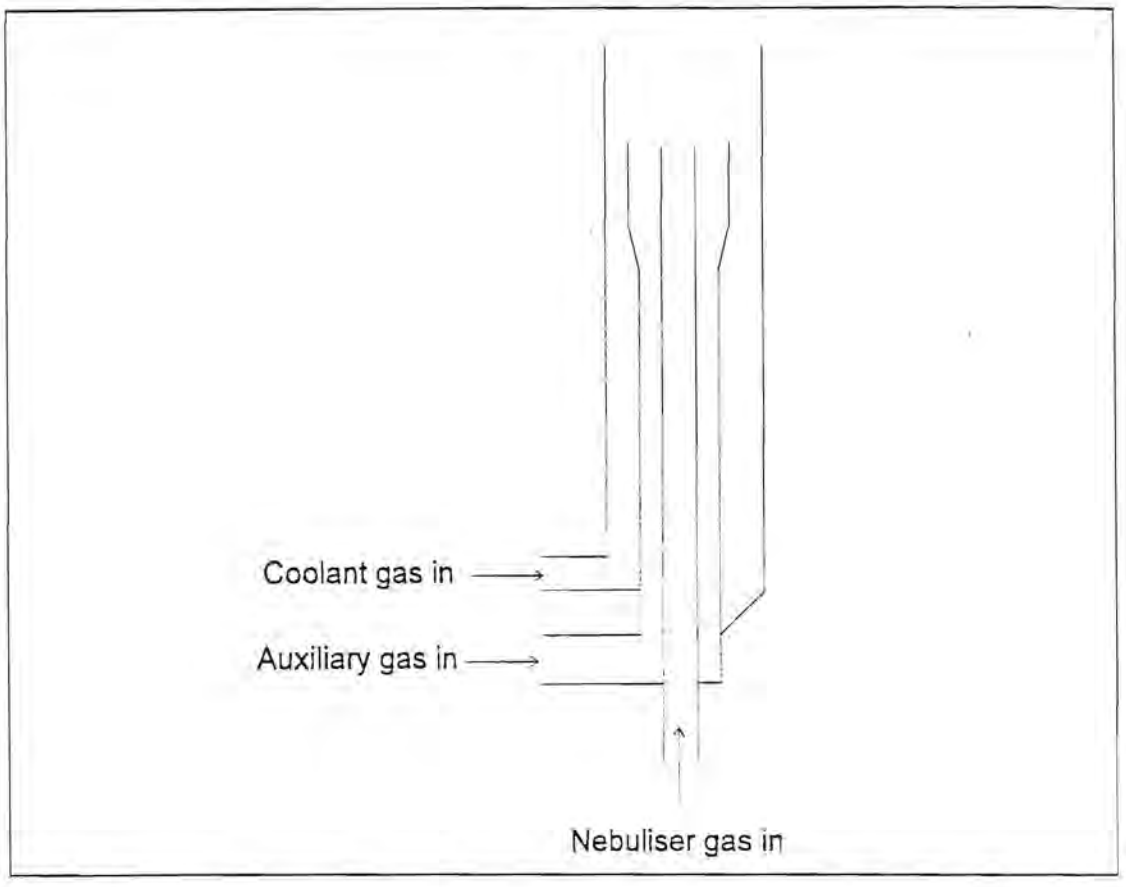

Figure 1.2: Fassel type inductively coupled plasma torch.

while the temperature in the induction region of the plasma may be as high as 10000 K, in the central channel the gas kinetic temperature is probably between 5000 and 7000 K at the mouth of the torch. The chemical composition of the sample solution can vary substantially without greatly affecting the electrical processes that sustain the plasma. This is mainly because the power is coupled mainly into the outer region which is physically distinct from the central channel through which the sample aerosol travels. The fact that the physical and chemical interferences in the inductively coupled plasma are not as severe compared to those seen in most other spectrochemical processes *[1]* may be attributed to this physical separation between the region where the electrical energy is added and the region containing the sample.

1.1.2 RF coupling [1]

The load coil and plasma present a low electrical impedance to the RF generator which feeds them energy. A matched load at the end of the coupling line to the load coil is necessary in order to provide efficient energy transfer and avoid mismatches which could produce high potentials from the reflected power. The load coil is essentially resistive and thus it absorbs the power delivered. The power required to maintain such a plasma is usually varies between 0.75

and 2.0 kW.

Mainly two types of generator are used. These include 1) free running systems, where the frequency is controlled by the oscillating circuit and load coil parameters and 2) crystal controlled systems where the operating frequency is determined by an oscillating quartz crystal and a servo controlled matching circuit is used to ensure correct matching of the load.

1.1.3 Sample introduction [1]

A sample which is introduced into central channel gas flow of the inductively coupled plasma needs to be a gas, vapour or aerosol of fine droplets or solid particles. A wide variety of methods and techniques may be used to produce these such as pneumatic or ultrasonic nebulisation for solutions, laser or spark ablation from a solid and generation of volatile hydrides or oxides from a reaction vessel among others. In a standard pneumatic nebuliser a fine droplet dispersion of the analyte solution is produced by a high velocity gas stream. A spray chamber removes the larger droplets and allows only those below approximately 8 μm to pass on to the plasma. These small droplets which reach the plasma carry only about 1% of the solution which is usually metered to the nebuliser by a peristaltic pump.

1.1.4 Sample history [1]

The ultimate aim of sample introduction is to produce sample ions at the entrance to the mass spectrometer. This is usually achieved by volatilisating, atomising and ionising a dispersion of fine solid particles in a carrier gas stream. In the most common case of pneumatic nebulisation the aerosol leaving the injector tube in the torch may still contain small liquid droplets, but these are quickly dried to produce solid microparticulates and at the increasingly higher temperatures which are experienced these are vaporised and the resulting vapour phase compounds dissociated. The transit through the center of the plasma takes several milliseconds and once atomised the sample is substantially ionised at the high temperature experienced.

Only 10^{-6} or less of the total atom population of the plasma consist of sample atoms. The degree of ionisation of the sample atoms is dependent on the ionisation conditions in the plasma, which in turn are dominated by the major constituents, usually argon, hydrogen, oxygen and electrons, as well as the ionisation constant and partition functions for the atom concerned. The temperature in the central channel is high enough to produce almost complete ionisation of many elements and a significant level for those elements of higher ionisation energy.

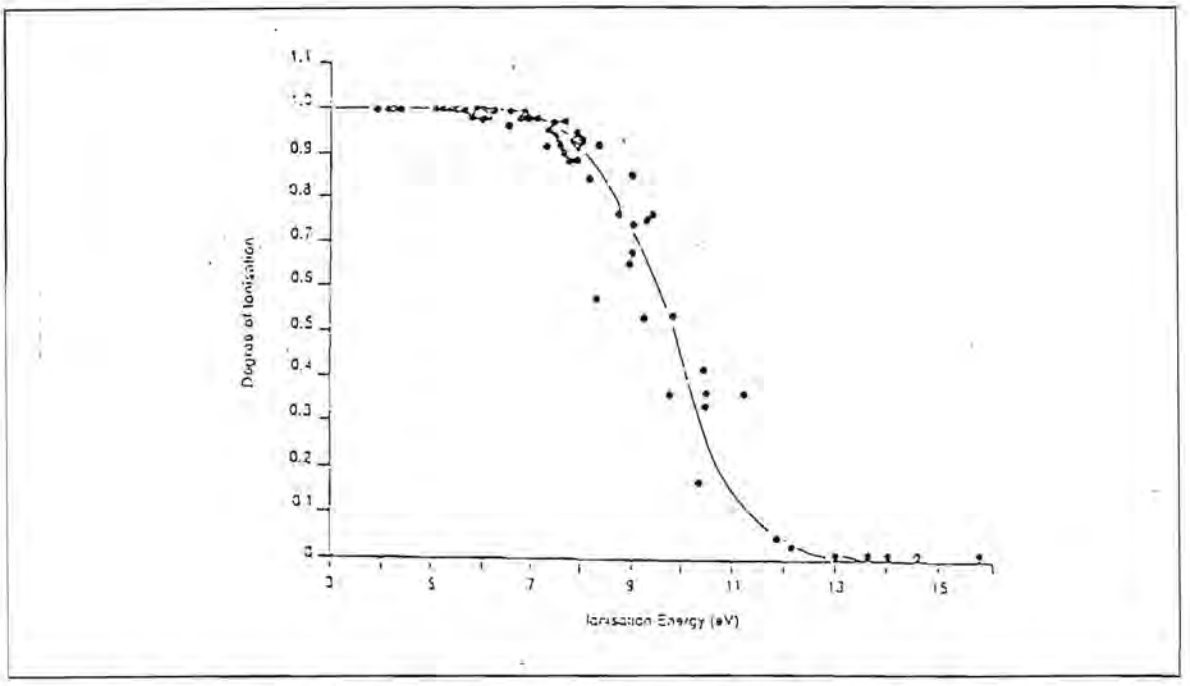

Figure 1.3: Degree of ionisation versus ionisation energy for singly charged ions in the inductively coupled plasma.

Although thermal equilibrium is not strictly achieved, it is approached at the plasma powers usually used. If it is however assumed, a reasonable estimate of experimental values for degree of ionisation may be obtained from the Saha equation. This is done using the generally accepted values from the literature for ionisation temperature T_i and electron population n_e. Values for most of the elements of the periodic table *[3]* are given in table 1.1. The general form of the dependence of degree of ionisation on ionisation energy for singly charged ions *[4]* is shown in figure 1.3, from which it may be seen that the response falls rapidly above 9 eV.

Table 1.1: Calculated values for degree of ionisation (%) of M^+ and M^{2+} at T_i = 7500 K, $n_e = 1x10^{18}$ dm^{-3}. Elements marked by an asterisk yield significant amounts of M^{2+} but partition functions are not available. (Values in brackets indicate % M^{2+} formed.)

H 0.1																He
Li 100	Be 75											B 58	C 5	N 0.1	O 0.1	F $9x10^{-4}$	Ne $6x10^{-6}$
Na 100	Mg 98											Al 98	Si 85	P 33	S 14	Cl 0.9	Ar 0.04
K 100	Ca 99(1)	Sc 100	Ti 99	V 99	Cr 98	Mn 95	Fe 96	Co 93	Ni 91	Cu 90	Zn 75	Ga 98	Ge 90	As 52	Se 33	Br 5	Kr 0.6
Rb 100	Sr 96(4)	Y 98	Zr 99	Nb 98	Mo 98	Tc	Ru 96	Rh 94	Pd 93	Ag 93	Cd 85	In 99	Sn 96	Sb 78	Te 66	I 29	Xe 8.5
Cs 100	Ba 91(9)	La 90(10)	Hf 98	Ta 95	W 94	Re 93	Os 78	Ir	Pt 62	Au 51	Hg 38	Tl 100	Pb 97(0.01)	Bi 92	Po	At	Rn
Fr	Ra	Ac	Unq	Unp	Unh	Uns	Uno										

Ce 98(2)	Pr 90(10)	Nd 99*	Pm	Sm 97(3)	Eu 100*	Gd 93(7)	Tb 99*	Dy 100*	Ho	Er 99*	Tm 91(9)	Yb 92(8)	Lu
Th 100*	Pa	U 100*	Np	Pu	Am	Cm	Bk	Cf	Es	Fm	Md	No	Lr

Table 1.2: Distribution of ionisation energies among the elements for singly and doubly charged ions at 1 eV intervals.

Ionisation energy (eV)	**Elements**	**2^+ ions**
<7	Li, Na, Al, K, Ca, Sc, Ti, V, Cr, Ga, Rb, Sr, Y, Zr, Nb, In, Cs, Ba, La, Ce, Pr, Nd, Pm, Sm, Eu, Gd, Tb, Dy, Ho, Er, Tm, Yb, Lu, Hf, Tl, Ra, Ac, Th, U	
7 – 8	Mg, Mn, Fe, Co, Ni, Cu, Ge, Mo, Tc, Ru, Rh, Ag, Sn, Sb, Ta, W, Re, Pb, Bi	
8 – 9	B, Si, Pd, Cd, Os, Ir, Pt, Po	
9 –10	Be, Zn, As, Se, Te, Au	
10 - 11	P, S, I, Hg, Rn	Ba, Ce, Pr, Nd, Ra
11 - 12	C, Br	Ca, Sr, La, Sm, Eu, Tb, Dy, Ho, Er
12 - 13	Xe	Sc, Y, Gd, Tm, Yb, Th, U, Ac
13 - 14	H, O, Cl, Kr	Ti, Zr, Lu
14 - 15	N	V, Nb, Hf
15 - 16	Ar	Mg, Mn, Ge, Pb
> 16	He, F, Ne	All other elements

It is clear from table 1.2 that most elements have first ionisation energies below 10 eV, corresponding to more than 50% ionisation while there are none whose second ionisation energies fall below 10 eV. Thus, although there are a number of elements such as the alkaline and rare earths, thorium and uranium which undergo some double ionisation, the majority do not and doubly charged ions should not present serious problems.

1.1.5 Plasma populations [1]

The gas pressure is 1 bar and at a gas kinetic temperature of 5000 K the total particle density is calculated from the gas laws to be 1.5×10^{21} dm^{-3}. The majority of this is argon. At an ionisation temperature of 7500 K the degree of ionisation of argon is calculated to be about 0.1%. As the second ionisation energy of argon is very high at 27 eV, the population of Ar^{2+} ions is negligible. In a "dry" plasma a typical value would be $n_{Ar+} = n_e = 1 \times 10^{18}$ dm^{-3}, but if a nebulised solution is introduced additional electrons are contributed by the ionisation of hydrogen and oxygen from the solvent, as well as H^+ and O^+ ions. At a nebuliser uptake of 1×10^{-3} dm^3 min^{-1} and an efficiency of 1% the populations of H^+ and O^+ are respectively about 2×10^{17} dm^{-3} and 1×10^{17} dm^{-3}. In addition, if the solution had been acidified with 1% nitric acid, as is usually done, there would be a population of N^+ of about 1×10^{15} dm^{-3}. These all contribute to the electron population and the value of n_e rises to about 1.3×10^{18} dm^{-3}. It is thus clear that the presence of water vapour in the aerosol contributes significantly to the ion and electron population of the axial channel.

The addition of trace elements to the nebulised solution produces far lower populations of the elements to be determined against this background of the "permanent" ions. An element at a concentration of 1 mg dm^{-3} in the sample solution, which is fully ionised in the plasma, contributes about 1×10^{13} ions dm^{-3} and accordingly the number is even lower for elements of higher ionisation energy. Thus, a fully ionised matrix element at 5 g dm^{-3} in the solution only contributes about 5×10^{16} dm^{-3} to the total level of n_e of 1.3×10^{18} dm^{-3} and produces a barely significant shift in the equilibrium. Thus, unless the concentration of the matrix element is extremely high, ionisation suppression in the plasma is generally not a major cause of matrix interference *[5]*.

1.1.6 Distribution of ions in the plasma [1]

As the plasma leaves the mouth of the torch it becomes accessible for ion extraction into the mass spectrometer. A simple visualization of the distribution of ions in the plasma may be

obtained from spatially resolved profiles made by moving the plasma across the ion extraction interface of an ICP-MS system. When no sample is introduced and the central channel contains only dry argon, the transverse profile of Ar^+ ions across the mouth of the torch is shown by the Ar^+ response in figure 1.4 *[1]*. On the torch axis the cooler central gas stream shows a relatively low Ar^+ population. A higher degree of ionisation of Ar occurs in the hotter induction region (plasma annulus) each side of the center. The ion population drops sharply at the edge of the plasma. If a similar plot is performed across the narrow central channel when a sample is being introduced, a profile such as that shown for Co^+ in figure 1.4 is obtained. The ions are concentrated mainly within 1 mm of the axis. Further along the axis away from the torch, the central channel diffuses into the annulus and similar profiles for Co at 5, 10 and 15 mm from the load coil are shown in figure 1.5 *[1]*.

From the distribution plots in figure 1.5 it seems as if the optimum position of the orifice is as close to the torch mouth as the load coil permits. However, it must be kept in mind that during its passage along the central channel of the plasma the sample must be converted to atomic ions as completely as possible and the processes of desolvation, volatilisation, dissociation and ionisation take several milliseconds. The time required depends particularly on the size of the initially desolvated microparticulates in the aerosol, which in turn depends on the level of dissolved solids in a nebulised sample solution, and on the bond strengths of the molecular species (which may be refractory) in the sample *[1]*. The time the sample resides in the hottest part of the plasma depends on the plasma operating parameters, but especially on plasma power and central channel gas flow.

The inductively coupled plasma thus forms a very convenient ion source with a high yield of singly charged analyte ions, few doubly charged and oxide or other molecular and adduct ions*[1]*.

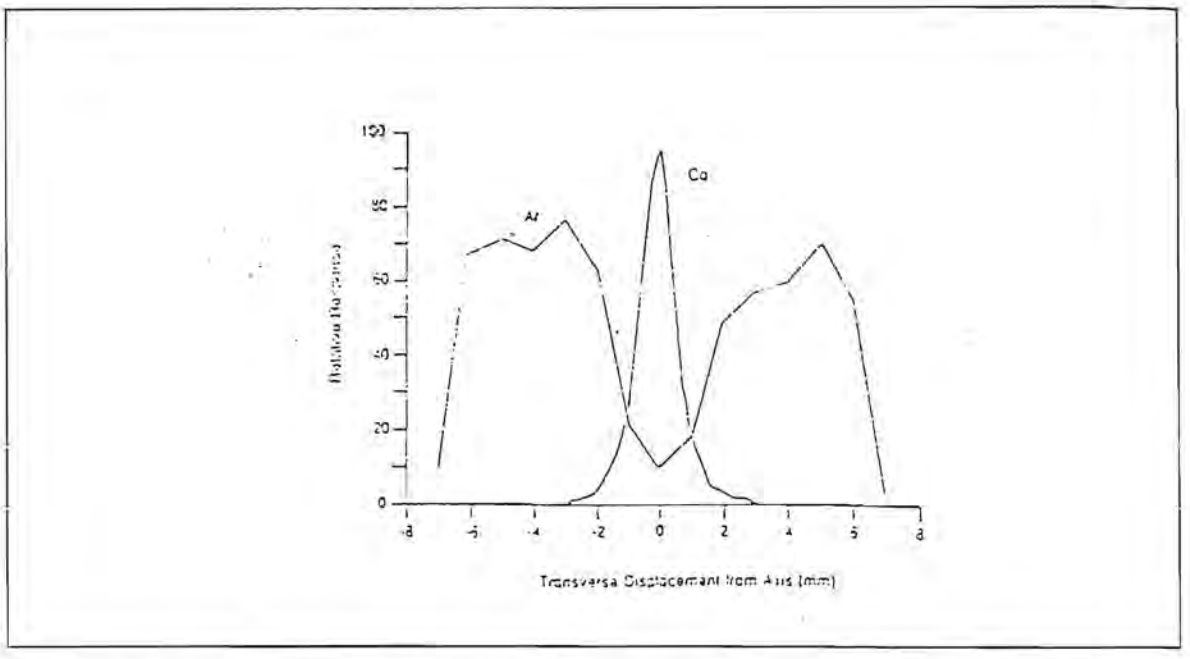

Figure 1.4: Transverse profiles of ions across the mouth of the plasma torch. Profile for Ar^+ shown for dry argon only. Profile for Co^+ from a nebulised solution at 100 μg dm^{-3}.

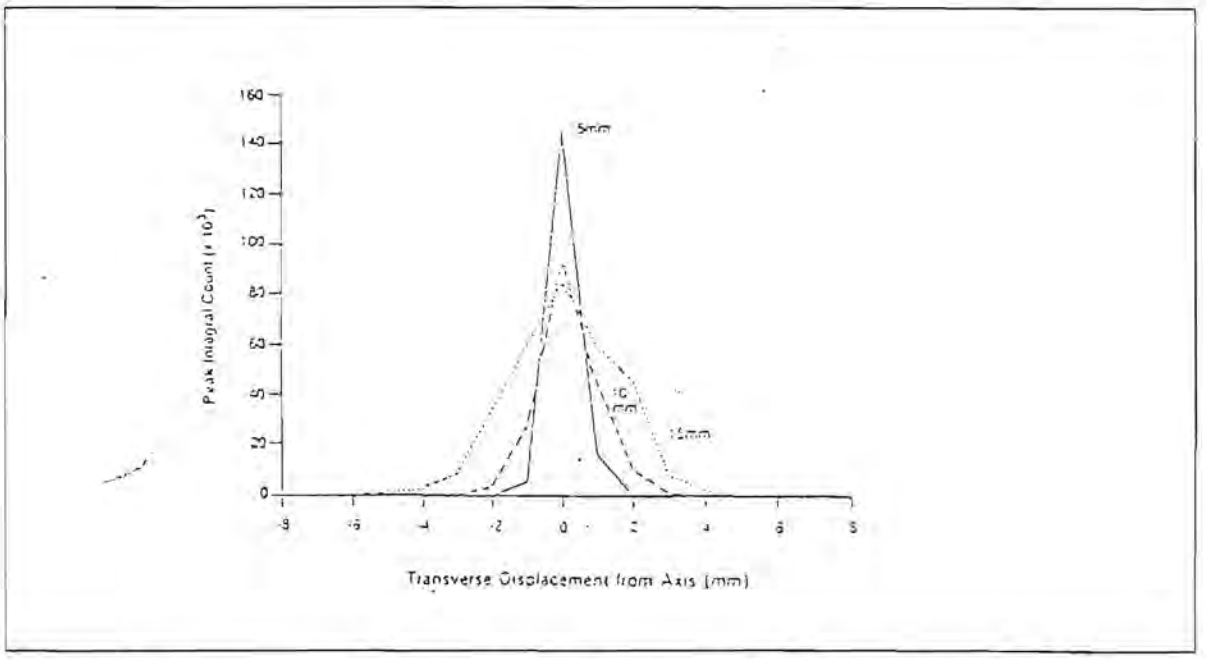

Figure 1.5: Transverse profiles across plasma flame at 5, 10 and 15 mm from load coil in steps of 1 mm. Nebulised solution containing Co at 100 μg dm^{-3}.

1.2 Ion extraction *[1]*

The extraction of ions from the plasma into the vacuum system is of critical importance in ICP-MS. Figure 1.6 shows a typical extraction interface. The ions first flow through a sampling orifice (diameter approximately 1 mm) into a mechanically pumped vacuum system, where a supersonic jet forms. The central section of the jet flows through the orifice of a skimmer cone (diameter also approximately 1 mm). The extracted gas containing the ions attains supersonic velocities as it expands into the vacuum chamber and reaches the skimmer orifice in only a few microseconds *[6]*. The sample ions change little in nature or relative proportions during the extraction process. To a first approximation, they simply flow through the orifice of the sampler cone and then through the orifice of the skimmer cone.

1.2.1 Boundary layer and sheath [1]

Figure 1.7 shows the two ways in which the plasma interacts with the sampling cone. Firstly, the plasma is deflected and cooled when it comes into contact with the metal cone. The temperature in the boundary layer of gas that forms between the plasma and the side of the cone is intermediate between the temperature of the plasma and that of the cone. Chemical reactions, such as oxide formation, occur readily in the boundary layer. However, in modern ICP-MS instruments the orifice of the sampler cone is large enough for the gas flow to puncture the boundary layer. Thus, the sampled gas is not cooled much while it is outside the sampler cone. There is still a thin, oblique boundary layer inside the lip of the orifice and care is taken in the design of the interface to ensure that oxides formed in this layer do not pass through the orifice of the skimmer cone. Oxide response is minimised if the diameter of the skimmer is less than that of the sampler *[7]*.

There is also an electrical interaction between the plasma and the conducting sampler cone. The plasma is electrically neutral since it contains equal numbers of positive ions and electrons (ignoring the negligible number of doubly charged and negative ions). A surface immersed in the plasma will collect both positive ions and electrons. Since the mobility of the electrons is much higher than that of the positive ions, the electron flux (current) to the surface is much higher than the positive ion flux. Thus, the potential of the surface of the sampler cone becomes negative with respect to the plasma. The sheath region that forms over the surface of the sampler cone is depleted in electrons, and positive ions are in excess. The negative potential of the surface of the sampler cone with respect to the plasma repels electrons and attracts ions to balance the two fluxes.

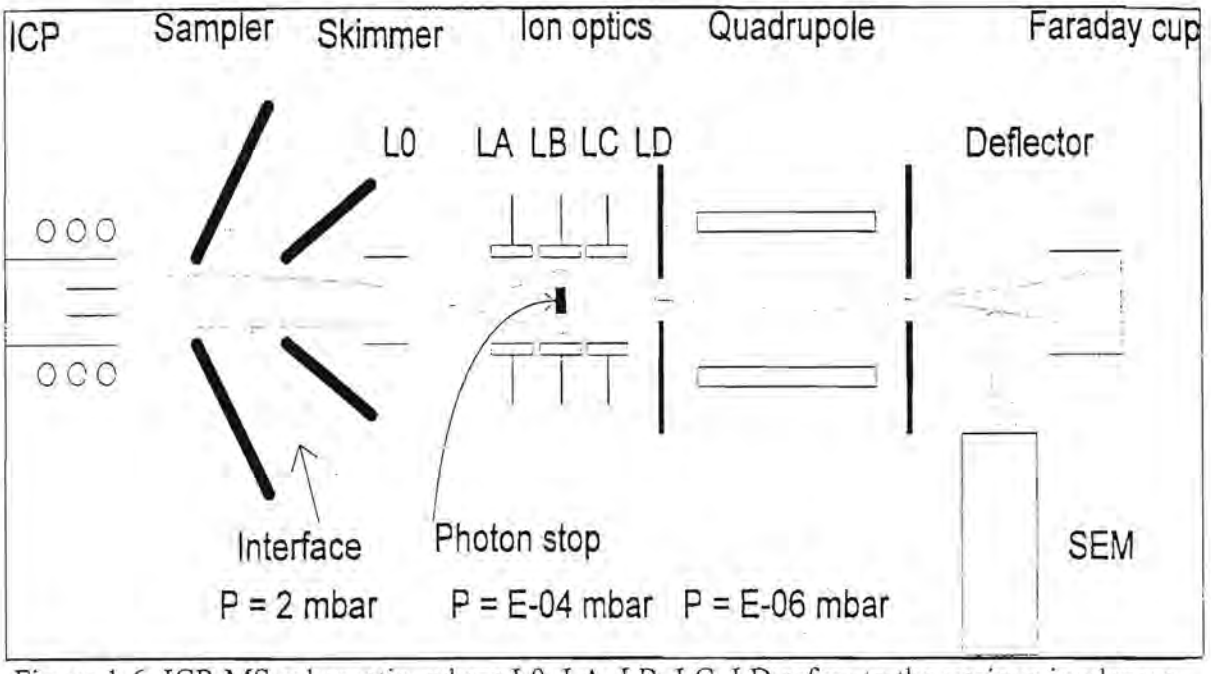

Figure 1.6: ICP-MS schematic, where L0, LA, LB, LC, LD refers to the various ion lenses and SEM refers to a secondary electron multiplier.

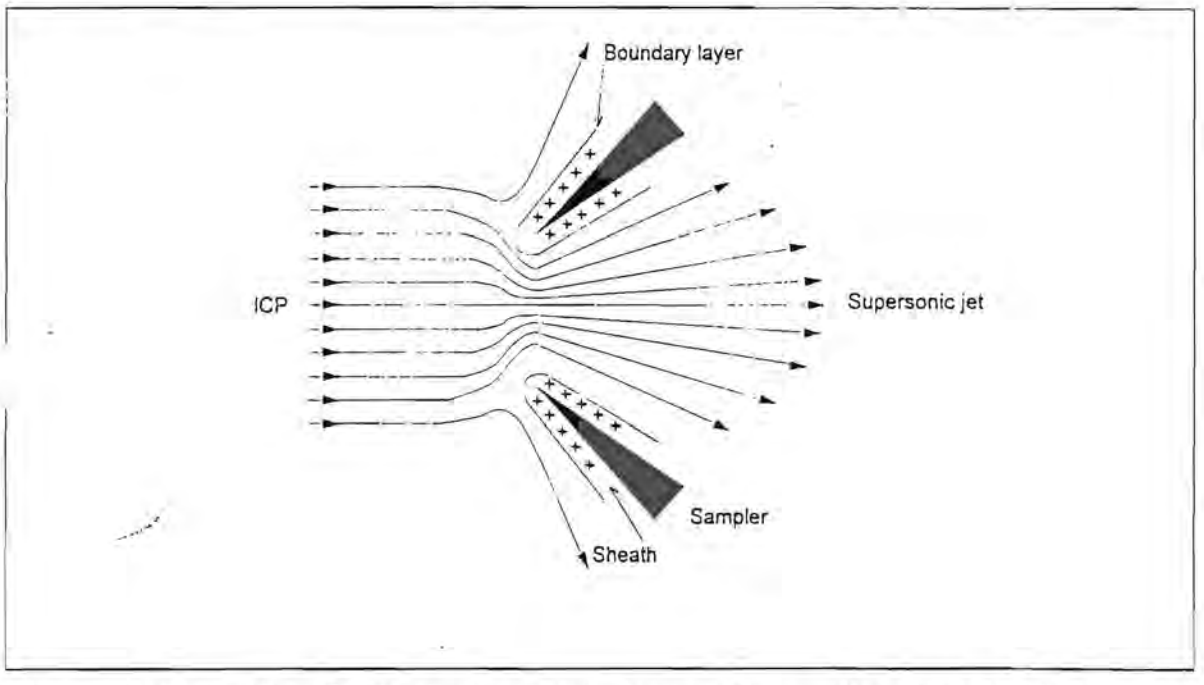

Figure 1.7: Interaction of inductively coupled plasma with sampling cone showing boundary layer, sheath and flow field into orifice. (Boundary layer not drawn to scale.) *[1]*

In ICP-MS the metal sampler cone is usually grounded. Since the potential of the sampler cone is fixed, the plasma appears to float at a positive potential, which is known as the plasma potential. The sheath co-exists with the boundary layer. The number of uncharged particles greatly exceeds the numbers of either positive ions or electrons, so the sheath is a dynamic region with particles constantly moving in or out via collisions. Although calculations indicate

the sheath to be much thinner than the boundary layer *[6]*, it still influences the ion extraction process by its interaction with the RF potential in the plasma, as described in the next section.

1.2.2 *Plasma potential and secondary discharge [1]*

The plasma is maintained by RF energy coupled to it by the load coil. Thus, current circulate at this frequency through the plasma, which is a good conductor. In addition to this inductive (magnetic) coupling, the load coil is also coupled capacitively (electrostatically) through the torch wall by the capacitance between the coil and the plasma. The arrangement of the electrical connections to the coil influences this capacitive coupling process *[1]*.

Normally, the one end of the load coil is connected to the high voltage RF source while the other end of the load coil is grounded. A potential gradient thus exists along the load coil, except at the moment when the field polarity reverses. When the plasma contacts the sampler cone and part of it is drawn through the orifice, the plasma is coupled to the sampler cone through the very thin sheath. Since the impedance of this sheath layer is much lower than that of the capacitive coupling between the plasma and load coil, the plasma acquires an RF potential which is determined by the ratio of these two impedances which act as a potential divider. An RF current flows through this coupling from the load coil. However, the RF current flow to the grounded cone is modified by the different mobilities of ions and electrons in the sheath layer. During negative half cycles, the current is carried mainly by electrons, which can flow to ground far more readily than the positive ions that carry current during positive half cycles.

These effects cause the plasma to assume a net mean positive DC potential. This offset or bias potential may be considerably larger than the floating potential due to the sheath alone *[8, 9]*.

If the plasma potential is high enough, it can cause an electrical discharge between the plasma and the sampler cone. This secondary discharge is manifest as a crackling discharge into the orifice. A severe discharge is detrimental in that it erodes the orifice, generates multiply charged ions, and induces high kinetic energies and a wide spread of kinetic energy in the extracted ion beam *[8, 10]*.

Minimising this secondary discharge was a key step in the early development of ICP-MS. Modification of the load coil arrangement was one successful approach. The plasma potential

can also be reduced by: a) use of a low aerosol gas flow rate (0.5 - 0.9 dm^3 min^{-1}), b) reducing the solvent load to the plasma, c) moving the sampling orifice close to the load coil and d) substituting a two-turn load coil (instead of the original three turns). These measures weaken the discharge but do not eliminate it fully, because the ion kinetic energy and certain properties of the spectra such as the ratio M^{2+}/M^{+} vary with operating conditions in a fashion that is not consistent with the expected changes in the plasma. The fundamental reasons why the plasma potential is sensitive to sampling position and operating conditions are not clear at this time*[1]*.

The center tapped load coil arrangement *[8,11]*, as well as the Colpitts oscillator circuit *[12]*, seems to eliminate almost totally the secondary discharge. With the widespread use of aerosol desolvation, dry sample introduction, and other empirical ways to minimise plasma potential with unbalanced load coils, excellent results can be obtained from either type of coil arrangement *[13]*.

1.2.3 Supersonic jet [1]

The gas flowing through the sampler cone expands into the first stage of the vacuum chamber, which is evacuated by a mechanical pump. The pressure ratio is more than sufficient for a supersonic jet to be formed inside the first stage. The supersonic jet consists of a freely expanding region often called the zone of silence surrounded by shock waves called the barrel shock and Mach disc. Figure 1.8 graphically depicts the sampler and skimmer cones as well as the shock waves. The barrel shock and Mach disc are caused by collisions between fast atoms from the jet and the background gas, which reheat the atoms and induce emission. The position of the onset of the Mach disc is given by:

$$X_M = 0.67\, D_0\, (P_0/P_1)^{1/2}$$

where X_M is the position of the Mach disc from the sampling orifice along the central axis,

D_0 is the diameter of the sampling orifice,

P_0 is the pressure in the inductively coupled plasma and

P_1 is the background pressure in the extraction chamber *[14]*.

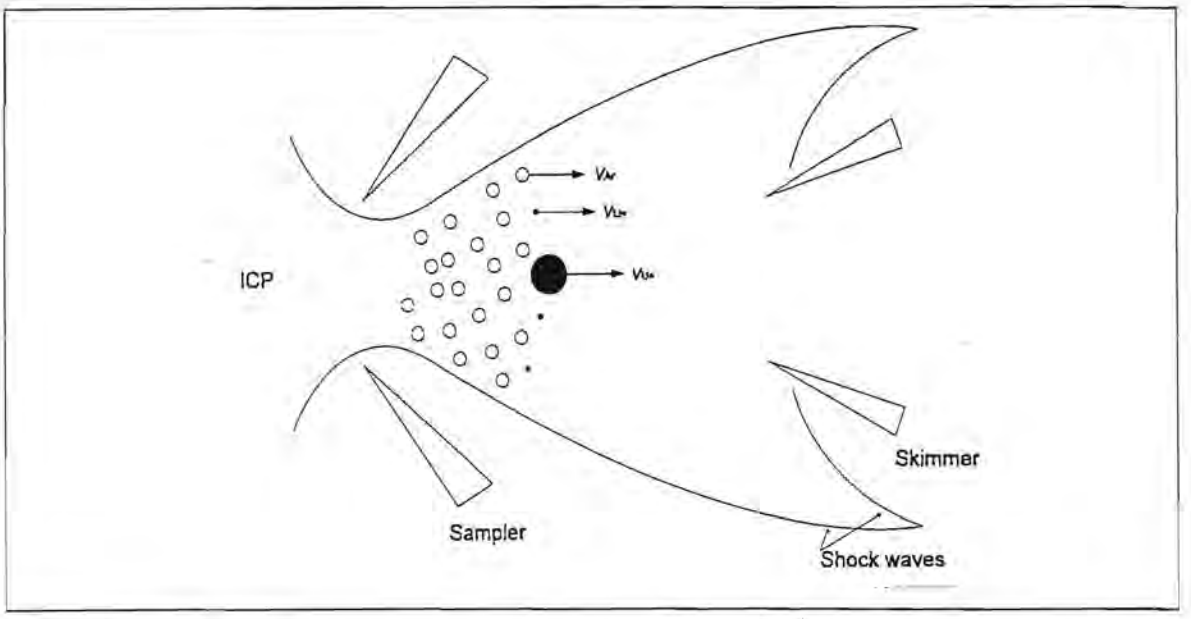

Figure 1.8: Sampler, skimmer and shock waves showing how light ions (·) and heavy ions (•) are all accelerated to the same velocity (v) as neutral Ar (○) in the supersonic jet.

In order to avoid losses of positive ions due to collisions and scattering, the skimmer cone is positioned with its tip open inside the Mach disc. This is done to ensure that the central core of the zone of silence passes through the skimmer cone into the second vacuum stage. The Mach disc is now replaced by a shock wave that forms outside the skimmer downstream from the tip. A sampler-skimmer separation of roughly two thirds of the distance to the onset of the Mach disc usually provides optimum positive ion transmission *[6, 15]*.

1.2.4 *Gas dynamics [1]*

The gas dynamic properties of the extraction process have been described *[6]*. Some of the points are given below.

The sampler collects gas from a region in the plasma of cross-sectional diameter roughly eight times that of the orifice of the sampler cone. The gas flow rate of an argon plasma at 5000 K is 10^{21} atoms s^{-1}. Of the gas that passes through the sampler, only about 1% (~10^{19} atoms s^{-1}) also traverses the skimmer. Furthermore, only the centerline flow gets through the skimmer, resulting in a spatial resolution in the plasma comparable to the diameter of the skimmer cone.

When the orifice of the sampler cone is large, the flow punctures the boundary layer cleanly and the gas is cooled very little until it gets inside the orifice. The presence of the metal sampler cone has little effect on the upstream plasma unless the secondary discharge is intense. Once

the sampled gas passes through the orifice of the sampler cone, collisions occur for the first few orifice diameters, after which the atoms continue to flow under essentially collisionless conditions. It is estimated that approximately 250 collisions occur between neutral argon atoms and other species during extraction. The extraction process takes roughly 3 μs and therefore there is little opportunity for ion loss by recombination between positive ions and electrons. There is also substantial experimental evidence for the lack of ion-electron recombination during extraction *[10, 16, 17]*.

The low number of collisions during the expansion and the short time duration thereof suggest that the sampling process is not complicated by extensive chemical reactions, and the ions extracted is more or less representative of the ions in the plasma *[6]*. The oxide ions (MO^+) observed are probably present mainly in the plasma, particularly if the orifice of the sampler cone is too close to the initial radiation zone. Some MO^+ ions can be formed from M^+ ions by reactions in the cool boundary layer in front of or inside the orifice of the sampler cone. Use of a skimmer orifice that is smaller than the sampling orifice helps prevent these additional MO^+ ions from passing through the skimmer to the mass spectrometer *[7]*. The origins of the other polyatomic ions are less clearly established.

1.3 Ion focusing *[1]*

After the positive ions leave the skimmer cone they are conveyed to the mass analyser by means of ion lenses.

1.3.1 Operation of ion lenses [1]

The general problem of transmitting and focusing ions through an ion lens are shown in figure 1.9. Suppose a positive ion of charge z is formed in a region of potential $V_{initial}$. It has a potential energy $zV_{initial}$. This ion will travel through a given region as long as the potential in that region is below $V_{initial}$, otherwise it will turn around and go back towards the source. This implies that the ion in figure 1.9 will travel to the right if the potentials V_1 and V_2 are less than $V_{initial}$.

When the ion moves into a region of potential V, the kinetic energy of the ion becomes $z(V_{initial} - V)$. The velocity (v) of the ion is therefore $v = [2z(V_{initial} - V)/m]$, where m refers to the mass of the positive ion. Consider the first cylinder (V_1) in figure 1.9. Once inside the cylinder, the ion

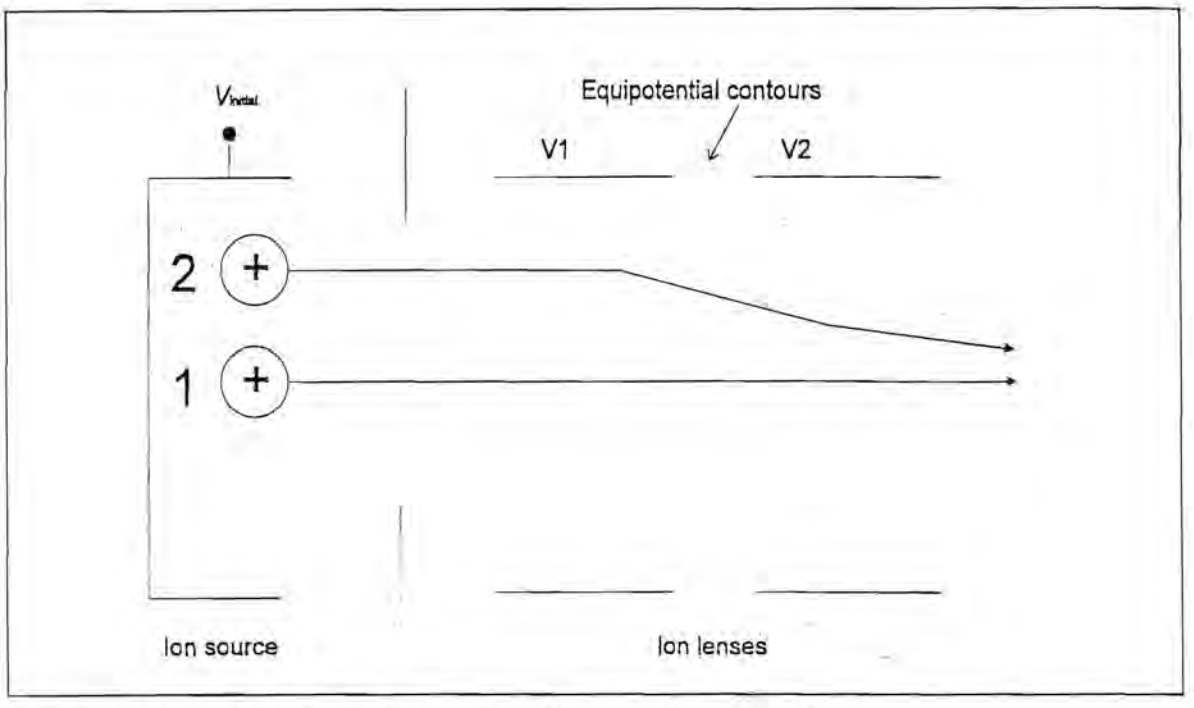

Figure 1.9 Schematic diagram illustrating the operation of ion lens.

experiences a uniform potential and moves at constant velocity in the same direction as when it entered the cylinder. By imparting a directed velocity to the ion, the lens draws it toward the mass analyser and retains it inside the vacuum system while the unwanted neutral particles flow to the pump. As the ion nears the exit of the first cylinder, it enters a new field region, which may be used as a lens to constrict or focus the stream of ions. This focusing action can improve the fraction of ions leaving the source that are transmitted downstream to the mass analyser.

Consider the region between the two cylinders in figure 1.9. If V_1 is not equal to V_2, the potential between the cylinders varies in space. The figure depicts curved equipotential contours in this region. These curved equipotential surfaces between cylinders provide the focusing action. Ion 1, which leaves the source on center, is acted upon symmetrically and passes straight through the lens. This ion is easily collected anyway. The real improvement lies for ion 2, which initially leaves the source displaced from the axis of the lens. The forces acting on ion 2 in the region between the two cylinders are unbalanced. If V_1 and V_2 are adjusted properly, ion 2 can be deflected closer to the axis. Once inside the second cylinder, the ion travels along a straight path, which may cross the axis and diverge again. More electrodes can be used downstream from V_2 to provide additional focusing action and to further adjust the ion path.

1.3.2 *Ion lenses in ICP-MS [1]*

In each lens several electrodes are strung together in order to confine the ions on their way to the mass analyser. Each lens incorporates a central disc in order to prevent photons originating from the plasma from reaching the detector. The sampler and skimmer cones stare into the heart of the inductively coupled plasma, which is a good source of vacuum ultraviolet radiation that can activate the detector. 50 - 80% of the positive ions are probably lost here, as shown by measurements of ion current with the stop removed.

Generally, the skimmer cone is grounded. The positive ions gain kinetic energy during extraction from both the gas dynamic effect of the supersonic expansion and any plasma potential above that of the sampler cone. The positive ion beam also has an energy spread of a few electron volts. Also, positive ions of different masses have different kinetic energies and thus follow different paths through the lens.

Different ion optical conditions are required to transmit positive ions of different *m/z* and the sensitivity for different elements is not as even across the mass range as the high ionisation efficiencies of the different elements would indicate. The extent of the mass discrimination effect depends on ion lens settings and ion energy, the latter of which can be influenced by plasma potential and plasma operating conditions.

1.3.3 *Space charge effects [1]*

A few ions are lost due to recombination during the extraction process and thus the ion current through the sampler cone remains quite high at about 0.1 A. The current through the skimmer cone is about 1 mA. In the plasma and in the supersonic jet, an equal electron current balances this ion current, so the beam acts more or less as if it was neutral *[6]*. As the beam leaves the skimmer cone, the electric field due to the lens collects positive ions and repels electrons. The electrons are no longer present to keep the positive ions confined in a narrow beam, resulting in the beam not being quasi-neutral, and the ion density still being very high. The mutual repulsion of ions of like charge limits the total number of positive ions that can be compressed into a beam of a given size. Space charge effects should become substantial in ICP-MS at total beam currents of the order of 1 μA *[18, 19]*, roughly three orders of magnitude below the actual beam current cited above. A simplified description of ion lenses, using the Laplace equation, assumes that the positive ions do not interact while in the ion lens, so the high ion current causes space-charge effects that are further reasons for non-ideal behaviour in ion optics in ICP-MS.

Ion trajectory calculations *[19]* show that the ion beam expands greatly due to space-charge effects. This expansion makes it difficult to collect all the ions leaving the skimmer cone and is probably a major source of ion loss in ICP-MS. Also, if the same space-charge force acts on all the positive ions, the light ions are affected the most and are deflected more severely. A greater fraction of light ions is deflected outside the acceptance volume of the ion lens than is the case for heavy ions, which could contribute to the generally poorer sensitivity for light elements and for the need for different focusing voltages for light and heavy ions.

The transmission of the ion lens now depends on the total beam current and the mass of the positive ions comprising the beam. Gillson et al. *[19]* showed that even a small change in the total ion current caused by addition of just a modest amount of matrix element can change the fraction of analyte ions that passes through the lens. Heavy matrix ions are deflected to a lesser extent and stay closer to the center of the ion beam where they can do the most damage.

These space-charge effects are a major cause of matrix interferences in ICP-MS. Many workers have reported that matrix effects are more severe in ICP-MS than in inductively coupled plasma emission spectrometry *[20 - 23]*. The masses of both the interferent and the analyte are of importance. Heavy matrix ions suppress analyte signals more extensively than matrices comprising of light ions, and heavy analyte ions are suppressed less severely than light ones *[19, 24 - 26]*. Most of these observations can be explained via the space-charge phenomenon. Alleviation of these effects and their analytical symptoms would greatly improve the analytical capabilities of ICP-MS. Caruso and co-workers have described a scheme in which the ion lens voltage is adjusted to maximise the analyte signal with the sample matrix present *[27]*.

1.4 Quadrupole mass spectrometers *[1]*

The ion lens provides little or no *m/z* separation of the extracted ion beam. In most ICP-MS instruments this function is performed by a quadrupole mass analyser. This section describes the operating principles and pertinent properties of these mass analysers.

1.4.1 Quadrupole configuration [1]

Figure 1.10 shows a diagram of a typical quadrupole mass filter. Four straight metal rods or metallised surfaces are suspended parallel to and equidistant from the axis. Ideally, the surfaces of these rods have a hyperbolic shape, although round rods that approximate hyperbola are usually used instead. Opposite pairs are connected together. DC and RF voltages of amplitude

U and V, respectively, are applied to each pair. The DC voltage is positive for one pair and negative for the other pair. The RF voltages on each pair have the same amplitude but of opposite sign, i.e. they are 180° out of phase.

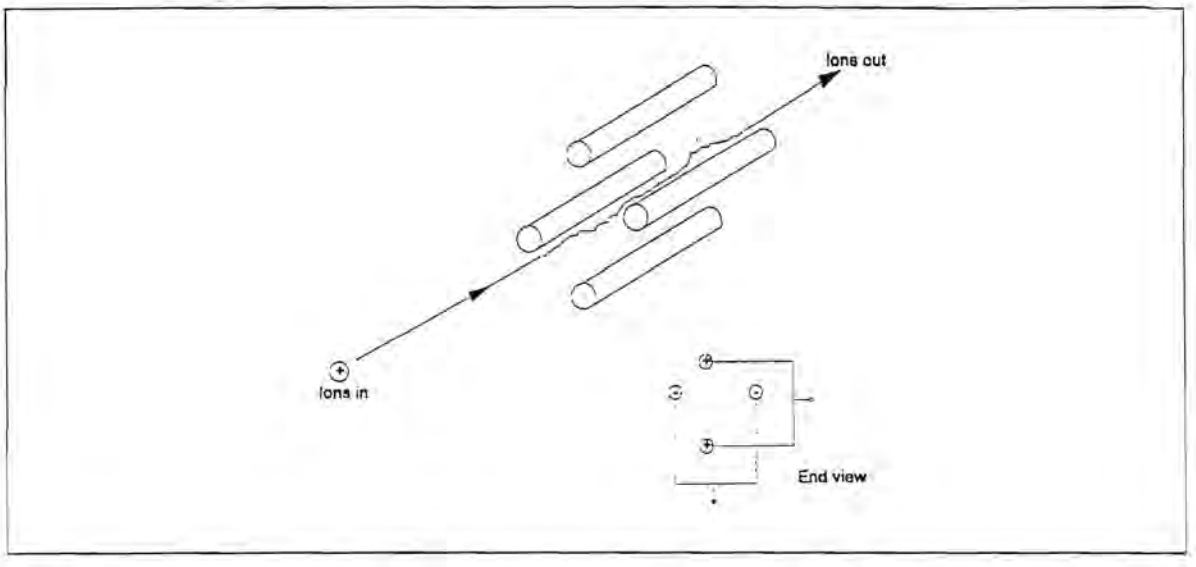

Figure 1.10: Diagram of quadrupole rods showing ion trajectory and applied voltages.

The ions to be separated are introduced along the axis into one end of the quadrupole system at velocities determined by their energy and mass. Due to the applied RF voltages all the ions are deflected into oscillatory paths through the rods. If the RF and DC voltages are selected properly, only ions of a given m/z ratio will have stable paths through the rods and will pass through the quadrupole system. Other ions will be deflected too much and will strike the rods and be neutralized and lost there. Thus, the dimensions of the ion trajectories relative to the boundaries of the rods are of critical importance.

1.4.2 *Ion trajectories [1]*

In the positive rod plane (figure 1.11), the lighter ions tend to be deflected too much and strike the rods, while the ions of interest and the heavier ions have stable paths. In this plane the quadrupole acts like a high pass mass filter. In the negative rod plane the heavier ions tend to be lost preferentially and the analyte ions and the lighter ions have stable paths. Thus the quadrupole acts like a low pass mass filter in the negative plane. The negative and positive planes are superimposed physically, so these filtering actions occur on the same ion beam at the same time. This juxtaposition of high pass and low pass mass filtering produces a structure that transmits ions only at the m/z value of interest.

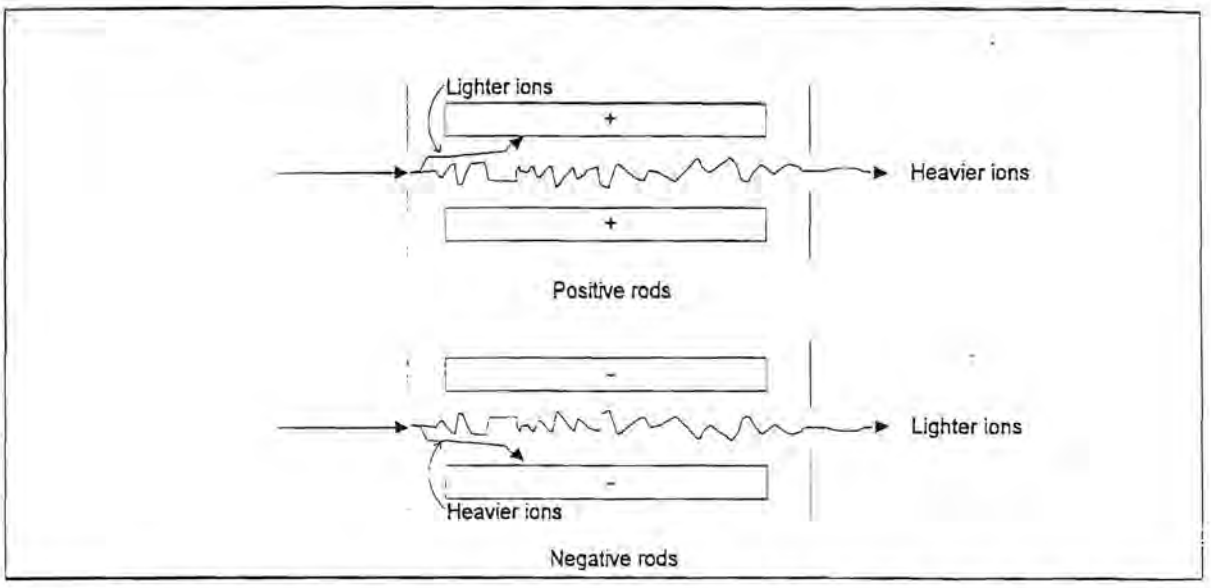

Figure 1.11: Side views of the ion separation processes in the two rod planes of a quadrupole.

1.4.3 *Characteristics of mass spectra from quadrupoles [1]*

Quadrupoles can operate at fairly high pressures (~1.3×10^{-2} Pa) as long as the mean free path is greater than the length of the device and the pressure is low enough to prevent electrical discharges inside the rods. Since the inductively coupled plasma operates at atmospheric pressure this causes the gas load to be high and the tolerance of the quadrupole to relatively high operating pressures simplifies the vacuum requirements. The typical operating pressures in ICP-MS instruments are limited largely by the detector (electron multiplier) rather than by the mass analyser system.

Quadrupoles perform best with positive ions that have low kinetic energies. The resolution is not greatly sensitive to the ion energy spread in the axial direction if the maximum ion energy stays below a certain value, usually about 20 eV. In the case of the ions having a too high energy they pass through the quadrupole system too quickly and do not experience enough RF cycles for proper resolution. The peaks resulting from such high-energy ions tend to be broad and/or split.

Only ions of a given *m/z* value are transmitted at any given time. The *m/z* value can be scanned or switched very rapidly, but ions of different *m/z* cannot be simultaneously monitored with a conventional quadrupole.

1.4.4 Scanning and data acquisition [1]

If U and V are not changed, the mass filter transmits only one m/z value continuously. This mode is called selected ion monitoring or single ion monitoring. It provides a 100% duty cycle on the m/z value of interest but precludes acquisition of spectral information elsewhere. For multi-element measurements, the values of U and V can be changed continuously in one scan. Also, U and V can be changed under computer control rapidly between selected discrete values (peak hopping), or the quadrupole can be scanned repetitively through the m/z region of interest (multi-channel scanning).

1.5 Ion detection *[1]*

1.5.1 Channeltron electron multipliers [1]

These are the most common detectors used in ICP-MS instruments. Figure 1.12 shows a diagram of such a Channeltron electron multiplier. The operating principles are similar to those of a photomultiplier, but there are no discrete dynodes. Instead, an open glass tube with a cone at one end is used. The interior of the tube and cone is coated with a lead oxide semiconducting material whose exact composition is proprietary. Electrical connections are made to the semiconducting coating through metal strips. For detection of positive ions, the cone is biased at a high negative potential (~-3 kV) and the back of the tube near the collector is held near ground. Relative to either end, the resistance of the interior coating varies continuously with position. Thus, when a voltage is applied across the tube, a continuous gradient of potential exists with position inside the tube.

When a positive ion leaves the quadrupole system it is attracted to the high negative potential at the cone. As the ion hits this surface it causes one or more secondary electrons to be ejected. Inside the tube, the potential varies continuously with position, so the secondary electron(s) move further into the tube to regions closer to ground. The secondary electrons hit another section of the coating causing more secondary electrons to be emitted. This process is repeated many times as the secondary electrons pass down the tube. The result is a discrete pulse containing as many as 10^8 electrons at the collector after an ion strikes the entrance of the detector.

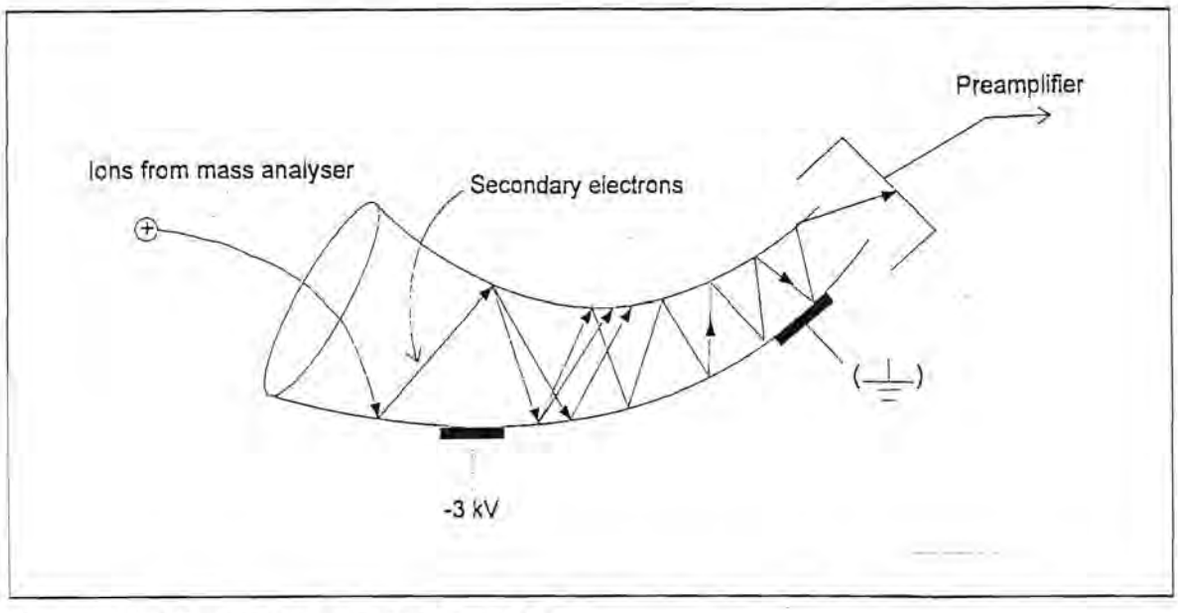

Figure 1.12: Channeltron electron multiplier.

As long as the high voltage is switched off first Channeltrons can be vented to air repeatedly without damage. A pressure below a value of approximately 6.7×10^{-3} Pa is required during operation, else spurious discharges form in the detector chamber.

1.5.2 *Signal measurement by pulse counting [1]*

Despite the use of pulse counting and careful blocking of the optical axis (in order to block photons that can activate the detector) between the detector and plasma, the actual background during operation is generally 10 to 50 counts s^{-1}, substantially higher than the dark count rate of the multiplier. The phenomena responsible for this background are not known precisely *[28]*.

The upper end of the dynamic range is limited by two phenomena. Firstly, the electron multiplier can only sustain a given maximum current flow. At a gain of 10^8 and an ion count rate of 10^6 ions s^{-1}, the current flow at the collector is about 16 μA. At high count rates the gain decreases because the electron current exceeds the standing current in the semiconducting coating of the detector. The fraction of ion pulses that are too low to be counted therefore increases. Secondly, pulse pile-up (the arrival of two pulses in a time interval shorter than the response time constants of the counting circuit) is a problem that could also limit linearity.

Both these effects cause the calibration curve to droop toward the horizontal axis at relatively high count rates. A peak that is split in the center is another symptom of count rates that exceed the linear range of the system.

CHAPTER 2

OPTIMISATION OF INSTRUMENT PARAMETERS IN INDUCTIVELY COUPLED PLASMA MASS SPECTROMETRY

2.1 Introduction

In ICP-MS various instrument parameters need to be set in order to optimise for analyte signals and to minimise background, doubly ionised and oxide signals. The plasma is optimised for the production of a large population of ions and the efficient transport of these ions through the interface with minimum interferences. Analyte signals may further be divided into intensities for light elements, argon and heavier elements. Some of the instrument parameters that need to be considered are: 1) horizontal, vertical and axial setting of the torch, 2) coolant, auxiliary and aerosol carrier gas flow rates, 3) power and 4) ion lens settings.

The effects of these various parameters on the different signals were investigated and the results presented were compared with the results of other researchers.

2.2 Experimental

2.2.1 Instrument

The instrument used for this study was a Spectromass-ICP. The free running generator operates at a frequency of 27.12 MHz. It has a three stage vacuum system consisting of two turbomolecular pumps and two rotating pumps. The following were used: a Fassel torch, a Scott-type double-pass spray chamber, a Meinhard nebuliser, Ni sampler and skimmer cones with diameters of about 1 mm and <1 mm. The solution uptake rate was $1x10^{-3}$ dm^3 min^{-1}.

Since mainly the way in which the signals vary with inductively coupled plasma and mass spectrometer parameters were of interest for this study, the study was started with a specific set of conditions, one parameter was varied, set optimally and then the next parameter was varied. Values and scales used for torch settings and gas flow rates are "arbitrary scales" as used by the instrument manufacturers, i.e. they do not refer to specific units of measurement. According to the manufacturers the scales for gas flow rates may be converted to dm^3 min^{-1} in the following way: For the coolant gas flow rate (arbitrary scale unit x 0.40), for the auxiliary gas

flow rate (arbitrary scale unit x 0.05) and for the aerosol carrier gas flow rate (arbitrary scale unit x 0.033).

2.2.2 *Multi-element solution*

The analyte solution consisted of a 1 mg dm^{-3} multi-element solution in 1% v/v HNO_3. According to some workers *[29, 30]* it is inadvisable to optimise ICP parameters in isolation to the mass spectrometer since the interface links together directly and synergistically two instrument components operating at totally different pressures and temperatures (inductively coupled plasma at atmospheric pressure and 5000 - 7000 K while the mass spectrometer is at 10^3 to 10^1 Pa and ambient temperature). Potential problems with spectral overlap interferences may result from the individual or combined effects of background intensities, isotopes or different concomitant elements, doubly ionised ions, oxide ions or other polyatomic ions. These form in either the plasma or the interface or during the sampling process.

Table 2.1: List of *m/z* values at which signals were monitored.

Element / ion monitored	**Isotope / *m/z* monitored**
Li^+	^{7}Li
Na^+	^{23}Na
Mg^+	^{24}Mg
Ar^+	^{36}Ar
Cu^+	^{63}Cu
In^+	^{115}In
Ce^+	^{140}Ce
Pb^+	^{208}Pb
Background	^{93}Nb
Background	^{100}Tc
Ce^{2+}	*m/z* 70
CeO^+	*m/z* 156

Background values in ICP-MS results from scattered photons or stray ions in the mass spectrometer. Background positions were chosen as positions where no analyte species in the multi-element solution would interfere or be monitored. The mass positions chosen were mass 93 and mass 100.

The doubly ionised and oxide ions of Ce were monitored as interferences, i.e. Ce^{2+} and CeO^+ at masses 70 and 156, respectively.

Signals monitored were divided into: low mass elements (Li^+, Na^+, Mg^+), Ar^+, heavier elements (Cu^+, In^+, Ce^+, Pb^+), background positions ($^{100}Tc^+$, $^{93}Nb^+$) and interferences (Ce^{2+}, CeO^+). The Ce^{2+}/Ce^+ and CeO^+/Ce^+ ratios were also calculated. A list of the masses at which signals were monitored are shown in table 2.1.

2.3 Effect of parameters on ICP-MS signals

2.3.1 Effect of torch adjustment

Effect of torch adjustment on light elements

The effect of the horizontal adjustment of the torch on the light elements can be seen in figure 2.1. An amount of "1000 units" on the x-axis corresponds to a distance of 0.492 mm moved. As the plasma is moved horizontally across the aperture of the sampler cone the analyte signals increase, reach a maximum and then decrease again. This is as expected since the analyte flow through the centre of the torch constitutes only a small part of the total plasma. The maximum analyte signals are observed at the torch setting of approximately "-2500 units". Although the system is sensitive to variations in the horizontal setting of the torch, this parameter does not seem to be critical since at distances of 1.2 mm away from the maximum Mg^+ intensities are still about 0.5×10^6 and intensities for Li^+ and Na^+ are about 1.5×10^6.

Figure 2.2 shows the effect of the vertical displacement of the torch on the response curves for the light elements. An amount of "1000 units" on the x-axis corresponds to a distance of 0.396 mm moved. Maximum analyte signals are observed at a setting of "-6500 units". As with the horizontal variation of the plasma, the signals increase, reach a maximum and then decrease again. At distances of about 1 mm from the optimum position a decrease in signal intensity of approximately 40% can be seen.

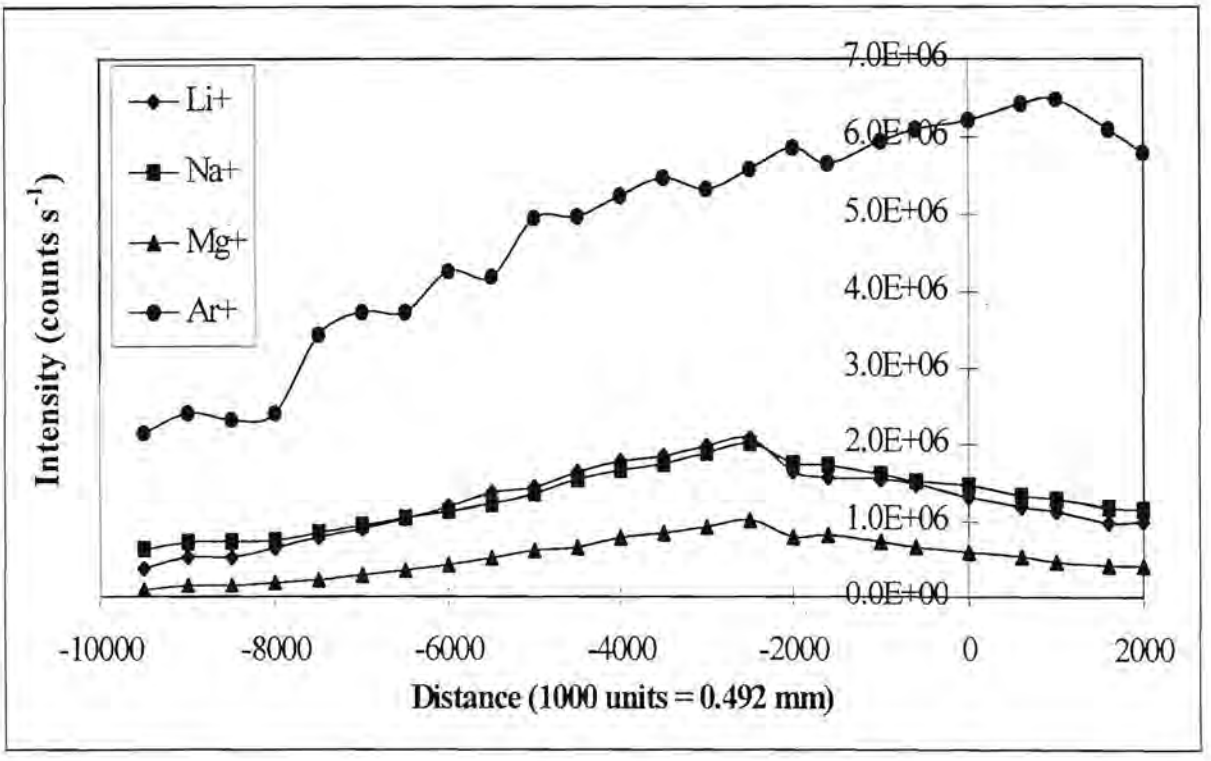

Figure 2.1: Effect of horizontal displacement of the torch on the response curves of light elements and argon.

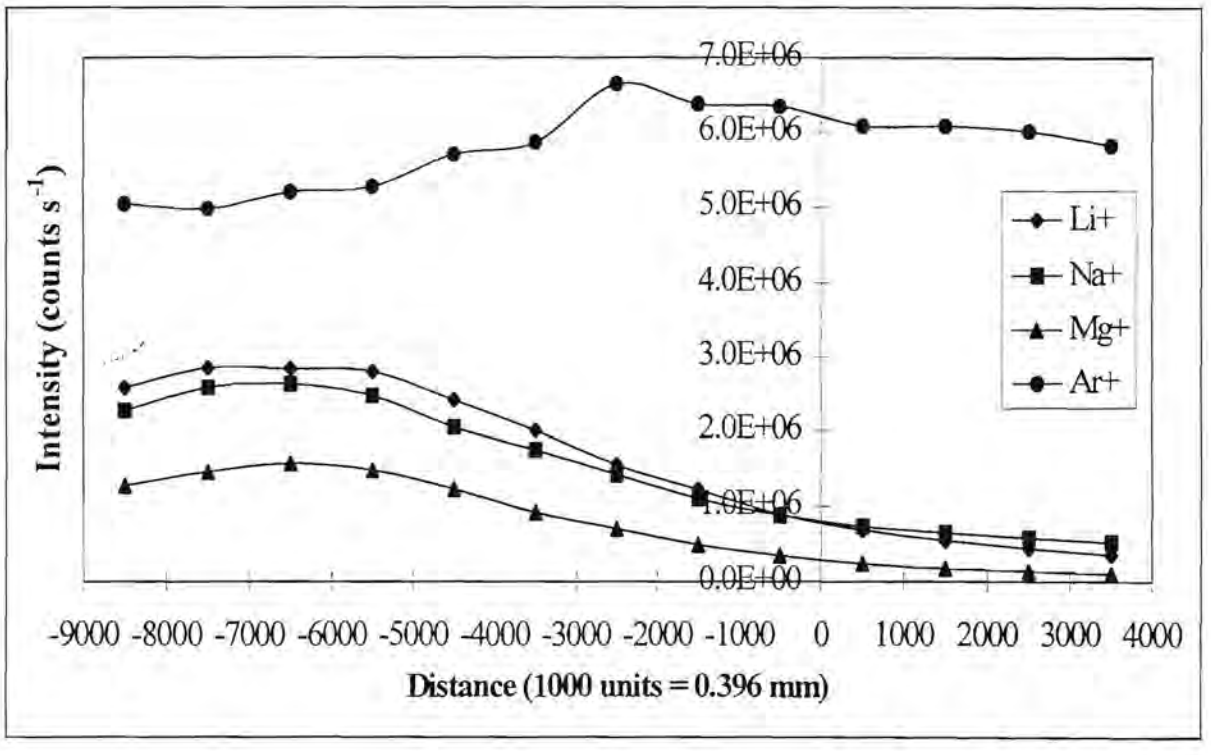

Figure 2.2: Effect of vertical displacement of the torch on the response curves of light elements and argon.

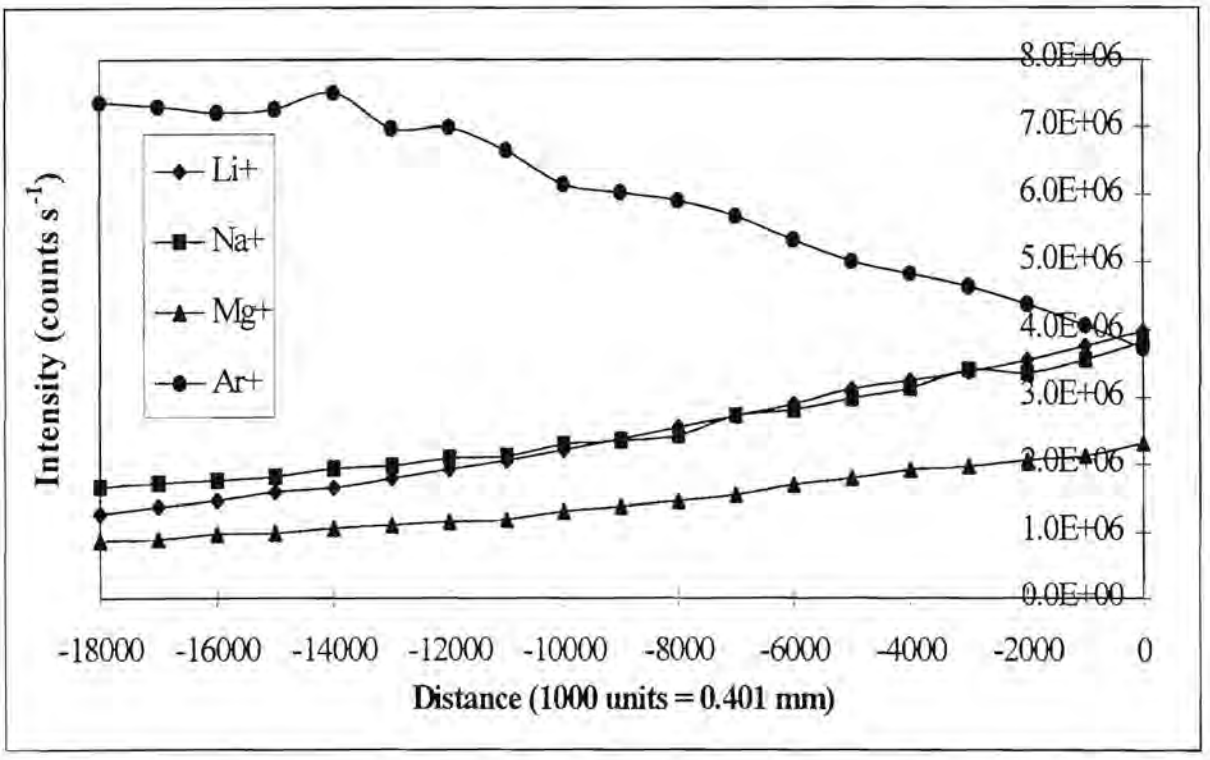

Figure 2.3: Effect of axial displacement of the torch on the response curves of light elements and argon.

From figure 2.3 the effect of the axial displacement of the torch on the analyte signal can be seen. "1000 units" on the x-axis corresponds to a distance of 0.401 mm moved. At the setting "0 units" the torch-sampler cone separation is 8.3 mm. As the torch is moved away from the sampling aperture, the analyte signals decrease and the argon signal increases. This can be explained by the fact that as the plasma is moved away less analyte ions reach the aperture and more argon reaches the sampler as the argon flow tends to enfold the analyte gas flow. Although higher analyte intensities are recorded nearer to the sampling aperture, other factors also have to be considered, e.g. lifetime of the sampler cone, time spent in the plasma by the analyte for processes such as desolvation, volatilisation, dissociation and ionisation to occur. The torch is usually set between "-3000 units" and "-6000 units". Many workers *[29 - 31]* also reported relative little change over a range of depths (axial displacement) with increasing signal loss at greater depths.

Effect of torch adjustment on heavier elements

Figure 2.4 shows the response of the heavier elements on the horizontal displacement of the torch. Similar trends are observed as for the light elements.

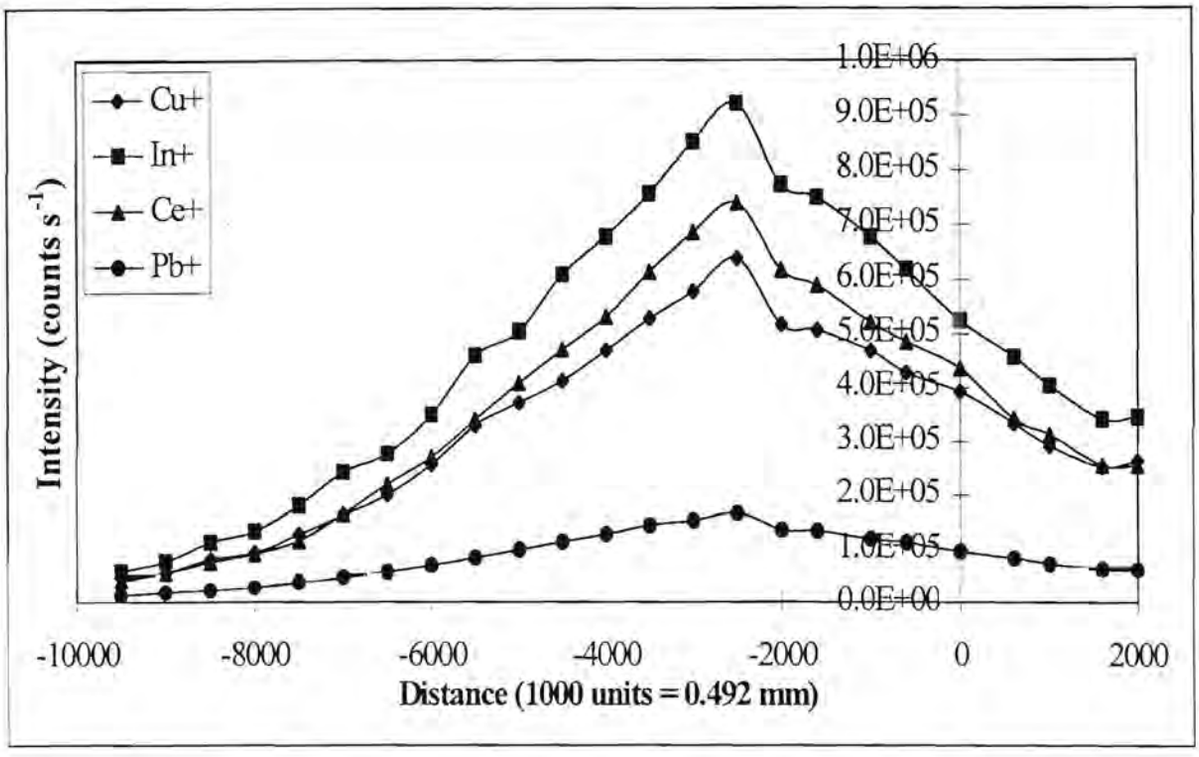

Figure 2.4: Effect of horizontal displacement of the torch on the response curves of heavier elements.

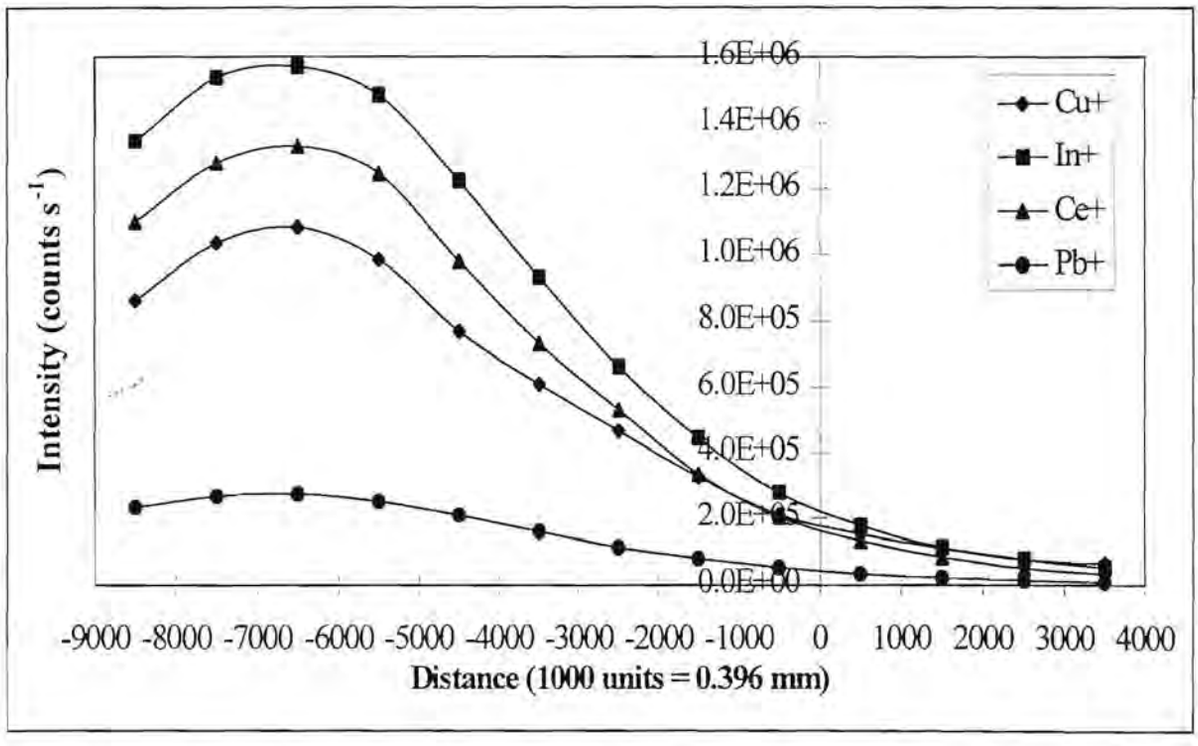

Figure 2.5: Effect of vertical displacement of the torch on the response curves of heavier elements.

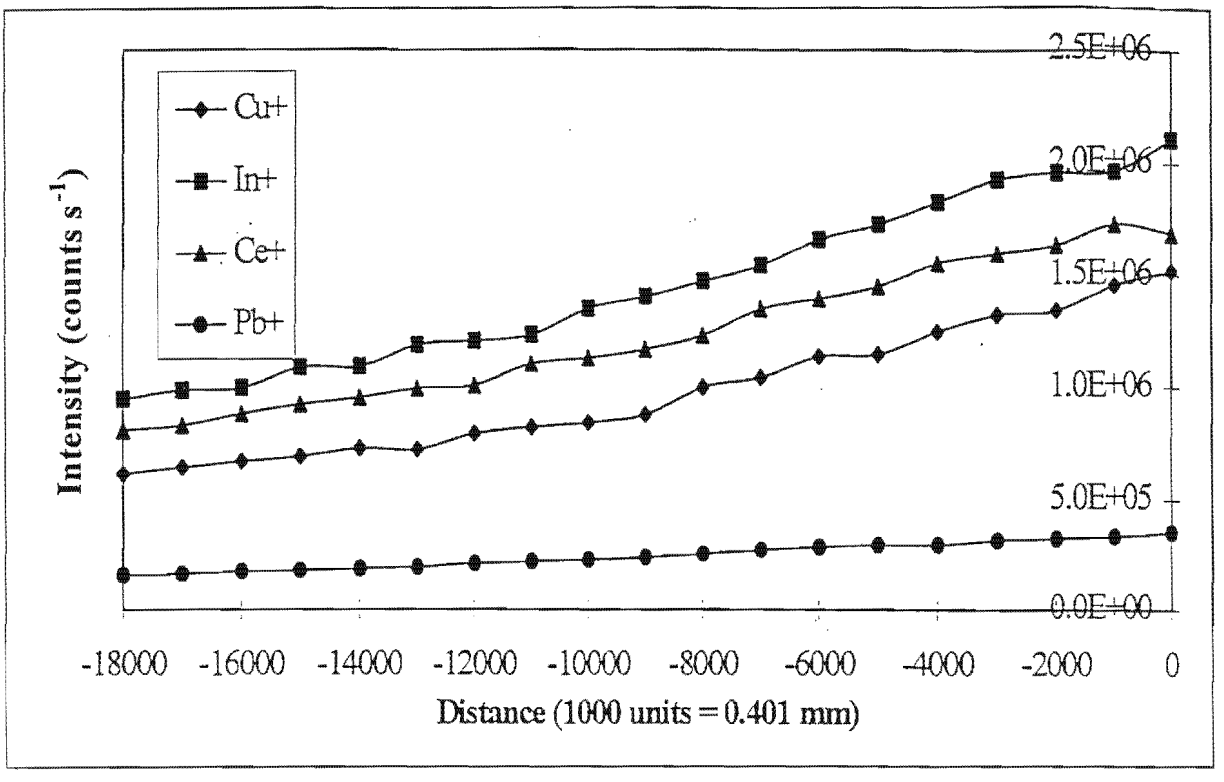

Figure 2.6: Effect of axial displacement of the torch on the response curves of heavier elements.

As the plasma is moved across the aperture the maximum analyte intensities are also observed at "-2500 units". At distances of 1.2 mm away from the maximum position the analyte signals decrease by about 40%. Even at these settings the signals observed are still above 1 x10^5.

The optimum vertical setting of the torch appears to be at "-6500 units" as can be seen from figure 2.5. The same trends as for the horizontal variation are observed.

Figure 2.6 shows the effect of axial displacement of the torch on the response curves of heavier elements. The trends observed are similar to those seen for the light elements. This is in accordance with results from Horlick *et al. [29]* and Vaughan *et al. [30]*.

Effect of torch adjustment on background intensities

From figure 2.7 the background intensities at various horizontal displacements can be seen. The background signals do not follow a specific trend but are below 80 counts s^{-1} over the whole range.

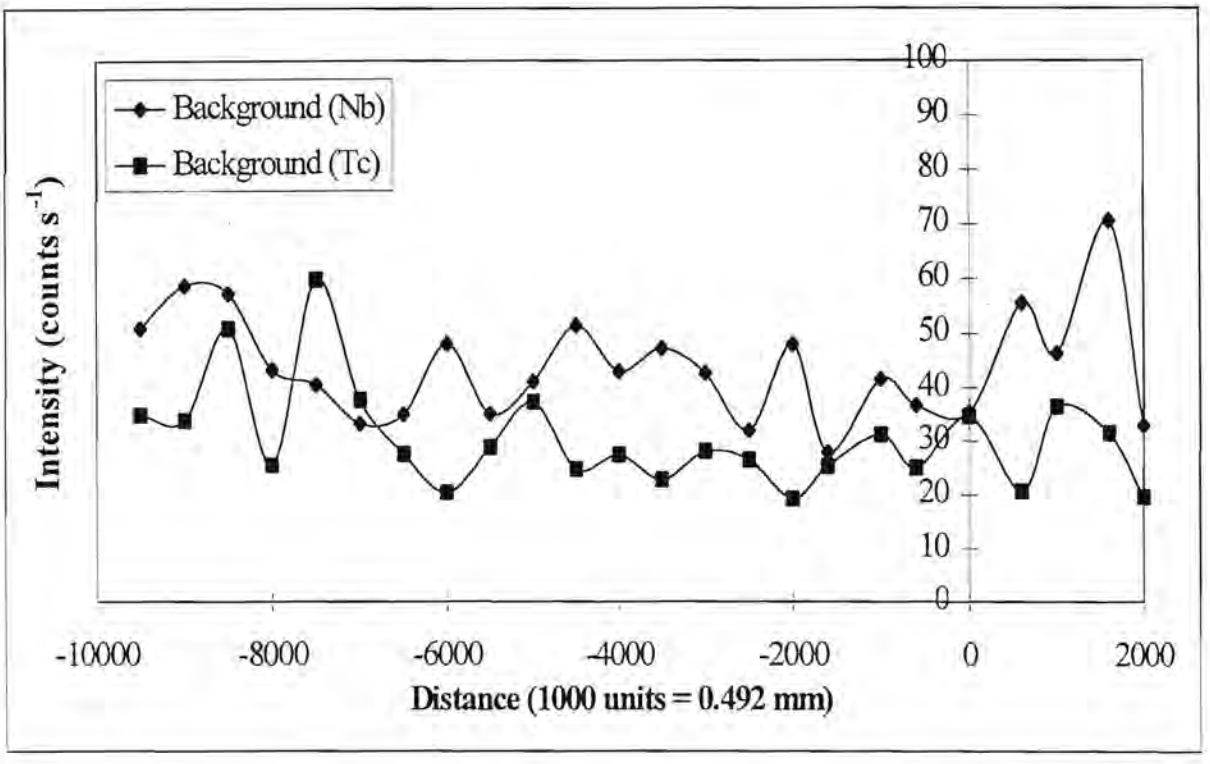

Figure 2.7: Effect of horizontal displacement of the torch on background intensities.

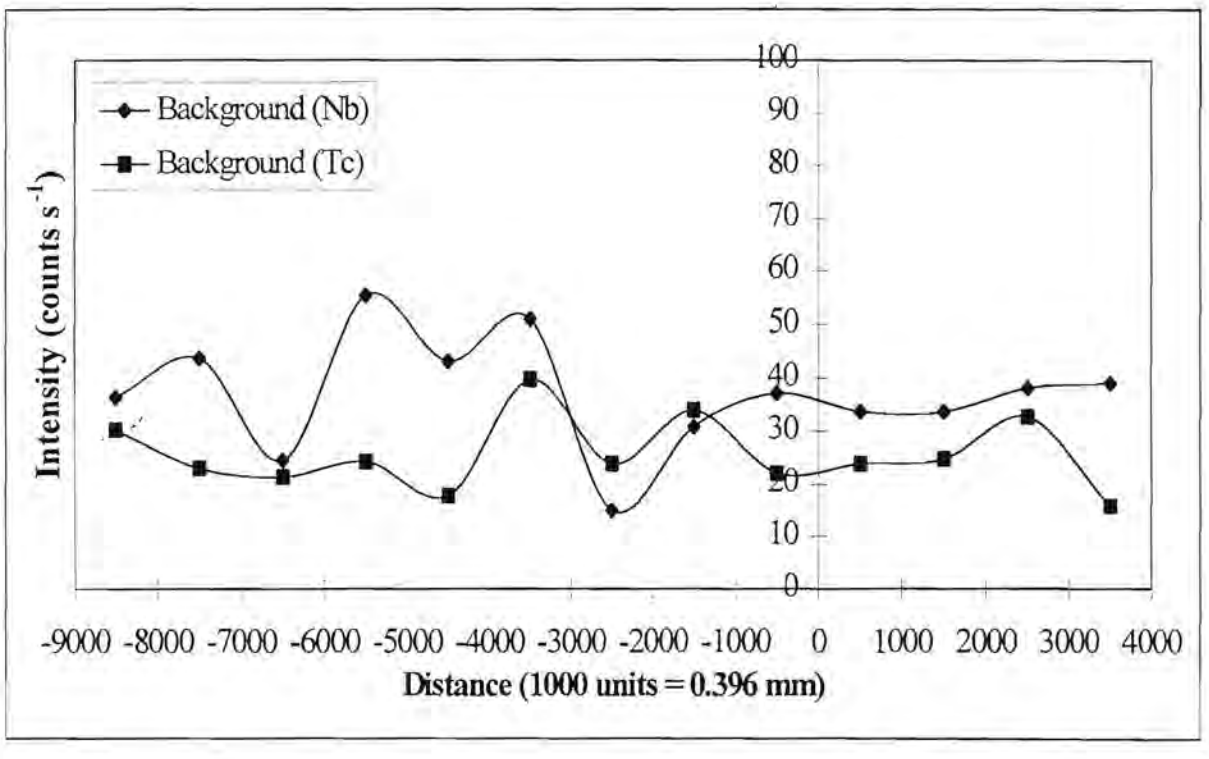

Figure 2.8: Effect of vertical displacement of the torch on background intensities.

Figure 2.8 shows that the background signals are below 50 counts s^{-1} for vertical displacement settings of the torch.

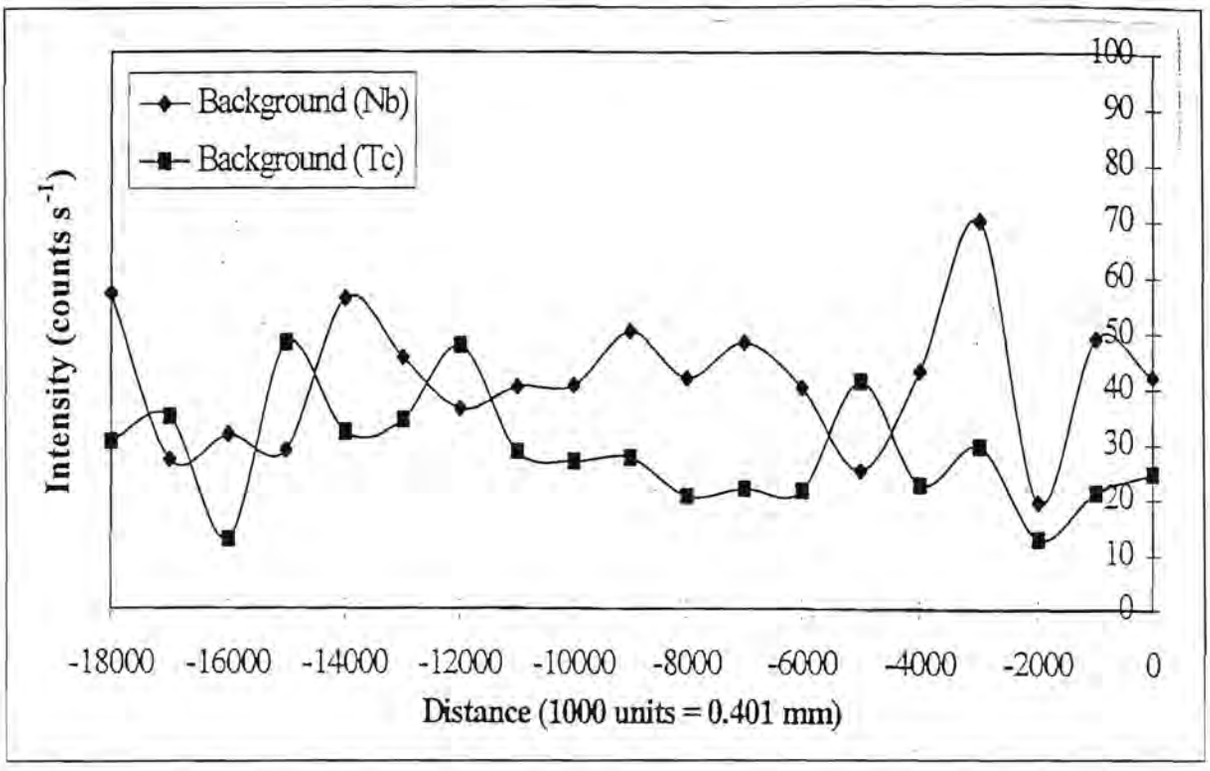

Figure 2.9: Effect of axial displacement of the torch on background intensities.

Axial settings of the torch have little or no effect on the intensities of the background signals. This can be seen from figure 2.9. Acceptable values of below 100 counts s^{-1} are observed over the whole range of axial displacements.

Effect of torch adjustment on doubly ionised ions and oxides

From figure 2.10 the signals from doubly ionised Ce and CeO^+ can be seen. Optimum values for these interferences are also obtained at a setting of "-2500 units". Figure 2.11 shows that the setting of the horizontal displacement of the torch has no significant effect on the M^{2+}/M^+ and MO^+/M^+ ratios. The Ce^{2+}/Ce^+ ratio is below the acceptable value of 2.5% and the CeO^+/Ce^+ ratio is about the acceptable value of 1% *[32]*.

The vertical displacement of the torch shows similar effects on the Ce^{2+} and CeO^+ signals (figure 2.12) and on analyte signals. Figure 2.13 shows that the vertical displacement of the torch does not have a significant effect on the Ce^{2+}/Ce^+ and CeO^+/Ce^+ ratios, except for the Ce^{2+}/Ce^+ ratio which increases significantly at settings of "500 units" to "3500 units".

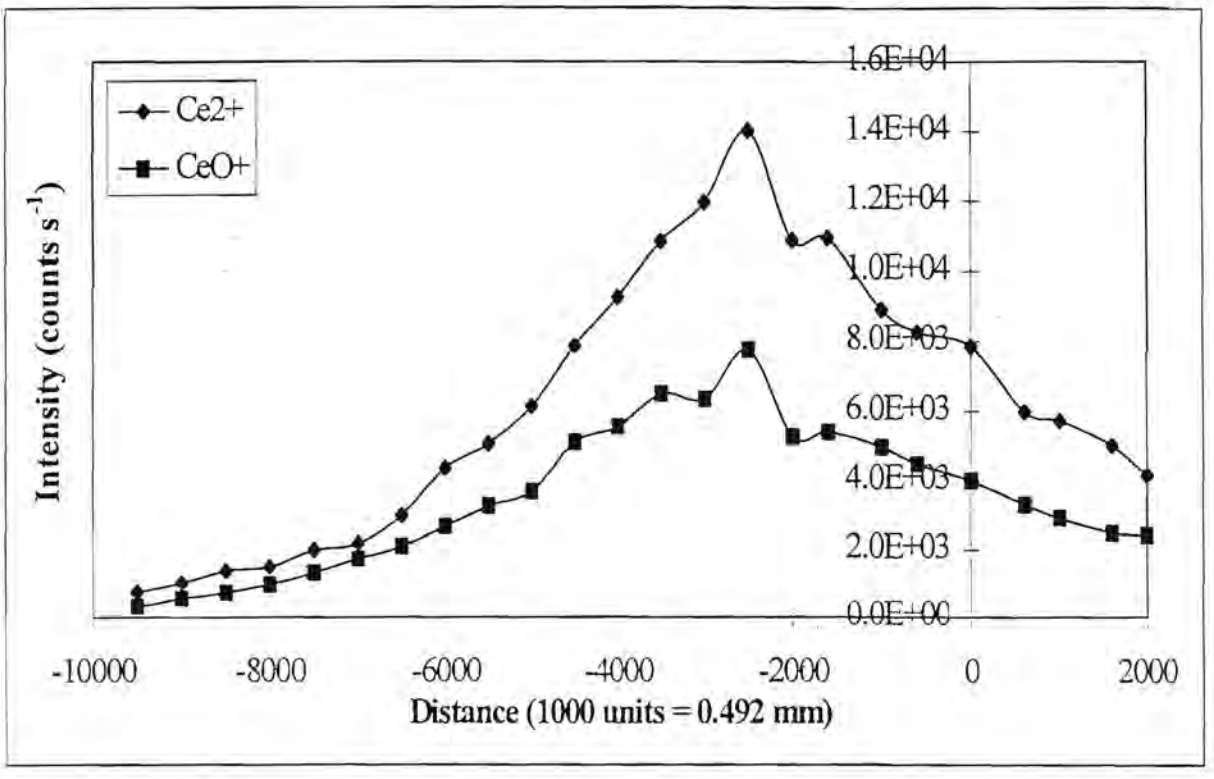

Figure 2.10: Effect of horizontal displacement of the torch on the response curves of doubly ionised and oxide ions.

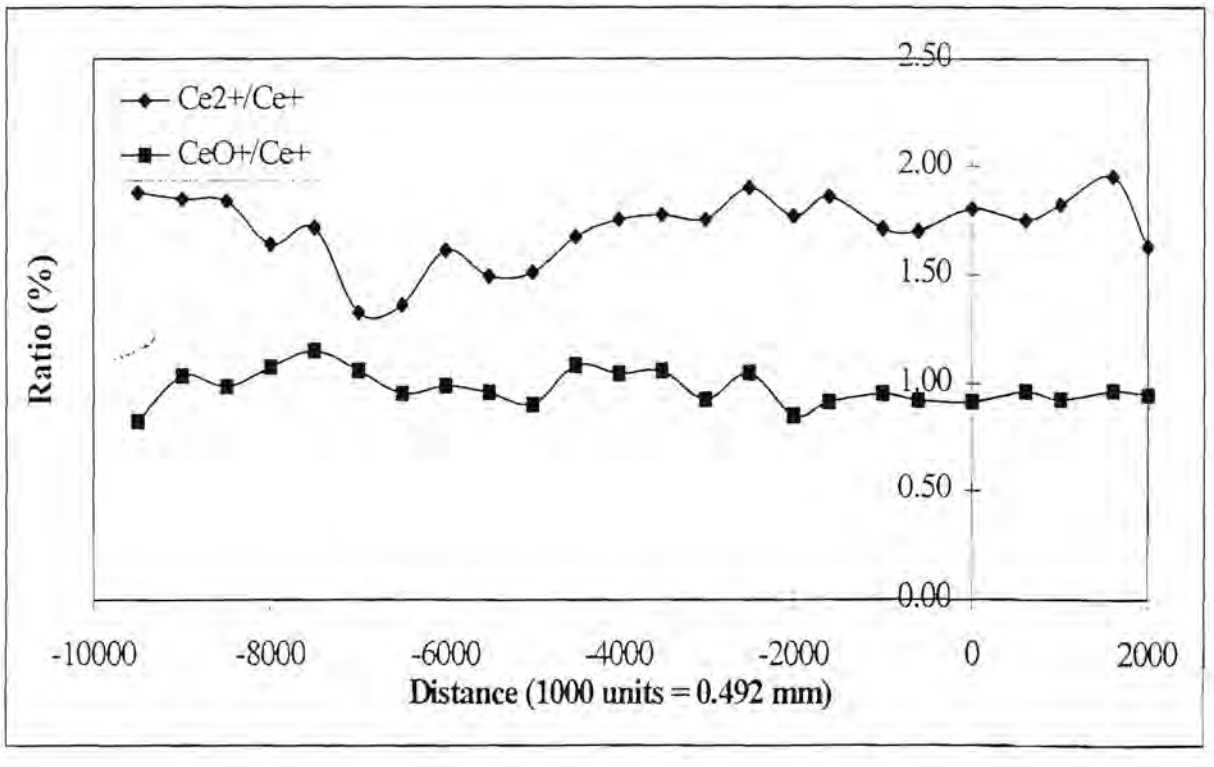

Figure 2.11: Effect of horizontal displacement of the torch on the ratios Ce^{2+}/Ce^{+} and CeO^{+}/Ce^{+}.

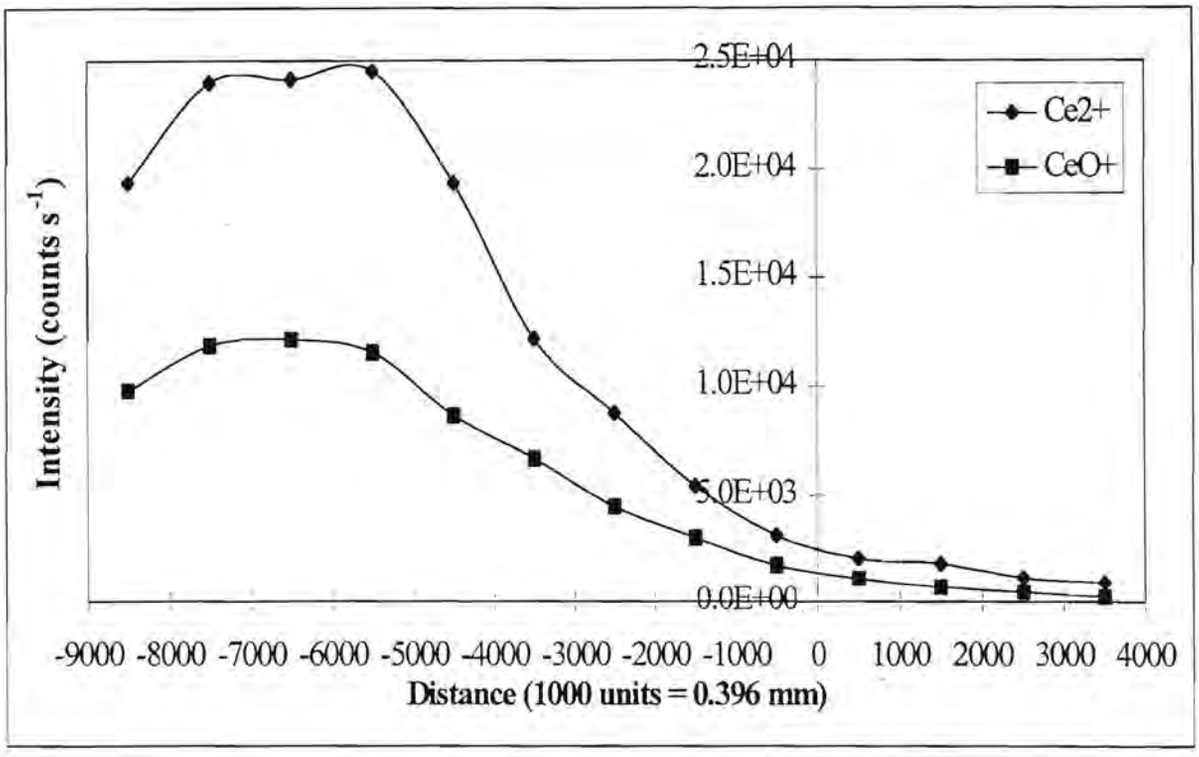

Figure 2.12: Effect of vertical displacement of the torch on the response curves of doubly ionised and oxide ions.

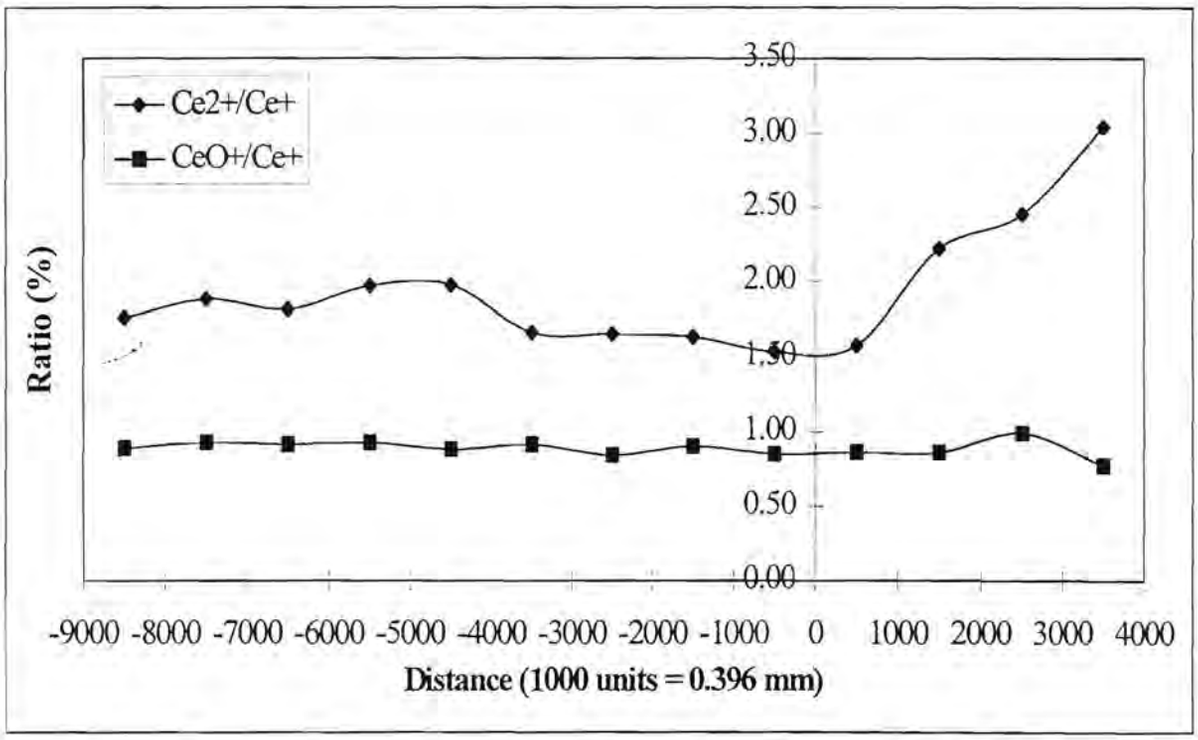

Figure 2.13: Effect of vertical displacement of the torch on the ratios Ce^{2+}/Ce^{+} and CeO^{+}/Ce^{+}.

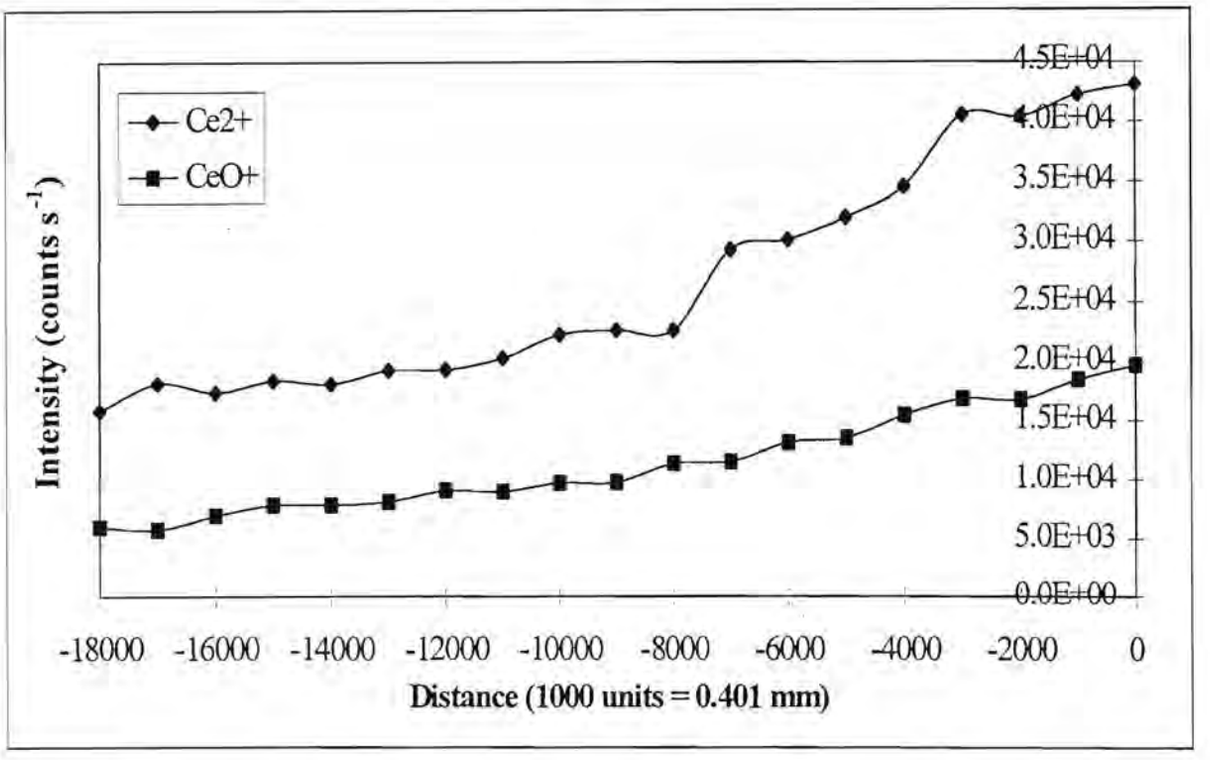

Figure 2.14: Effect of axial displacement of the torch on the response curves of doubly ionised and oxide ions.

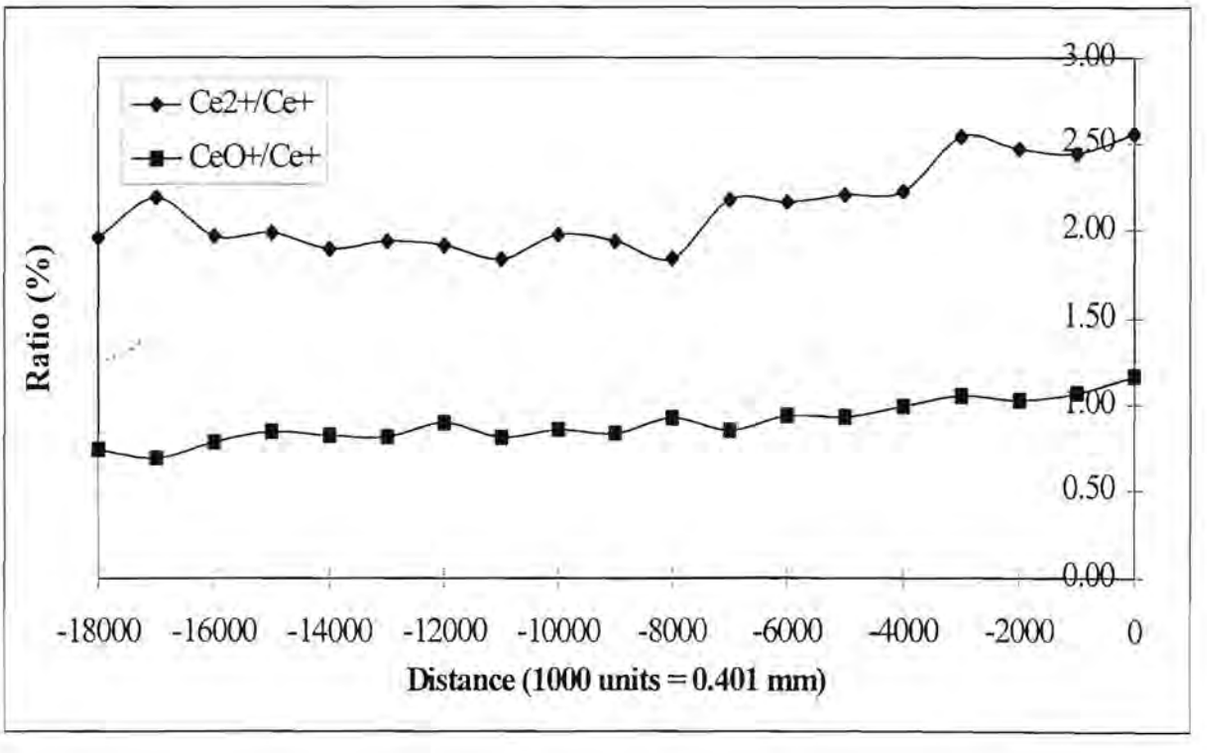

Figure 2.15: Effect of axial displacement of the torch on the ratios Ce^{2+}/Ce^{+} and CeO^{+}/Ce^{+}.

Figure 2.14 and figure 2.15 show that the amounts of Ce^{2+} and CeO^{+} produced, as well as the ratio of CeO^{+} to Ce^{+}, are not significantly affected by the axial displacement of the torch. The Ce^{2+}/Ce^{+} ratio increases slightly as the torch is moved closer to the sampling aperture. Distances closer than "-3000 units" should thus be avoided.

2.3.2 *Effects of coolant and auxiliary gas flow rates*

Effect of coolant and auxiliary gas flow rates on light elements

The effects of coolant and auxiliary gas flow rates on the light elements are shown in figure 2.16 and figure 2.17. The analyte signals increase with an increase in coolant gas flow rate and decrease with an increase in the auxiliary gas flow rate. Contrary to these results Horlick *et al. [29]* reported a slight increase in analyte signals with an increase in the auxiliary gas flow rate. The auxiliary gas flow rate has a smaller effect on the intensity of the signals than the coolant gas flow rate.

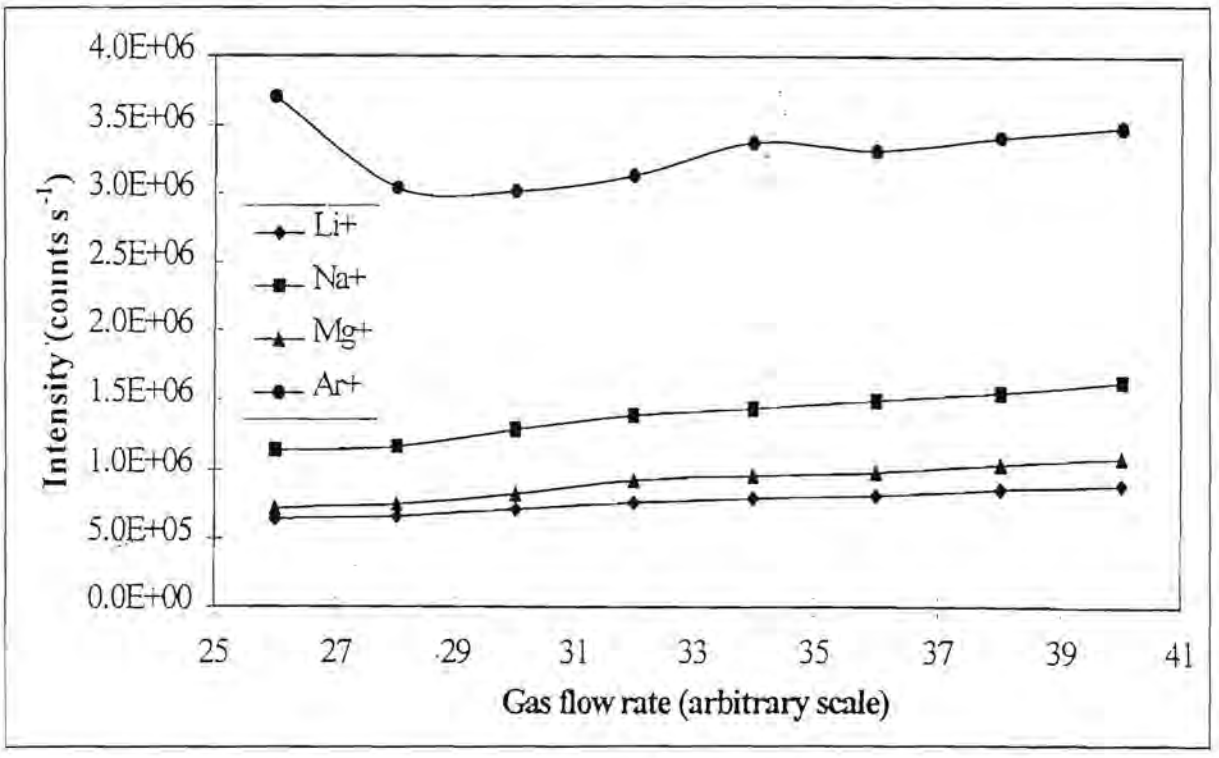

Figure 2.16: Effect of the coolant gas flow rate on the response curves of the light elements and argon.

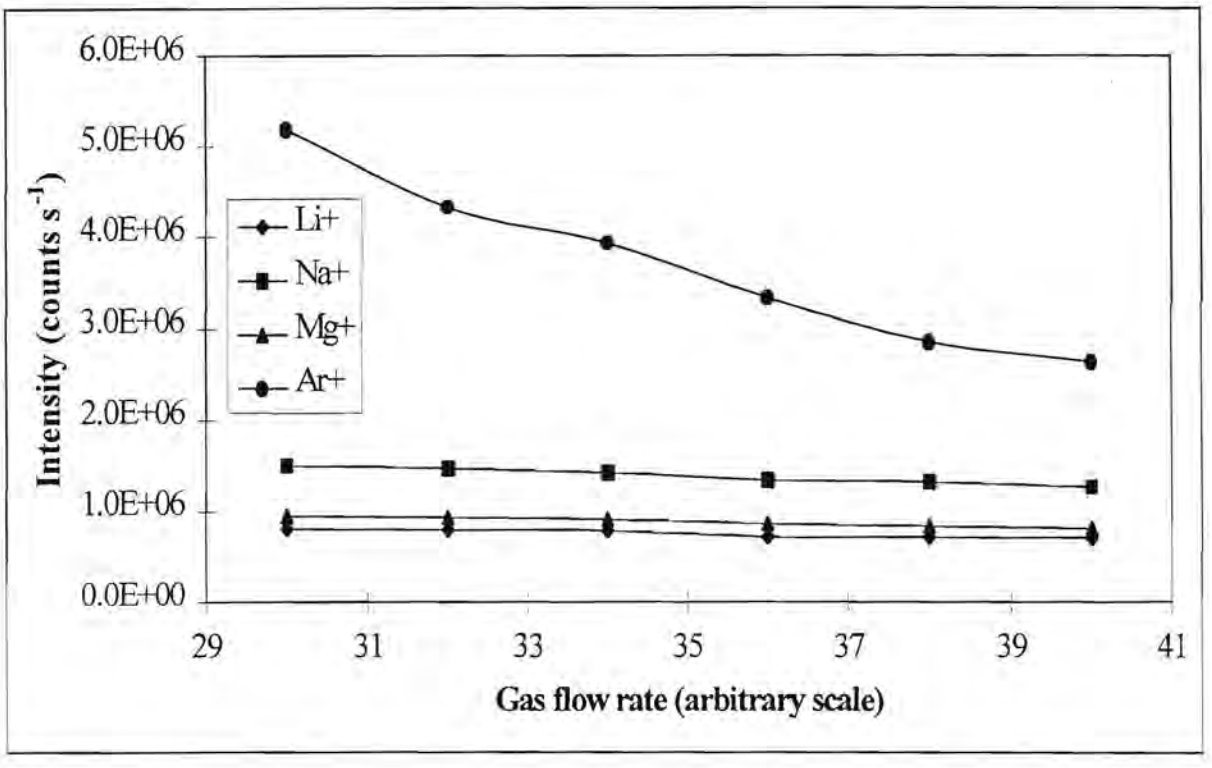

Figure 2.17: Effect of the auxiliary gas flow rate on the response curves of the light elements and argon.

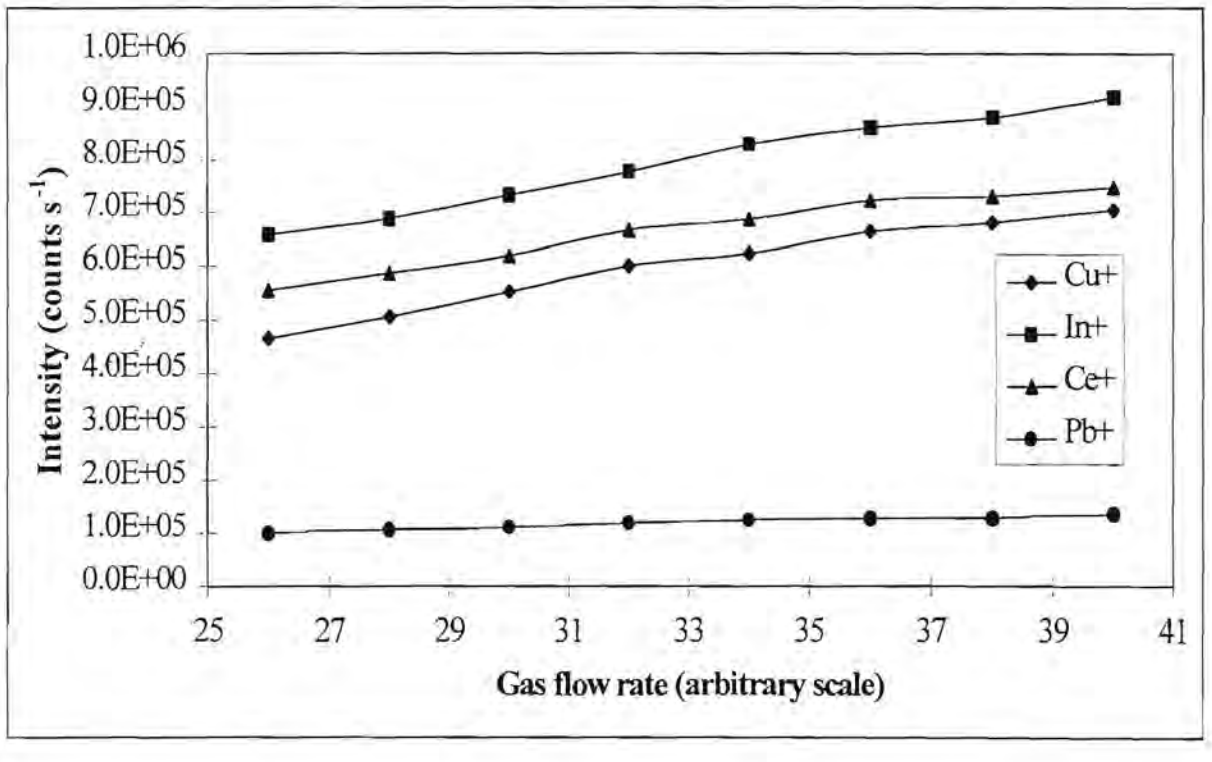

Figure 2.18: Effect of the coolant gas flow rate on the response curves of the heavier elements.

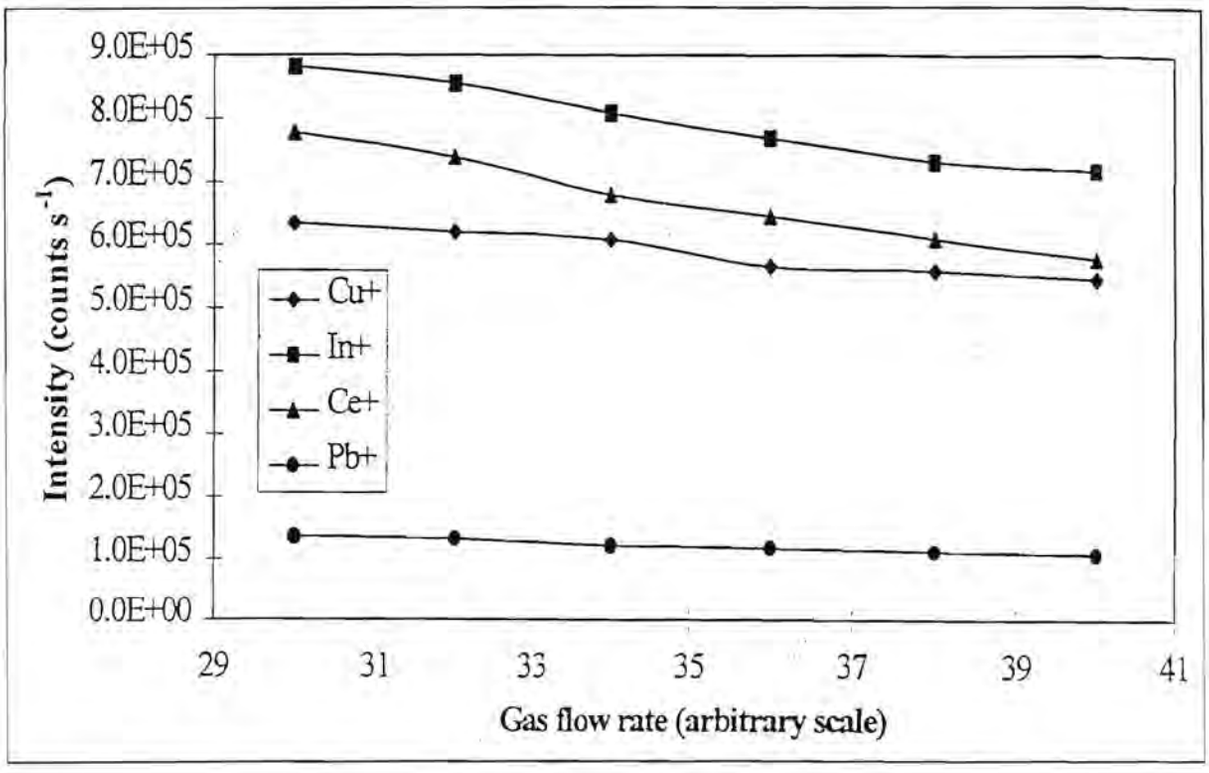

Figure 2.19: Effect of the auxiliary gas flow rate on the response curves of the heavier elements.

Effect of coolant and auxiliary gas flow rates on heavier elements

Figures 2.18 and 2.19 show similar trends for the heavier elements as for the light elements with increases in the coolant and auxiliary gas flow rates. Results from Long and Brown *[33]* show similar trends with the coolant flow identified as not having a great effect on analyte signals. They also found low auxiliary gas flow rates to be preferable.

Effect of coolant and auxiliary gas flow rates on background intensities

Changes in the coolant and auxiliary gas flow rates do not have a significant effect on the background intensities, which remain at approximately 50 counts s^{-1}. This is shown in figure 2.20 and figure 2.21.

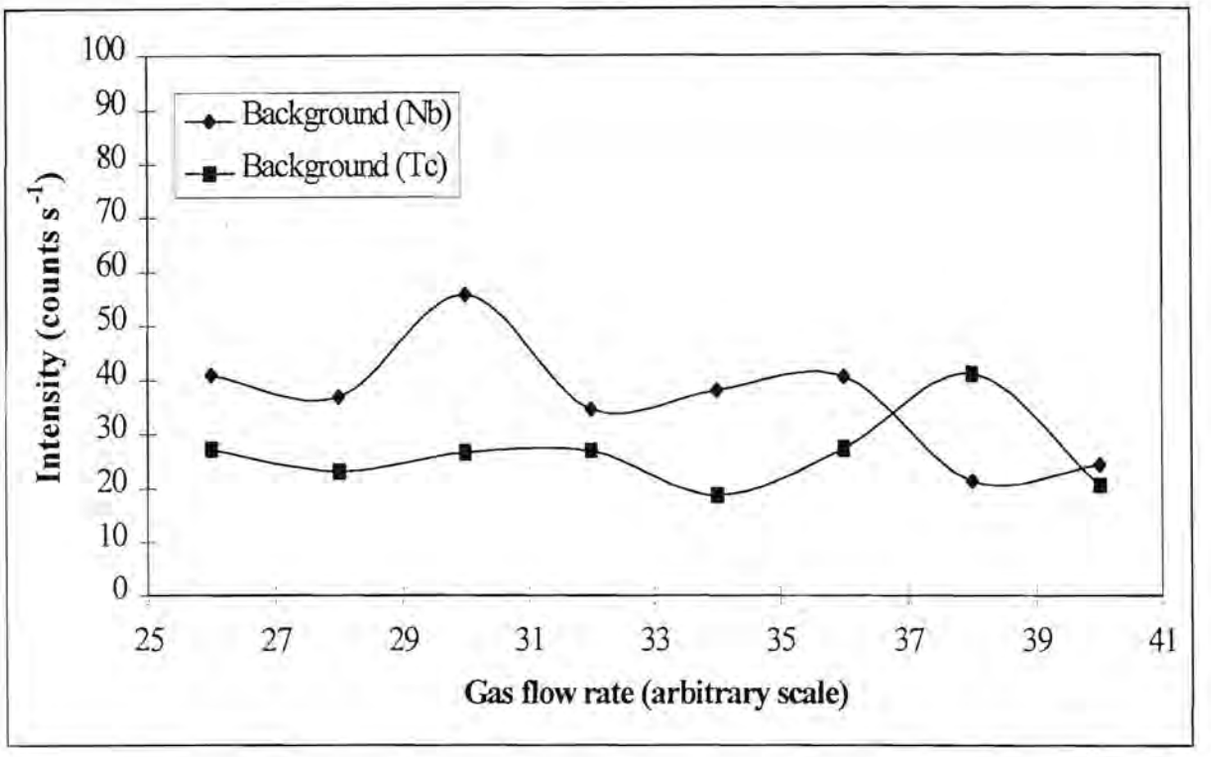

Figure 2.20: Effect of coolant gas flow rate on background intensities.

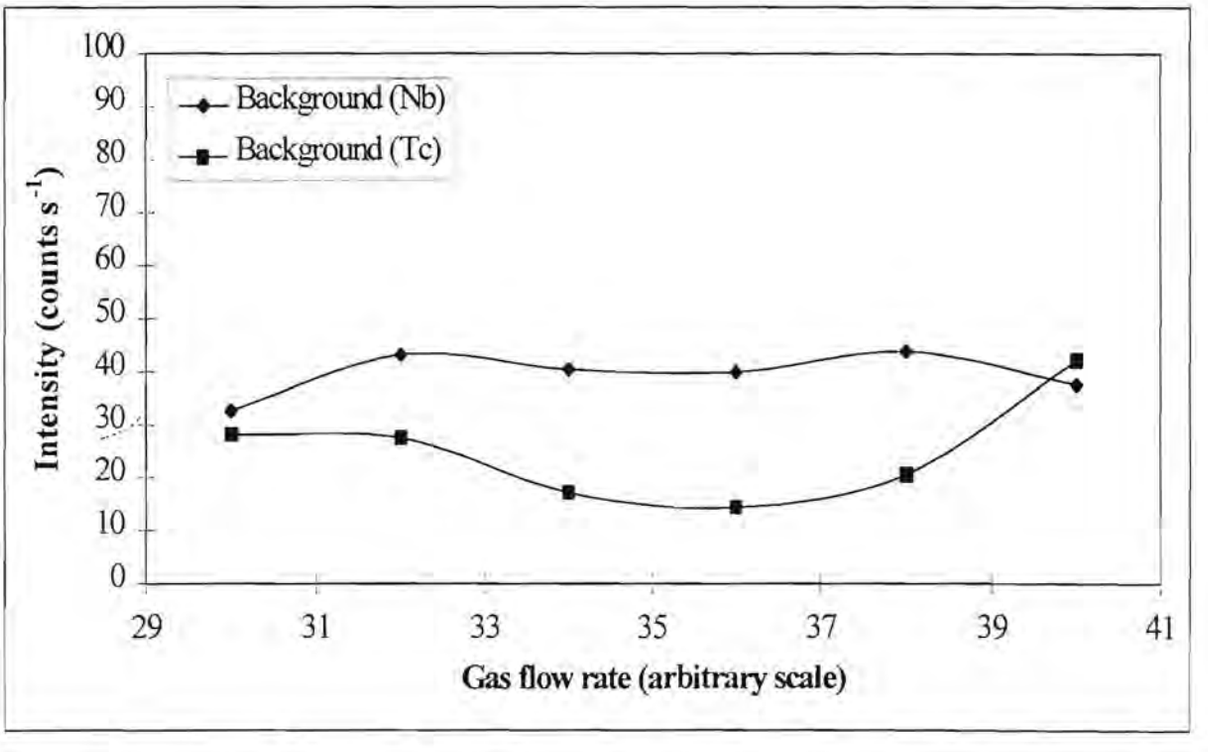

Figure 2.21: Effect of auxiliary gas flow rate on background intensities.

Effect of coolant and auxiliary gas flow rates on doubly ionised ions and oxides

Figures 2.22 and 2.23 show that the intensity of CeO^+ does not change much with variations in the coolant and auxiliary gas flow rates. The Ce^{2+} signal increases with increases in the coolant and auxiliary gas flow rates.

Figures 2.24 and 2.25 put these values into perspective by showing changes in the Ce^{2+}/Ce^+ and CeO^+/Ce^+ ratios with changes in the gas flow rates. Although the CeO^+/Ce^+ ratio remains unchanged at about 1%, the Ce^{2+}/Ce^+ ratio increases with increases in the gas flow rates.

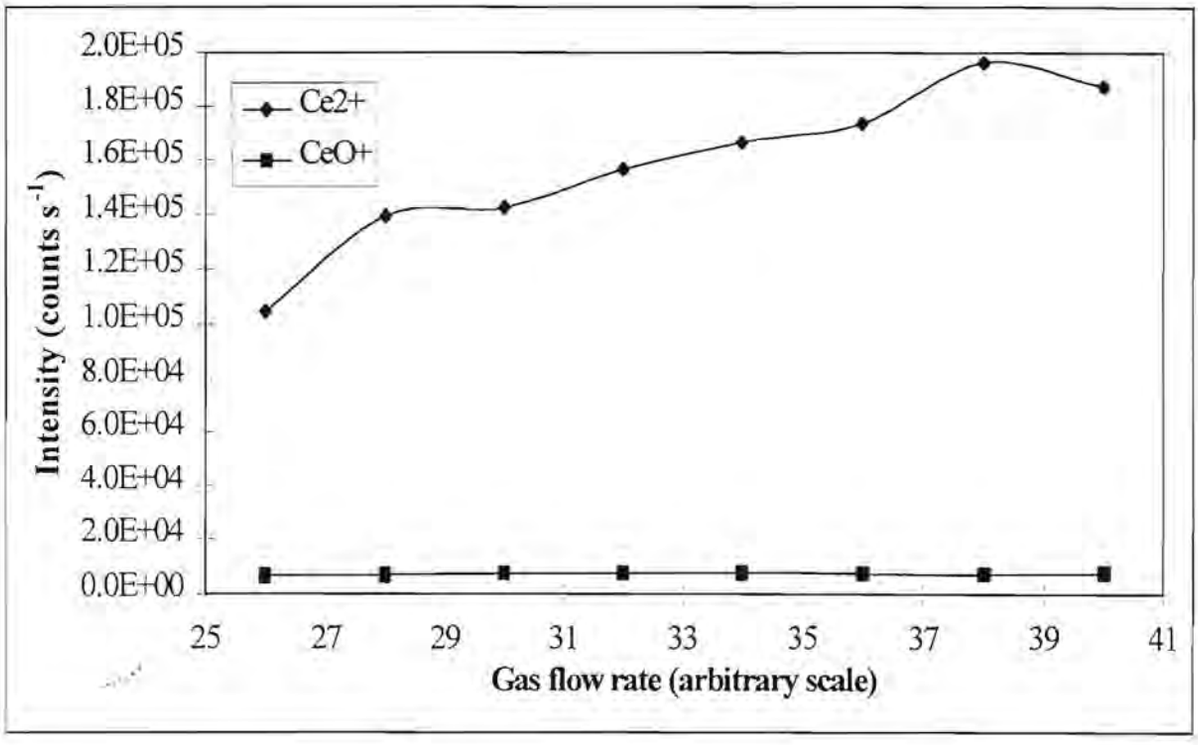

Figure 2.22: Effect of coolant gas flow rate on the response curves of doubly ionised and oxide ions.

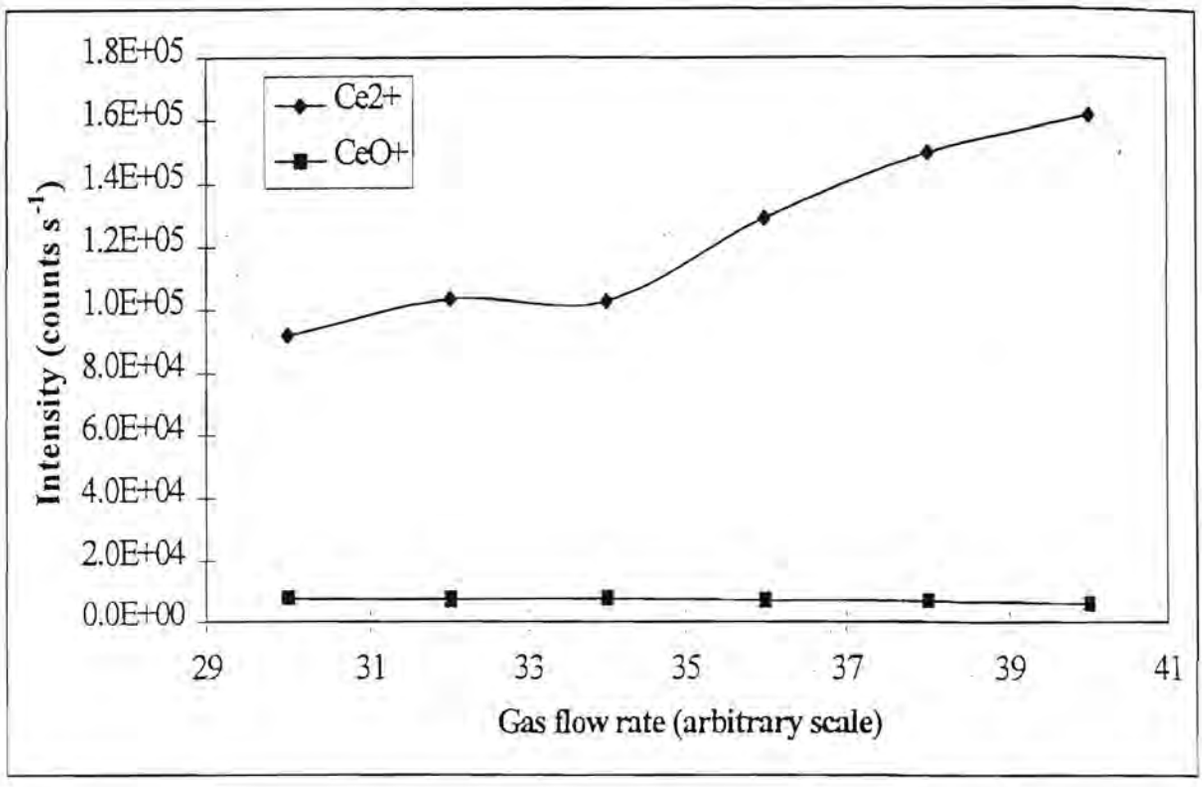

Figure 2.23: Effect of auxiliary flow on the response curves of doubly ionised and oxide ions.

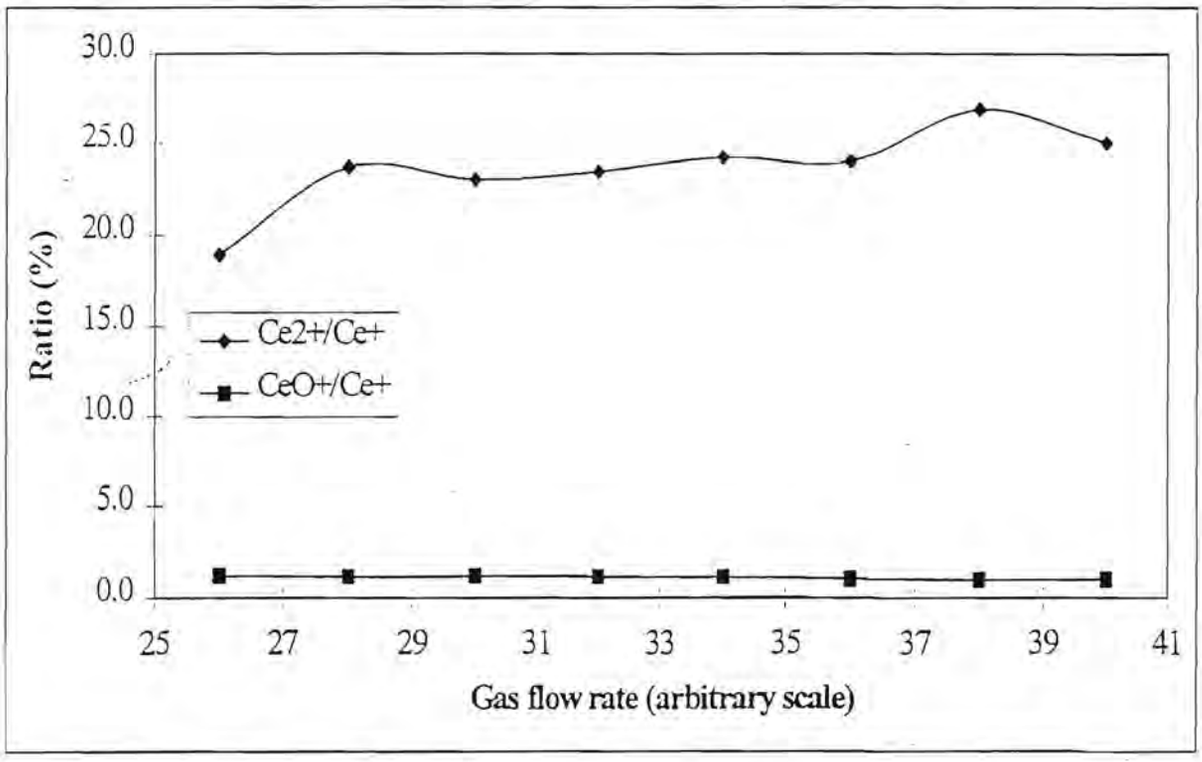

Figure 2.24: Effect of coolant flow on the response curves of the ratios Ce^{2+}/Ce^{+} and CeO^{+}/Ce^{+}.

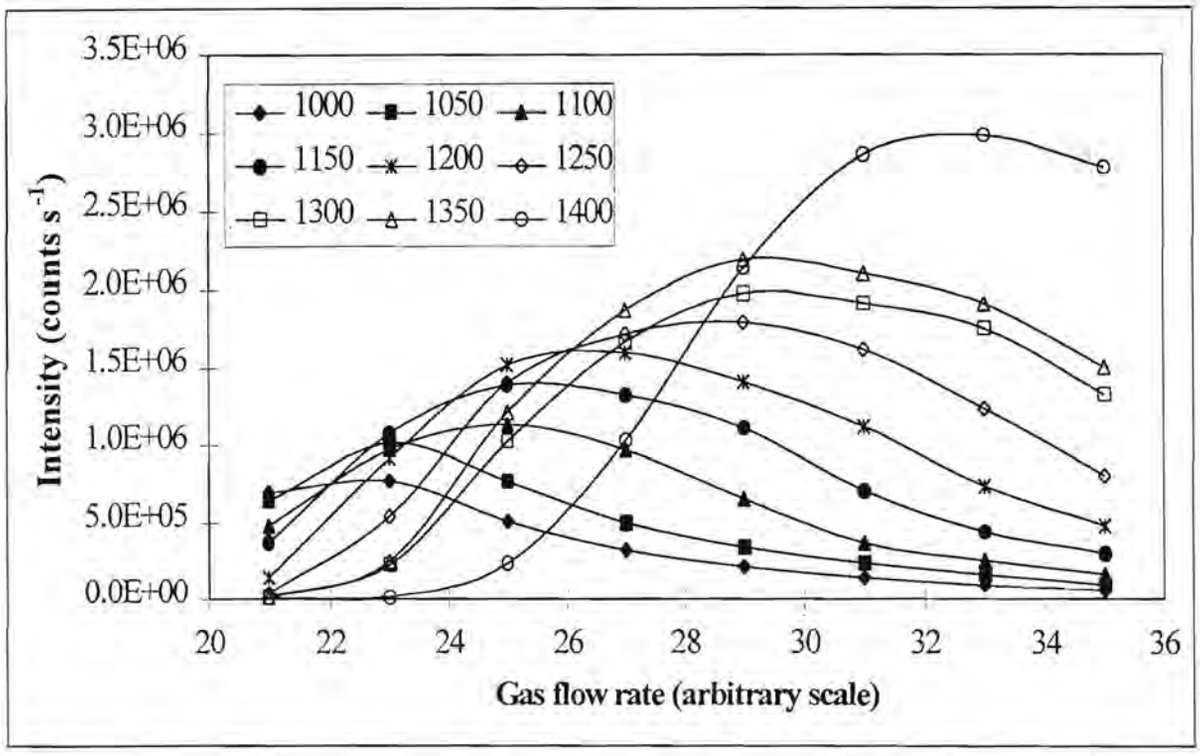

Figure 2.26: Effect of the aerosol carrier gas flow rate on the Li^+ signal at different power settings.

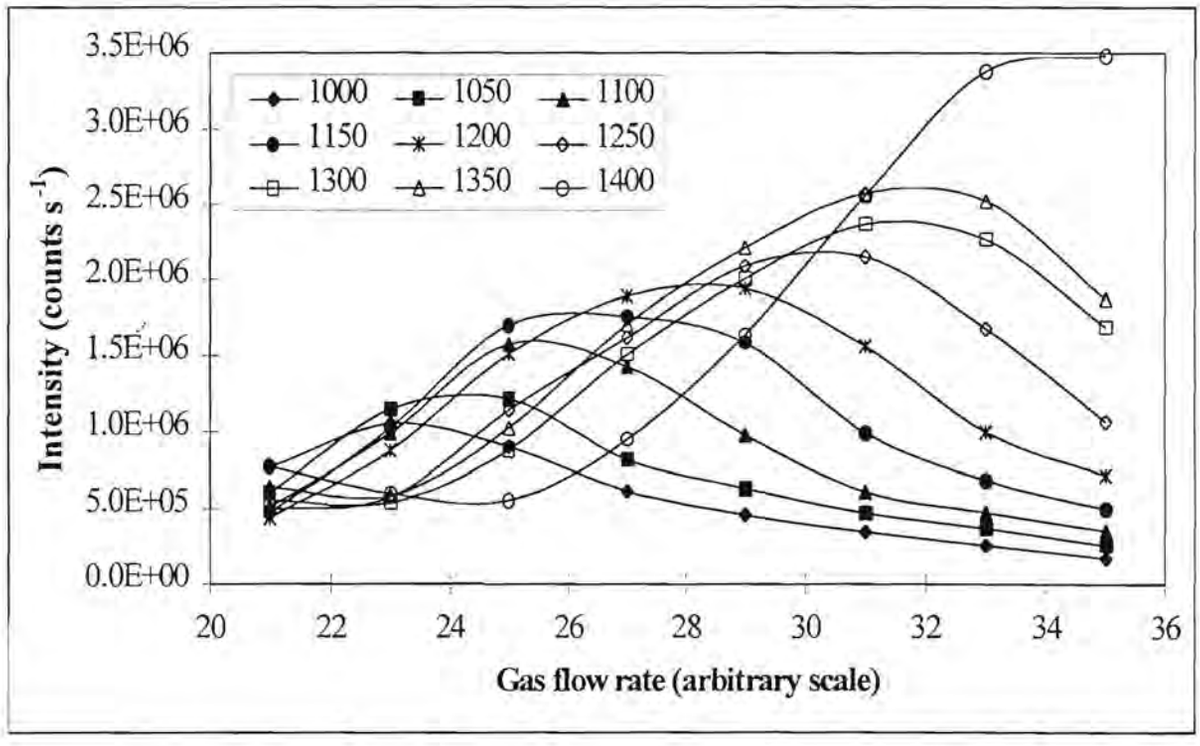

Figure 2.27: Effect of the aerosol carrier gas flow rate on the Na^+ signal at different power settings.

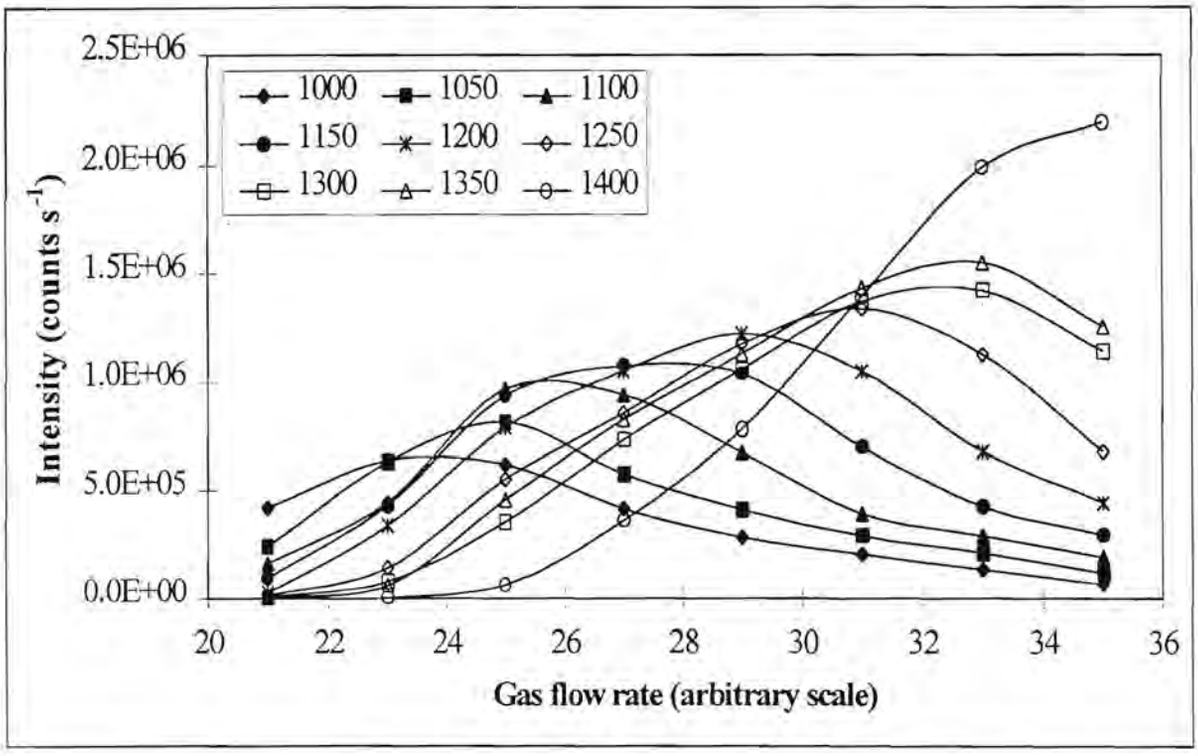

Figure 2.28: Effect of the aerosol carrier gas flow rate on the Mg^+ signal at different power settings.

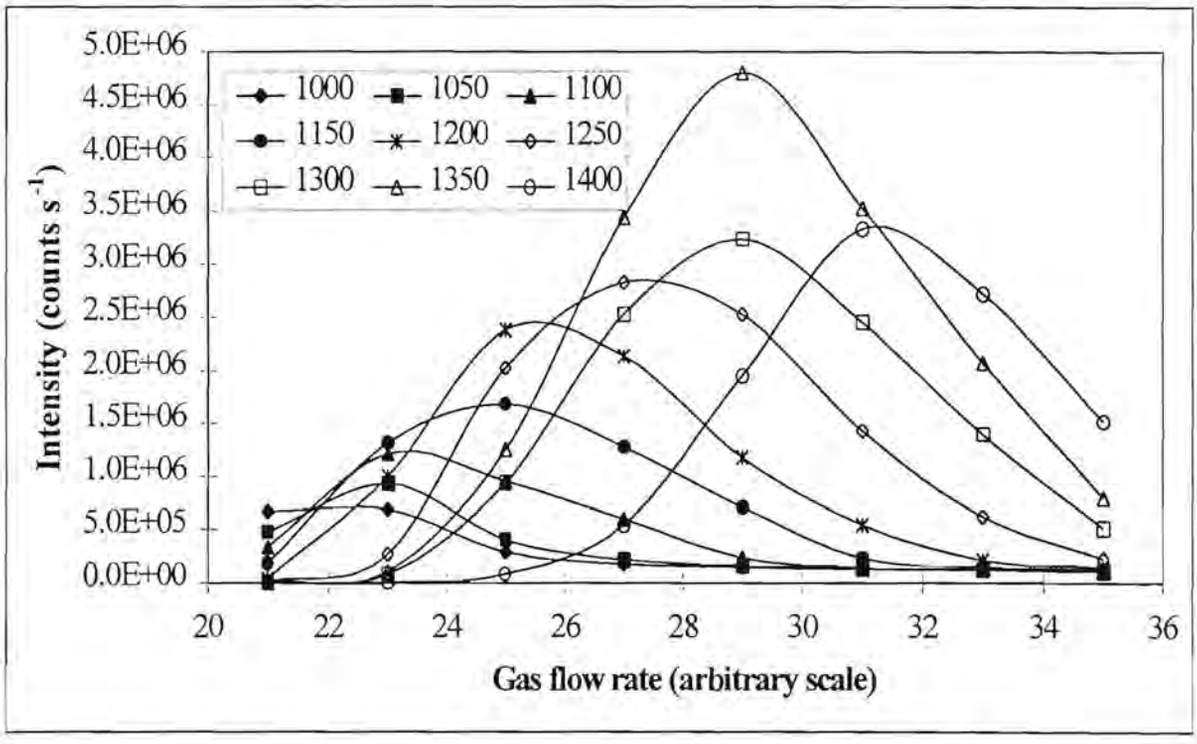

Figure 2.29: Effect of the aerosol carrier gas flow rate on the Ar^+ signal at different power settings.

Table 2.2: Aerosol carrier gas flow rates ("arbitrary scale" as used by instrument manufacturer) at which a maximum analyte signal is obtained for the power settings investigated.

Power setting	Li^+	Na^+	Mg^+	Ar^+	Cu^+	In^+	Ce^+	Pb^+	Ce^{2+}	CeO^+
1000 W	23	23	23	23	23	23	23	23	27	23
1050 W	23	25	25	23	25	23	23	23	29	25
1100 W	25	25	25	23	25	25	25	25	31	27
1150 W	25	27	27	25	27	27	25	25	33	27
1200 W	27	29	29	25	29	27	29	27	-	29
1250 W	29	31	31	27	31	29	29	29	-	29
1300 W	29	31	33	29	33	31	31	31	-	31
1350 W	29	31	33	29	33	31	31	31	-	31
1400 W	33	-	-	31	-	-	33	33	-	-

As the maximum intensity observed for an element increases with the power setting, it seems preferable to work at higher power settings. The curves show that the analyte signals are very sensitive to changes in the aerosol carrier gas flow rate at a specific power setting. Care should thus be taken when optimising the aerosol carrier gas flow rate.

Effect of power and aerosol carrier gas flow rate on heavier elements

Curves showing the effect of the aerosol carrier gas flow rate at different power settings can be seen in figures 2.30, 2.31, 2.32 and 2.33 for Cu^+, In^+, Ce^+ and Pb^+. The same trends as for the light elements are observed for the heavier elements. Table 2.2 shows that for the heavier elements the optimal aerosol carrier gas flow rate at a power setting of 1350 W is also about 31 ("arbitrary scale" as used by instrument manufacturer). As for the light elements, the data plotted indicate that analyte signals are very sensitive to changes in the aerosol carrier gas flow rate and higher power settings are preferable.

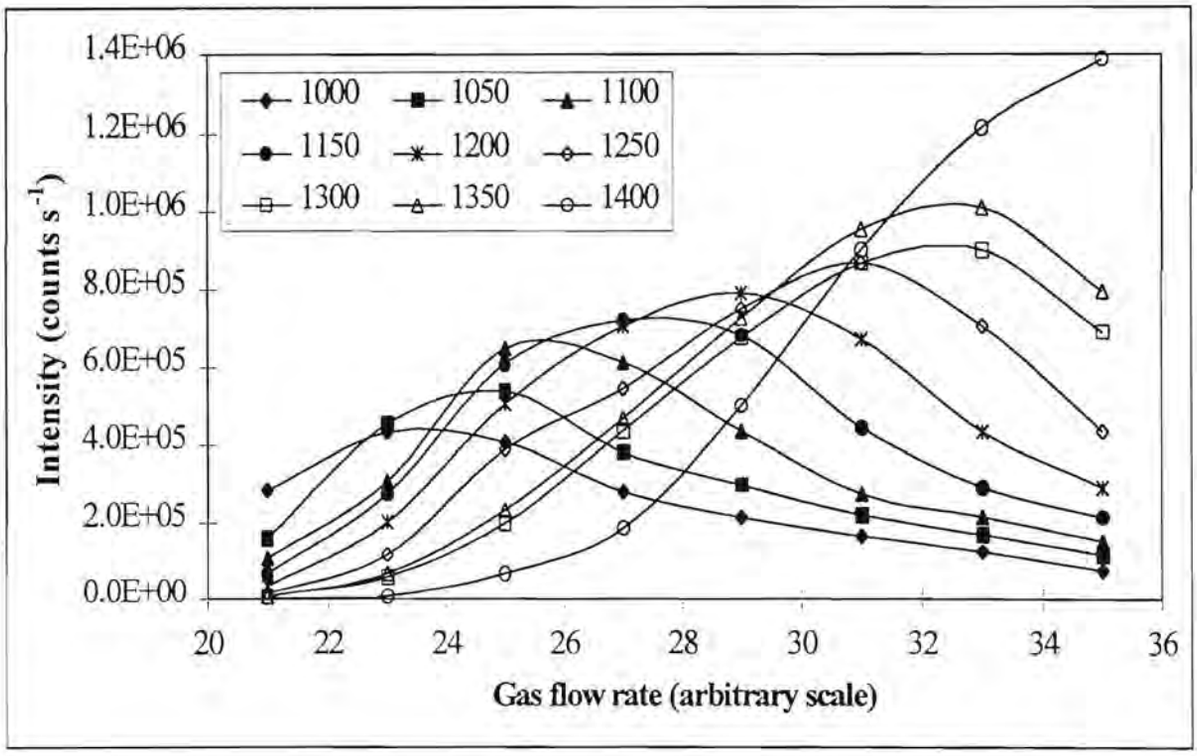

Figure 2.30: Effect of the aerosol carrier gas flow rate on the Cu^+ signal at different power settings.

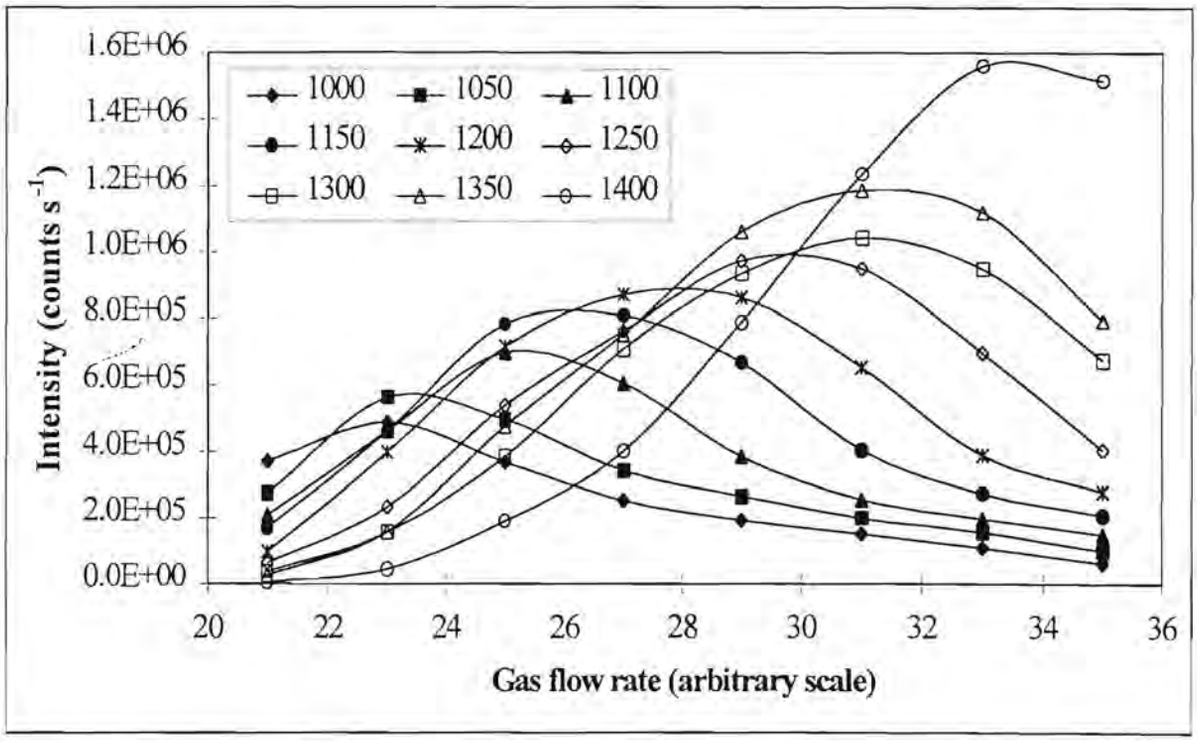

Figure 2.31: Effect of the aerosol carrier gas flow rate on the In^+ signal at different power settings.

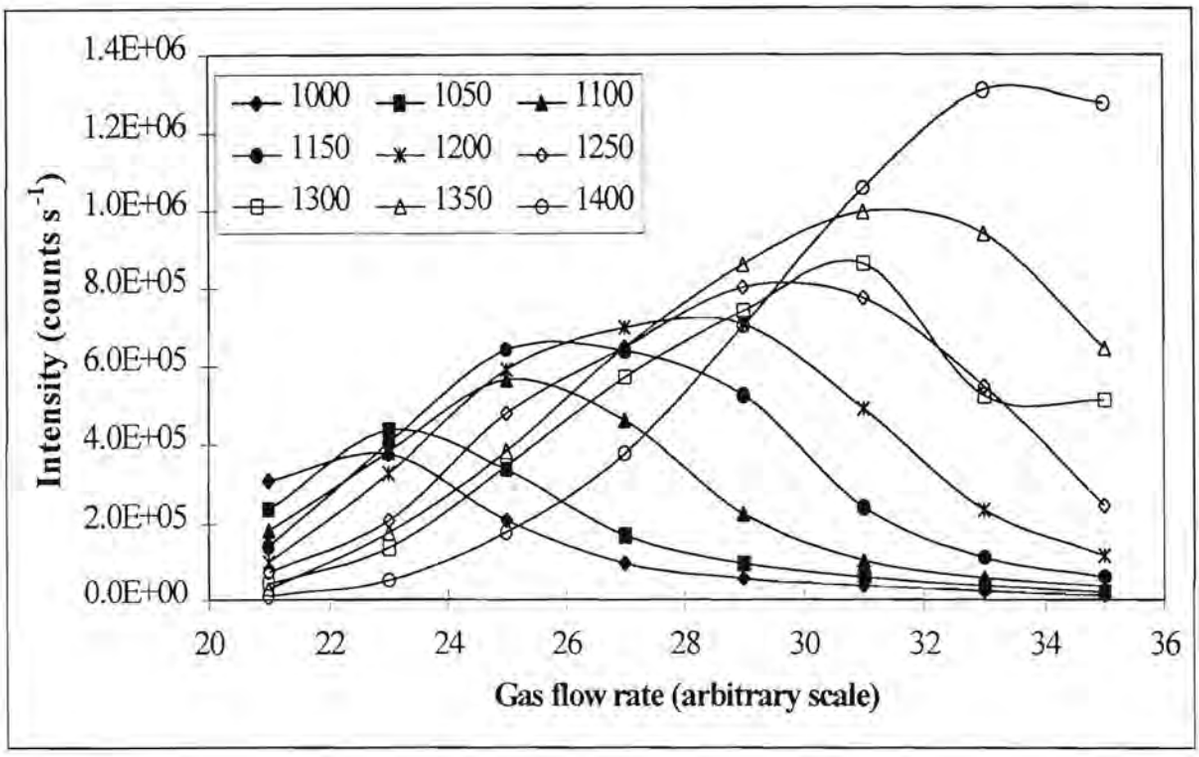

Figure 2.32: Effect of the aerosol carrier gas flow rate on the Ce^+ signal at different power settings.

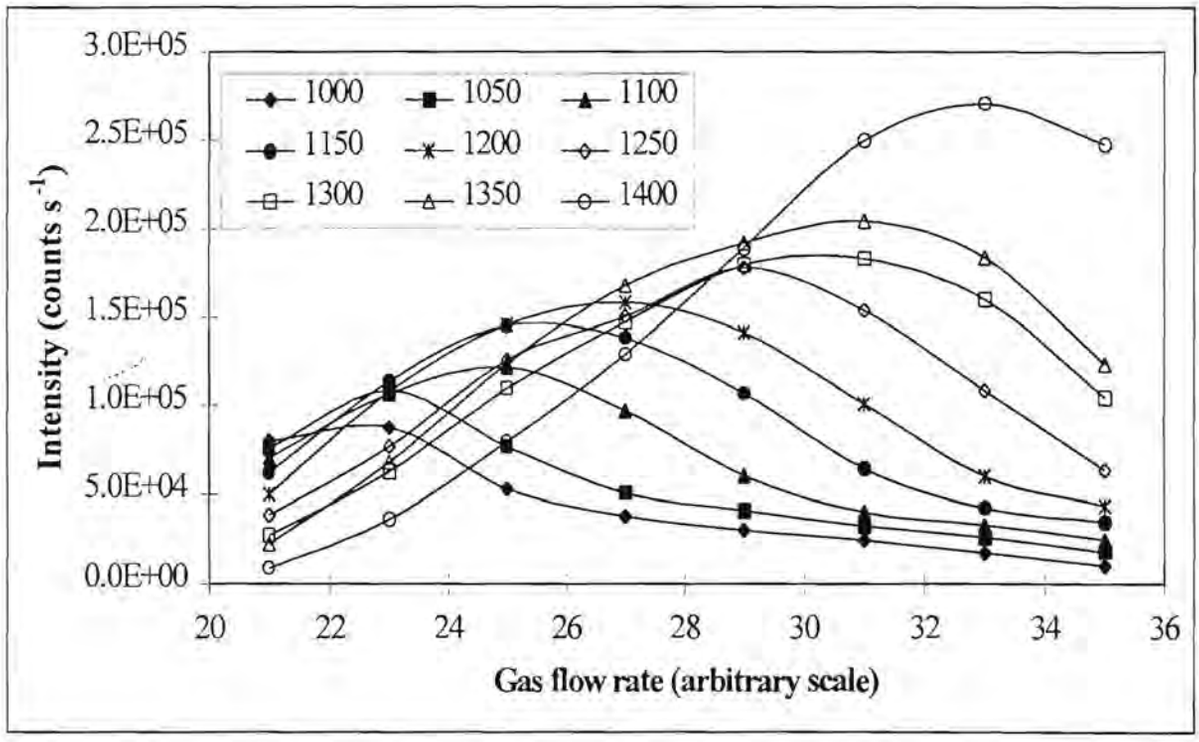

Figure 2.33: Effect of the aerosol carrier gas flow rate on the Pb^+ signal at different power settings.

Long and Brown *[33]* also found the aerosol carrier gas pressure to be of critical importance with definite settings for maximum analyte intensities. Their results showed that a compromise setting may be used that allowed multi-element analysis within 10% of the optimum sensitivity. In accordance to the results reported here, Long and Brown *[33]* further showed analyte signals to increase with an increase in power, to reach maximum values in the range 1.2 to 1.4 kW and then to decrease again. Their results, as well as those of other workers *[29, 30]*, also showed the optimum aerosol carrier gas pressure to increase with an increase in power. Zhu and Browner *[31]* reported that the response behaviour for aerosol carrier gas flow rate is largely independent of the concentration of the solution.

Effect of power and aerosol carrier gas flow rate on background intensities

Even though figures 2.34 and 2.35 indicate that the aerosol carrier gas flow rate does not have a significant effect on the background signals (values below 100 counts s^{-1}), lower background intensities are observed at lower power settings.

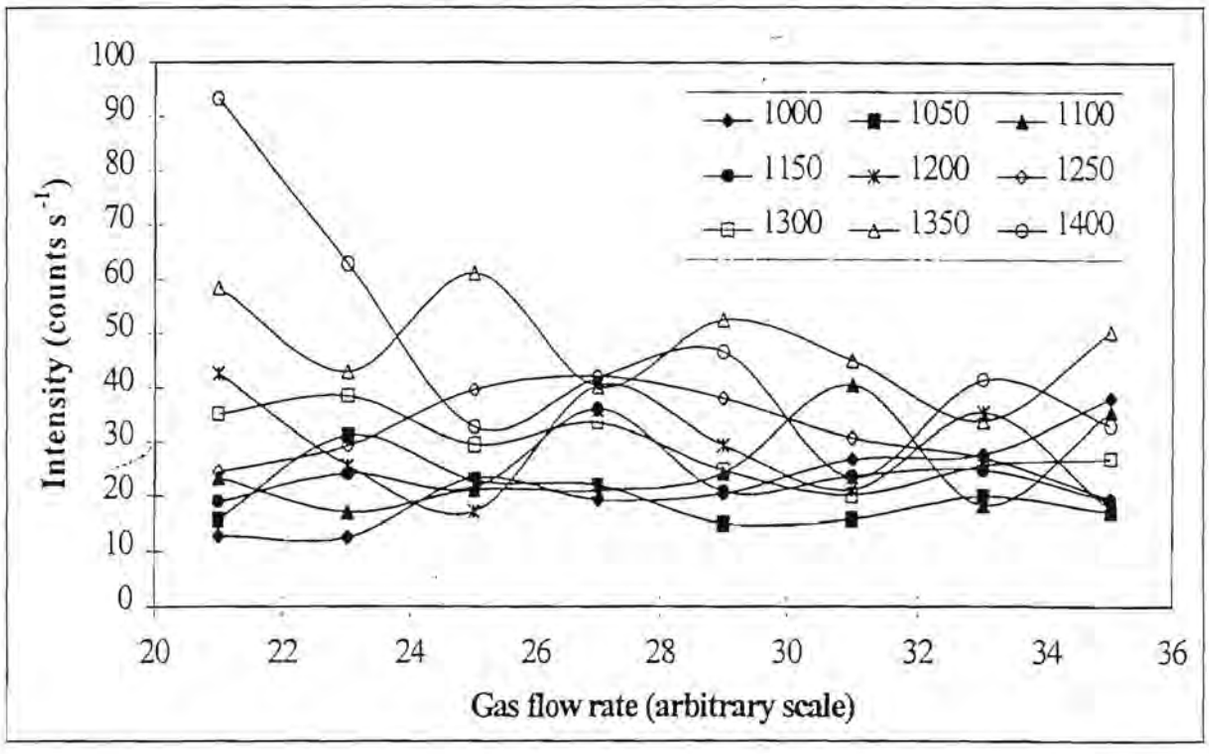

Figure 2.34: Effect of the aerosol carrier gas flow rate on background(Nb) signal at different power settings.

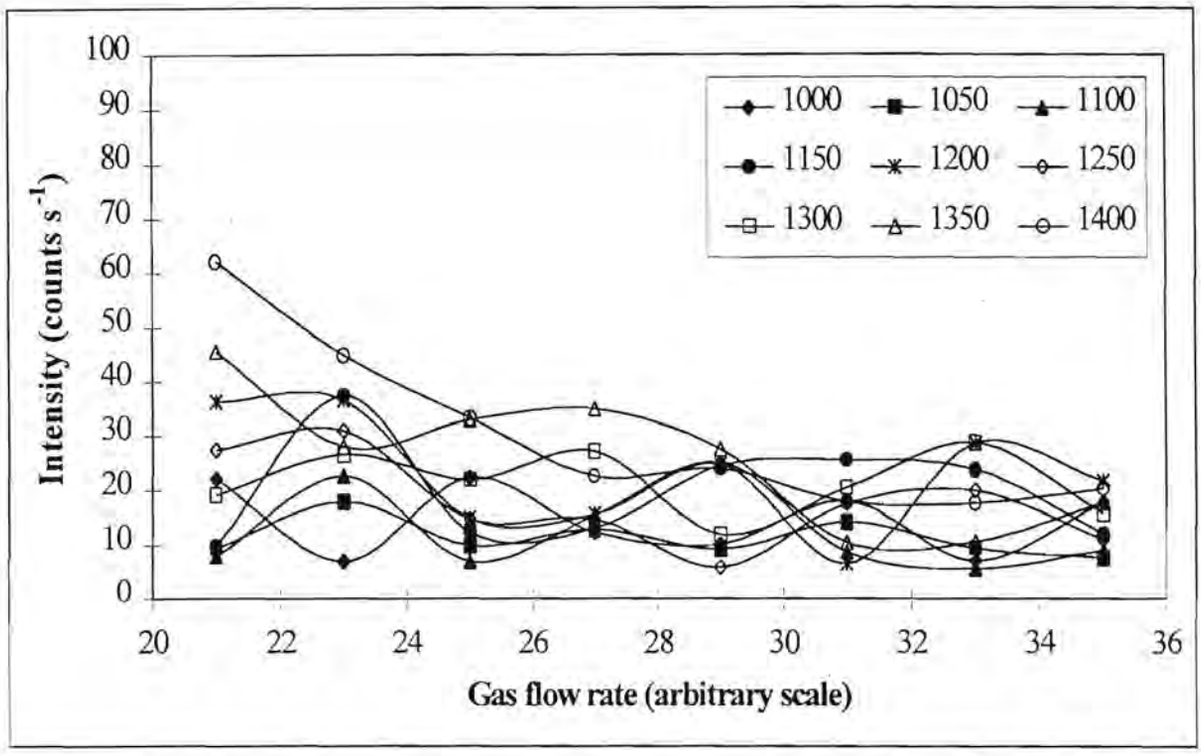

Figure 2.35: Effect of the aerosol carrier gas flow rate on background(Tc) signal at different power settings.

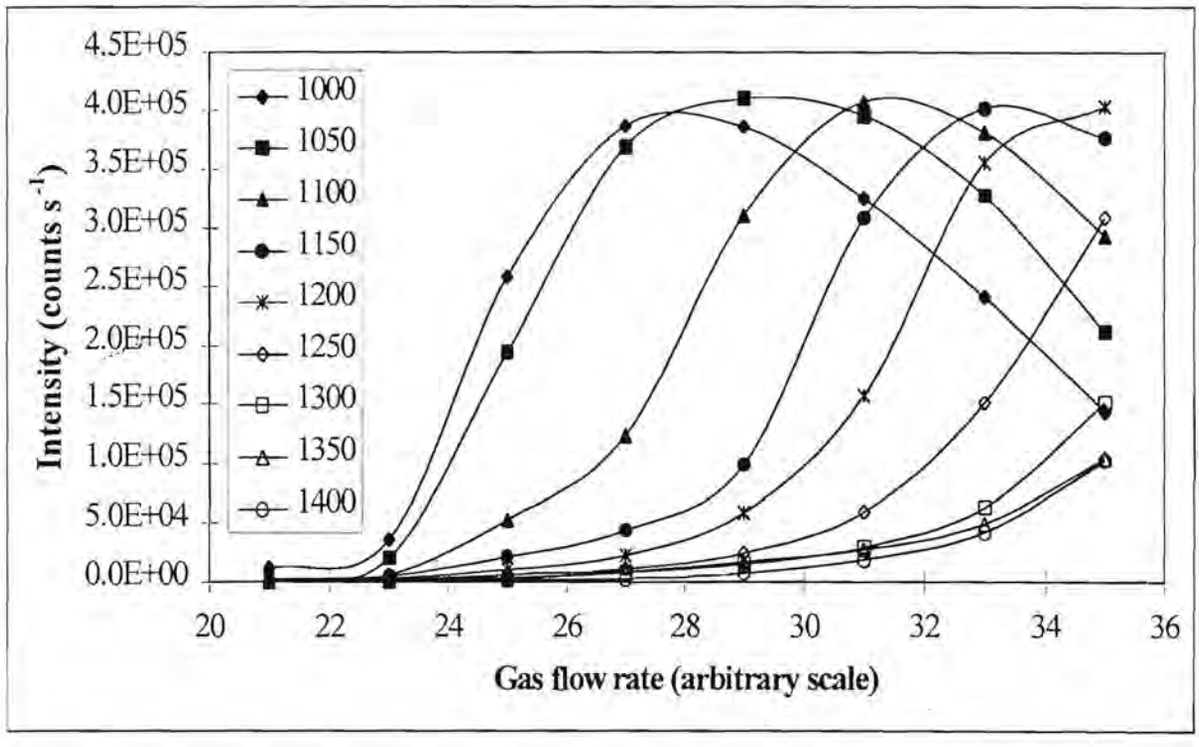

Figure 2.36: Effect of the aerosol carrier gas flow rate on the Ce^{2+} signal at different power settings.

Some workers *[33]* monitored background values at mass 130 and found a linear response with an increase in power. They found this to be more or less the same at 80 - 240 amu. They also reported a decrease in background intensity with an increase in aerosol carrier gas pressure. They stated that presumably, at high pressures the increased gas flow rate lowers the temperature in the plasma, thus increasing the number of scattered photons that are detected.

Effect of power and aerosol carrier gas flow rate on doubly ionised ions and oxides

According to Long and Brown *[33]* the three main reasons for decreases in the analyte signals as aerosol carrier gas pressure or power move away from the optimum are: 1) reduction in ion formation as a result of less efficient energy transfer from the RF load coil, via the plasma, to the analyte, 2) formation of neutrally charged species (not detected) and 3) formation of analyte oxide ions and doubly charged analyte ions. The effect of the aerosol carrier gas flow at various power settings on Ce^{2+} and CeO^{+} can be seen in figures 2.36 and 2.37. For Ce^{2+} signal maxima of approximately the same value can be seen for all power settings 1000 W to 1200 W. CeO^{+} curves show more or less the same trends as for the light and heavier elements.

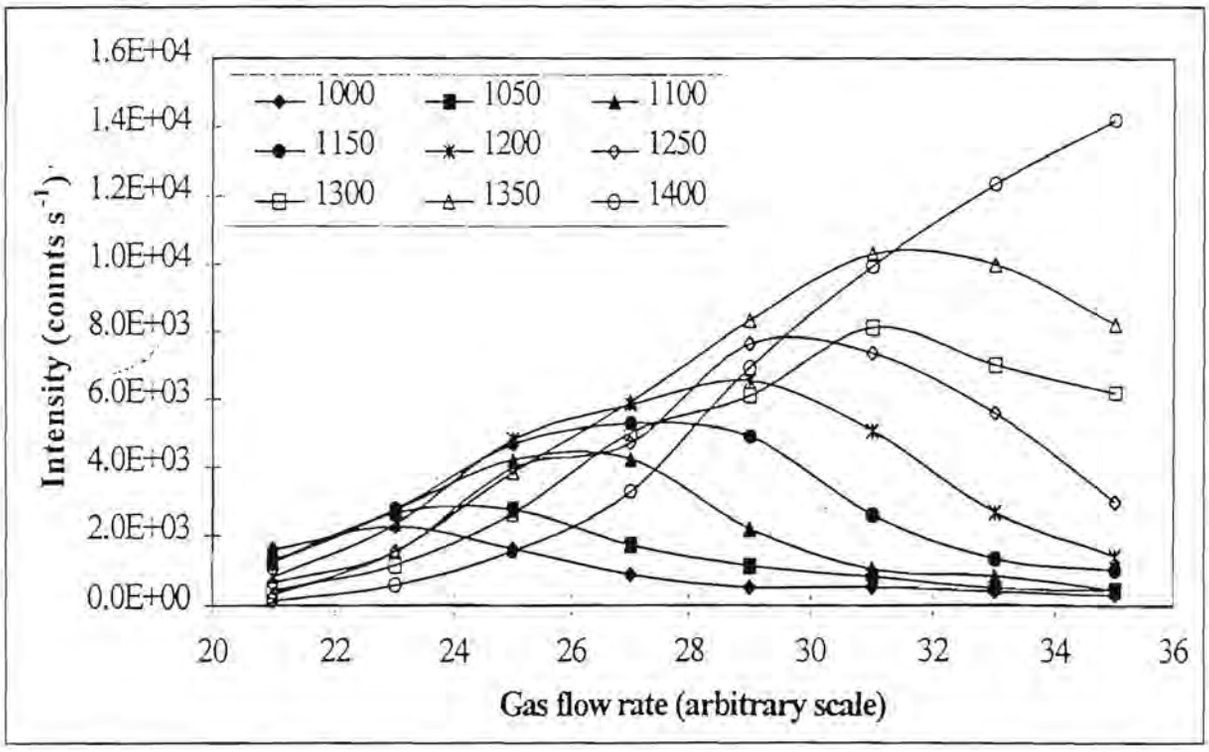

Figure 2.37: Effect of the aerosol carrier gas flow rate on the CeO^{+} signal at different power settings.

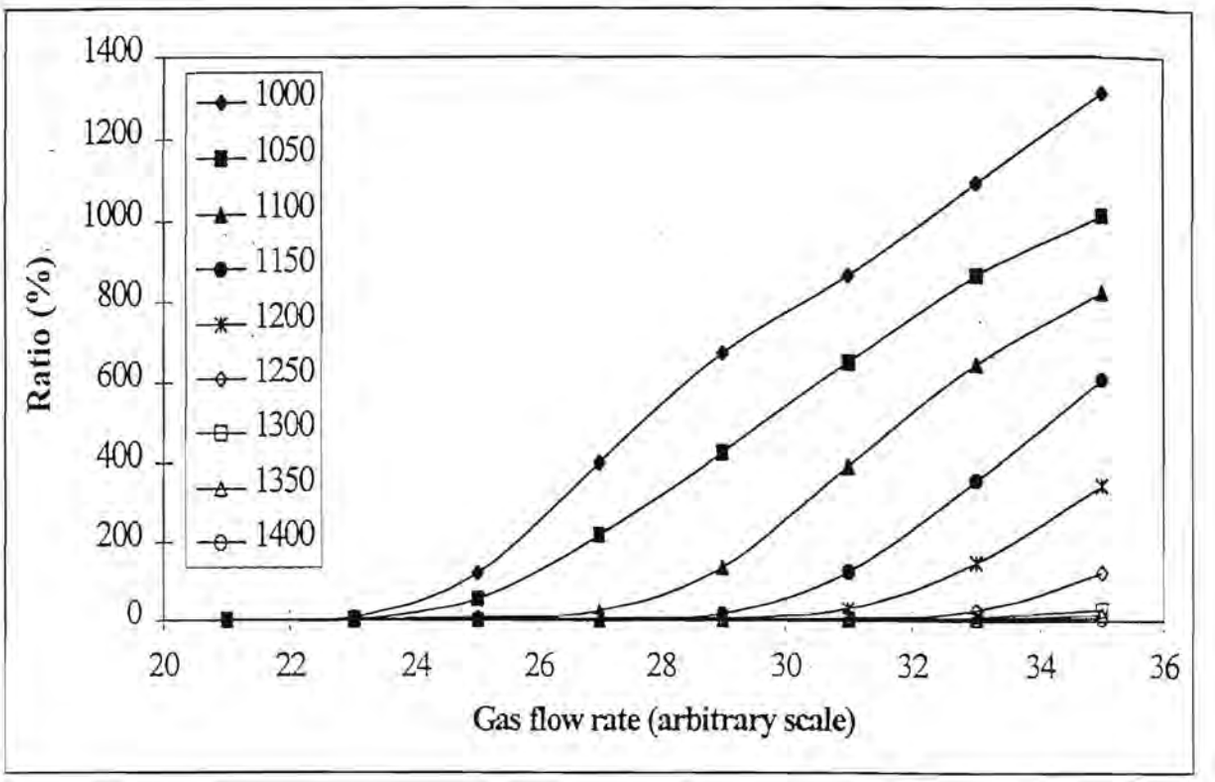

Figure 2.38(a): Effect of the aerosol carrier gas flow rate on the Ce^{2+}/Ce^{+} ratio at different power settings.

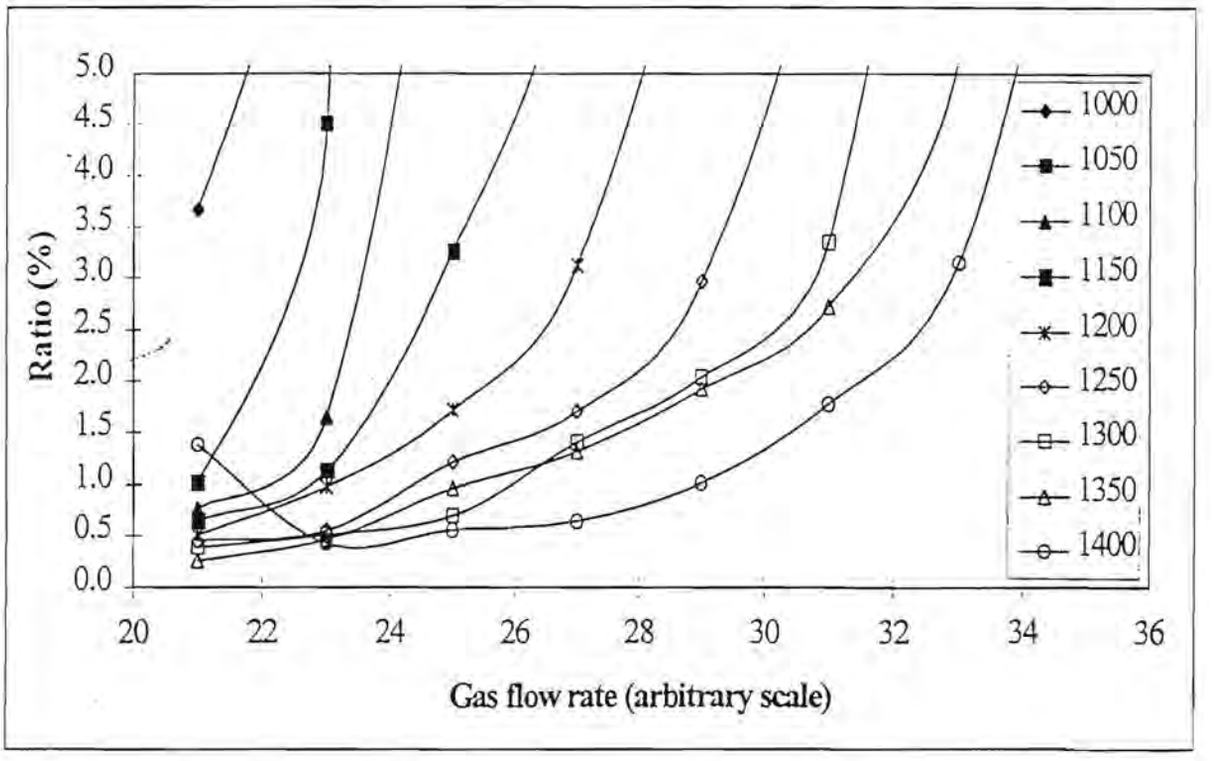

Figure 2.38(b): Effect of the aerosol carrier gas flow rate on the Ce^{2+}/Ce^{+} ratio at different power settings. (Only the 0 - 5% range is showed.)

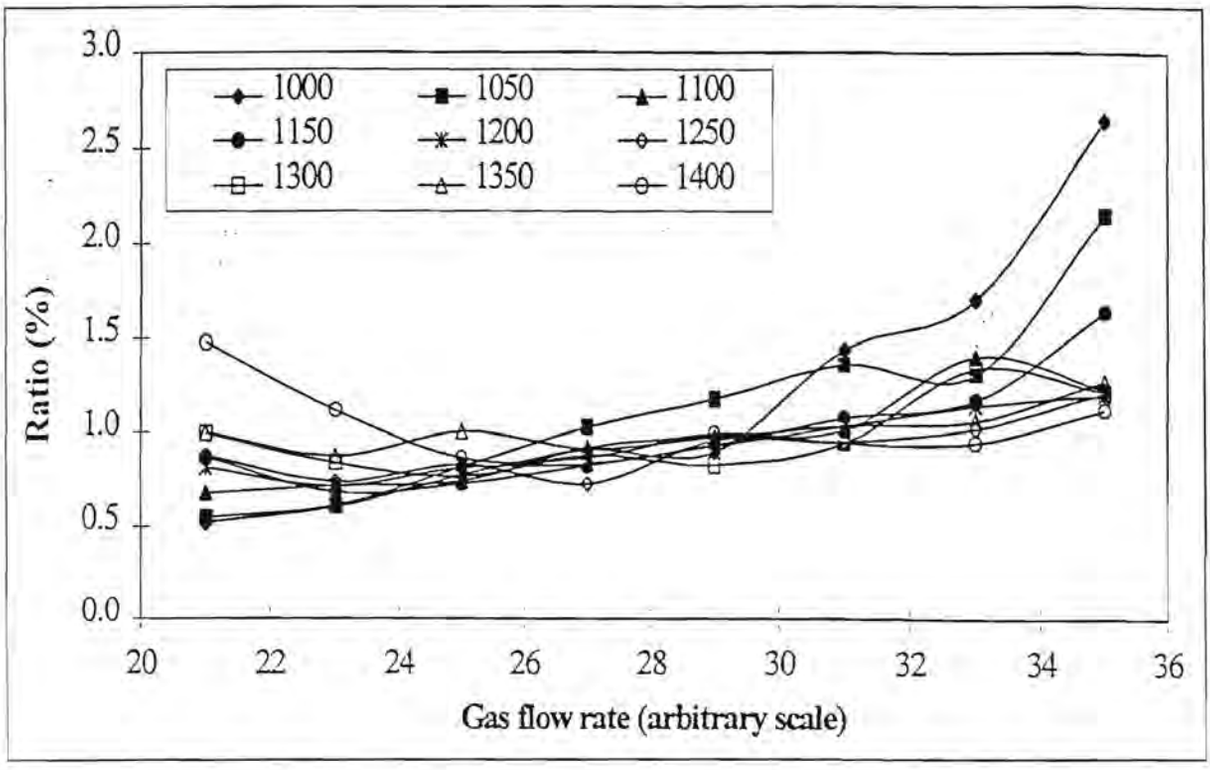

Figure 2.39: Effect of the aerosol carrier gas flow rate on the CeO^+/Ce^+ ratio at different power settings.

Figures 2.38(a), 2.38(b) and 2.39 give the trends followed by the Ce^{2+}/Ce^+ and CeO^+/Ce^+ ratios when the aerosol carrier gas flow rate is varied. Figure 2.38(b) shows that these parameters are critical in minimising the doubly ionised interferences. Table 2.3 gives the maximum flow rates that may be employed in order to maintain the Ce^{2+}/Ce^+ and CeO^+/Ce^+ ratios below the acceptable values of 2.5% and 1%.

These ratios are extremely sensitive to changes in the flow rate and great care must be taken in not choosing too high flow rates. For a power setting of 1350 W the maximum allowable flow rate seems to be 29 which is lower than the value of 31 for the analyte signals. Relative to these ratios the changes caused in the analyte signals by reducing the flow rate to 29 are small. Generally, the optimal flow rates for the analyte signals would not cause the CeO^+/Ce^+ ratio to increase above 1%, but lower flow rates have to be employed in order to minimise the Ce^{2+}/Ce^+ ratio. Long and Brown *[33]* reported M^+/MO^+ and M^+/M^{2+} ratios for Cs, Sm, Ba, Pb with variations in aerosol carrier gas pressure or power. They reported optimum aerosol carrier gas pressures with $M^+/MO^+ >$ 300 and $M^+/M^{2+} > 100$. They also concluded that lower pressures are preferable. Other researchers *[31]* obtained CeO^+/Ce^+ and Ce^{2+}/Ce^+ ratios of both lower than

3%. Similar to the results reported here, they found the CeO^+/Ce^+ ratio to increase slightly with increases in the aerosol carrier gas flow rate and decrease slightly with increases in the power settings. They also found the Ce^{2+}/Ce^+ ratio to increase with an increase in the aerosol carrier gas flow rate and decrease with an increase in power. Horlick *et al. [29]* stated that in order to minimise the CeO^+/Ce^+ ratio one has to lower the aerosol carrier gas pressure to a value lower than that providing maximum analyte counts. Gray and Williams *[34]* reported values of about 1% for the CeO^+/Ce^+ ratio.

Table 2.3: Maximum aerosol carrier gas flow rates ("arbitrary scale" as used by instrument manufacturer) at which acceptable values for Ce^{2+}/Ce^+ (2.5%) and CeO^+/Ce^+ (1%) ratios are still obtained for the power settings investigated.

Power setting	Ce^{2+}/Ce^+	CeO^+/Ce^+
1000 W	-	29
1050 W	21	25
1100 W	23	29
1150 W	23	29
1200 W	25	29
1250 W	27	31
1300 W	29	31
1350 W	29	29
1400 W	31	33

2.3.4 *Effect of ion lens settings*

Effect of ion lens settings on light elements

Figures 2.40(a) - (h) show the effects of various ion lens settings such as: lens parameters, field axis voltage and detector inner and outer diameter voltages on the response curves of the light elements. All the light elements appear to reach maximum values at more or less the same ion lens settings. The settings to which the analyte intensities are the most sensitive are: LA, LB, LC, ID and OD.

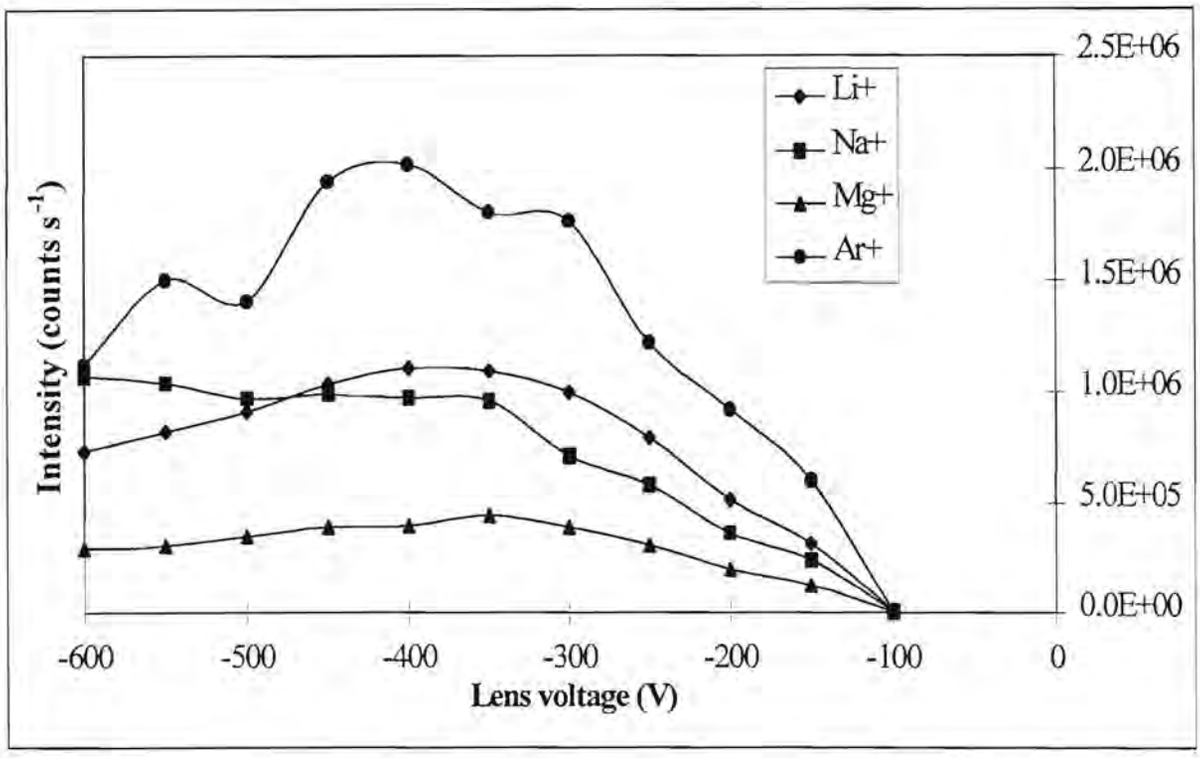

Figure 2.40(a): Effect of the lens parameter LO on the response curves of the light elements and argon.

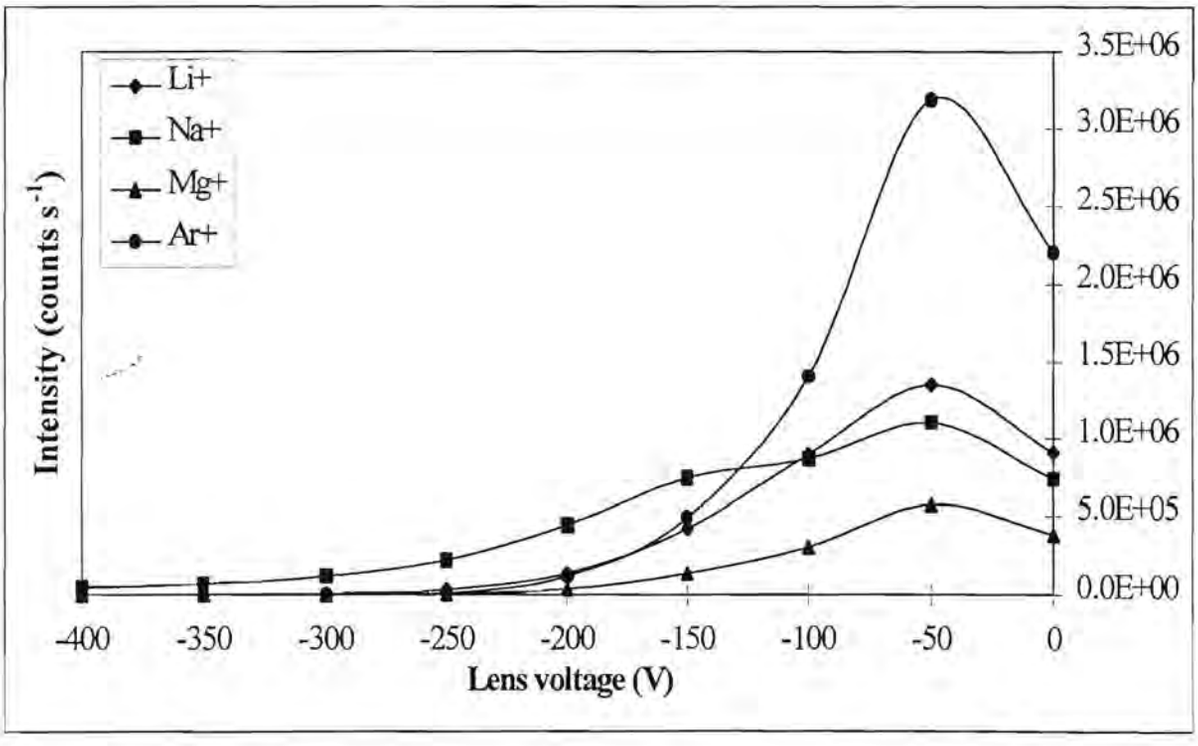

Figure 2.40(b): Effect of the lens parameter LA on the response curves of the light elements and argon.

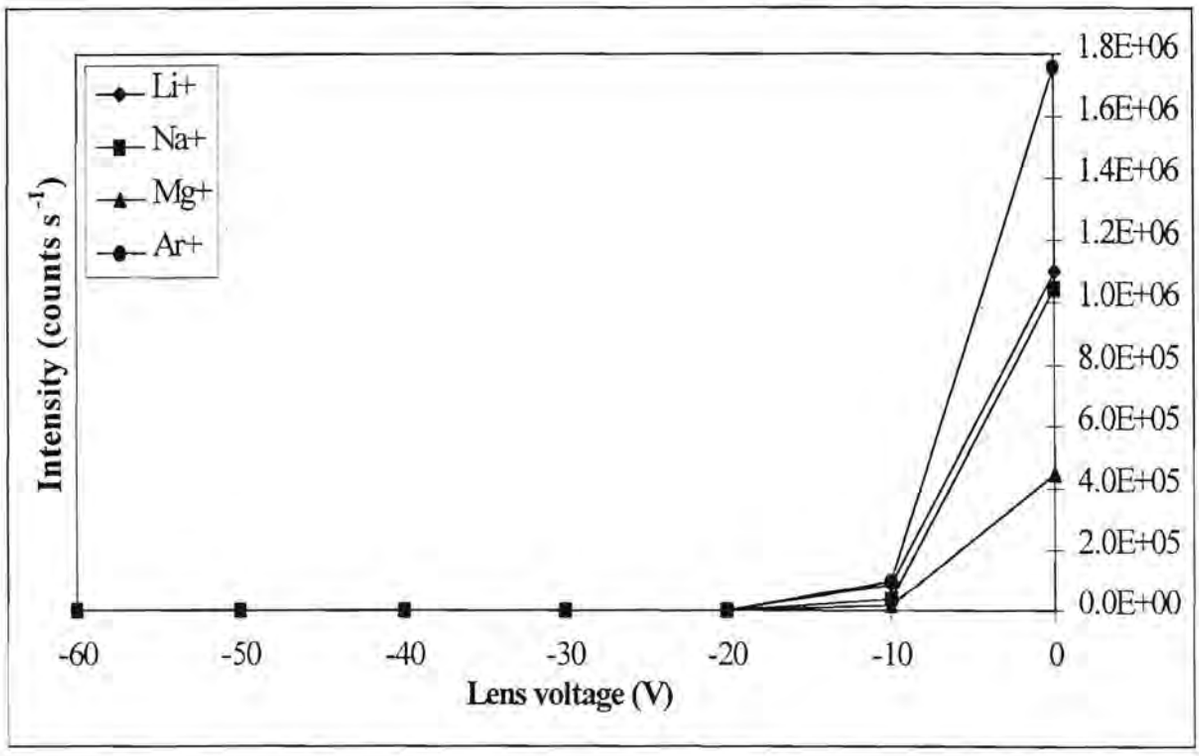

Figure 2.40(c): Effect of the lens parameter LB on the response curves of the light elements and argon.

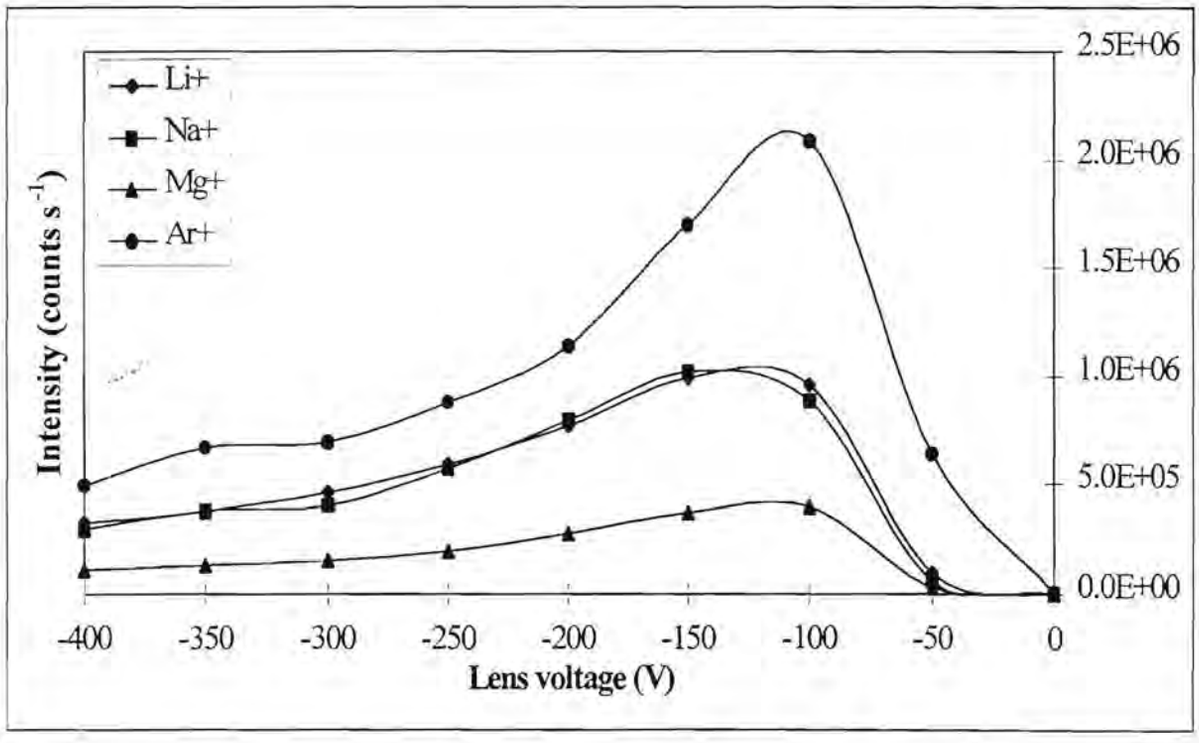

Figure 2.40(d): Effect of the lens parameter LC on the response curves of the light elements and argon.

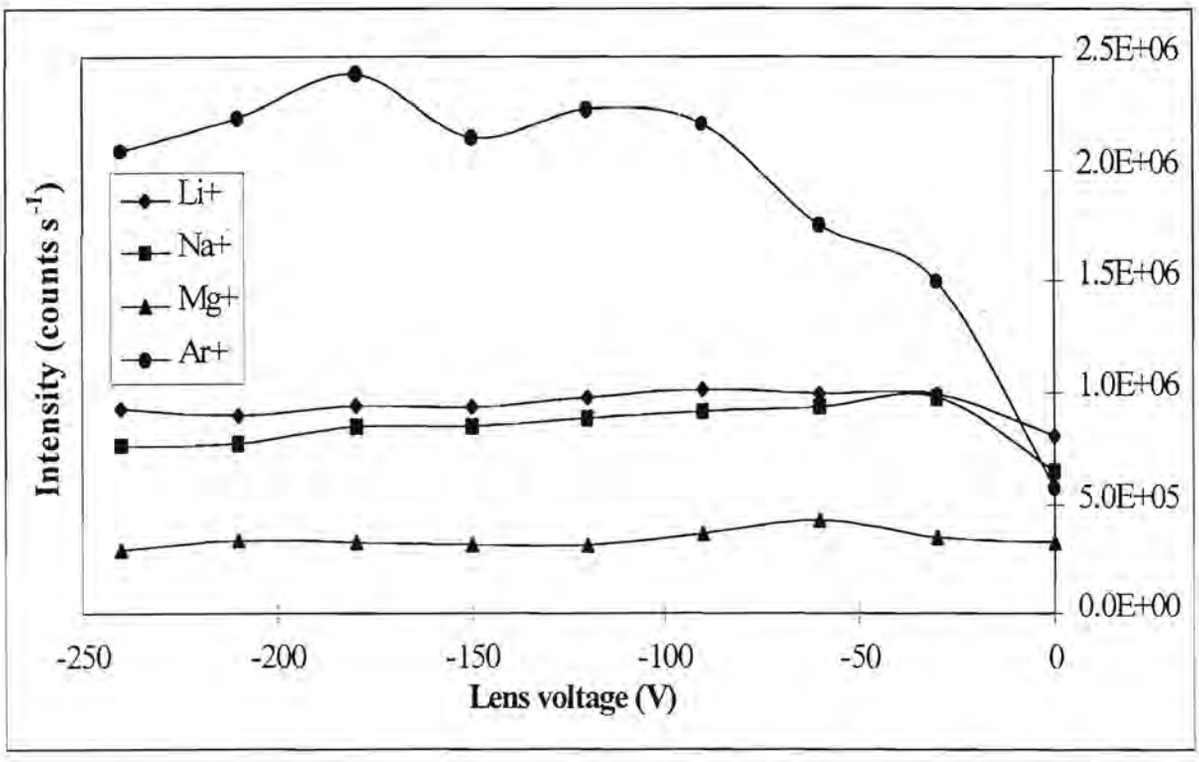

Figure 2.40(e): Effect of the lens parameter LD on the response curves of the light elements and argon.

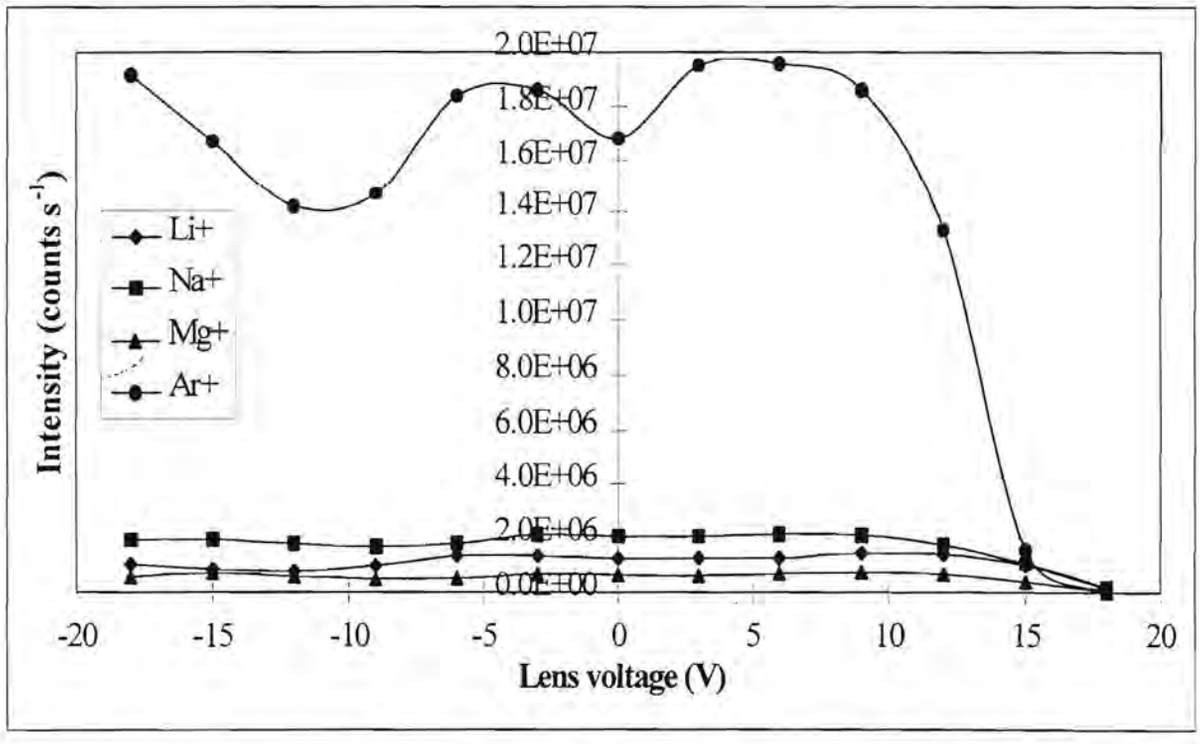

Figure 2.40(f): Effect of the field axis voltage FA on the response curves of the light elements and argon.

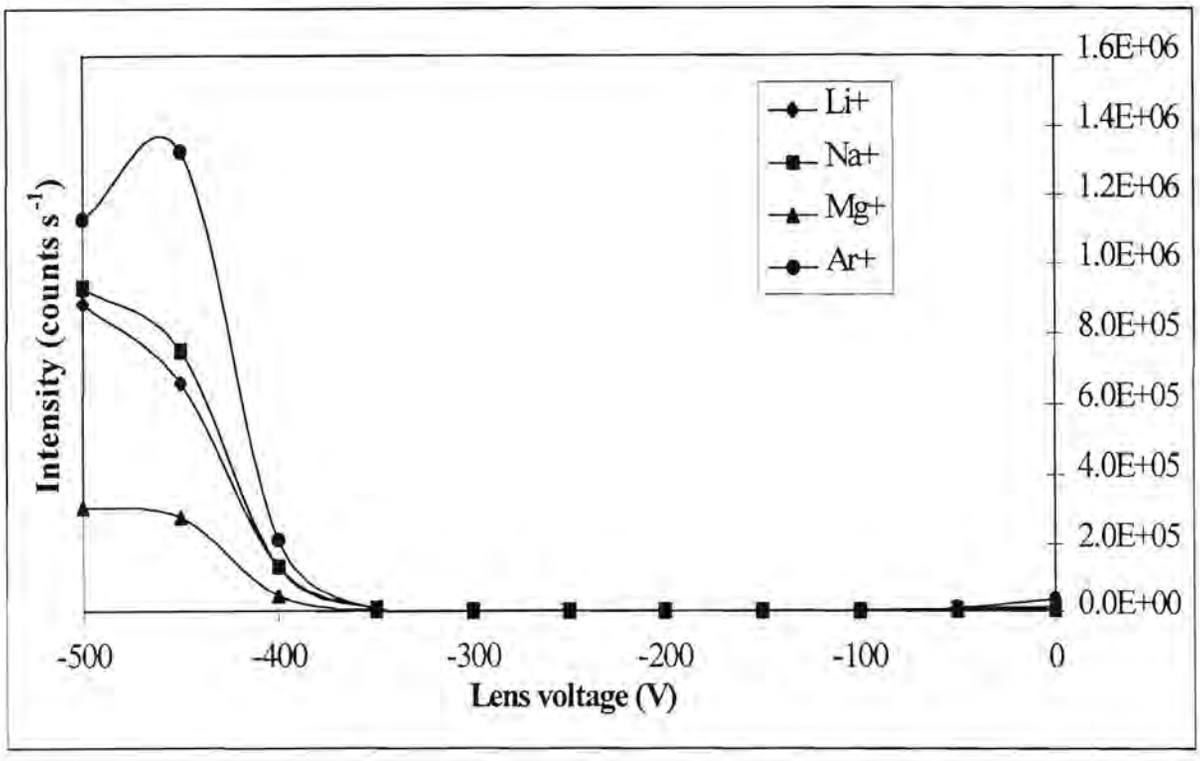

Figure 2.40(g): Effect of the detector inner diameter voltage ID on the response curves of the light elements and argon.

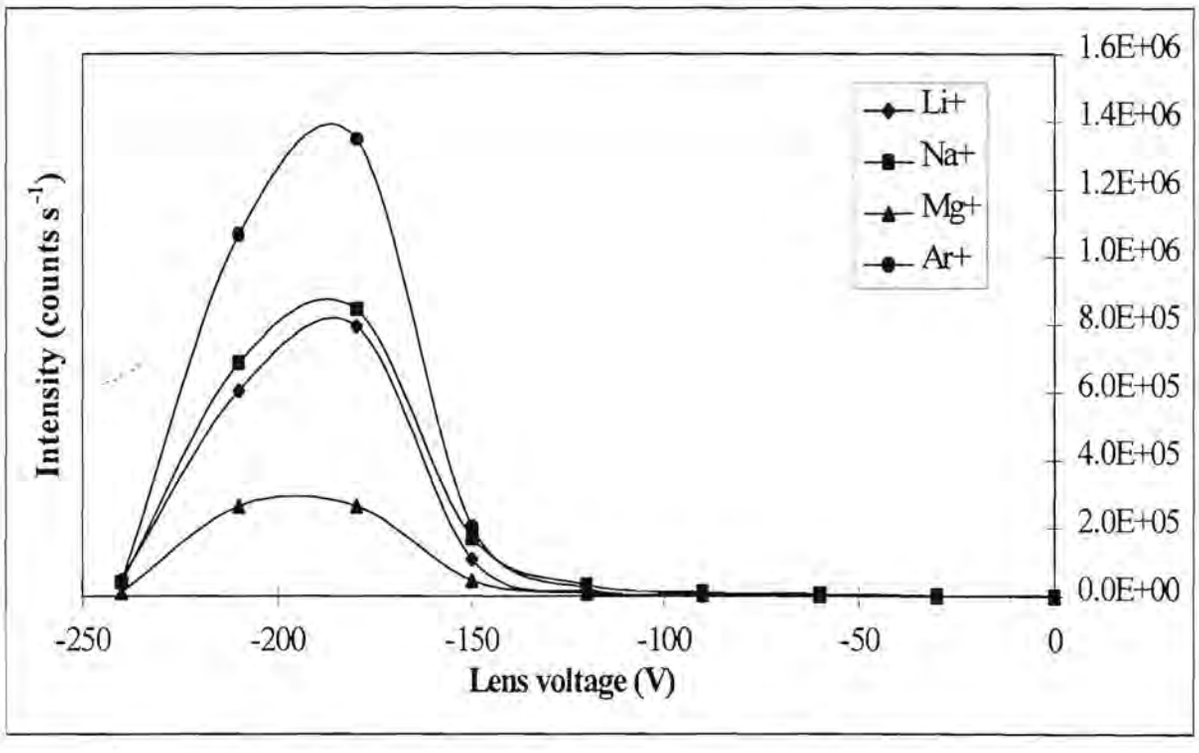

Figure 2.40(h): Effect of the detector outer diameter voltage OD on the response curves of the light elements and argon.

Effect of ion lens settings on heavier elements

From figures 2.41(a) - (h) it can be seen that the curves for the heavier elements show maxima at approximately the same ion lens settings than for the light elements. In some cases slightly more negative voltages are preferred. i.e. for the LO, LC and LD parameters.

Effect of ion lens settings on background intensities

Figures 2.42(a) - (h) show that none of the preferred ion lens settings for the light and heavier elements would cause the background signals to increase to values higher than 100 counts s^{-1}.

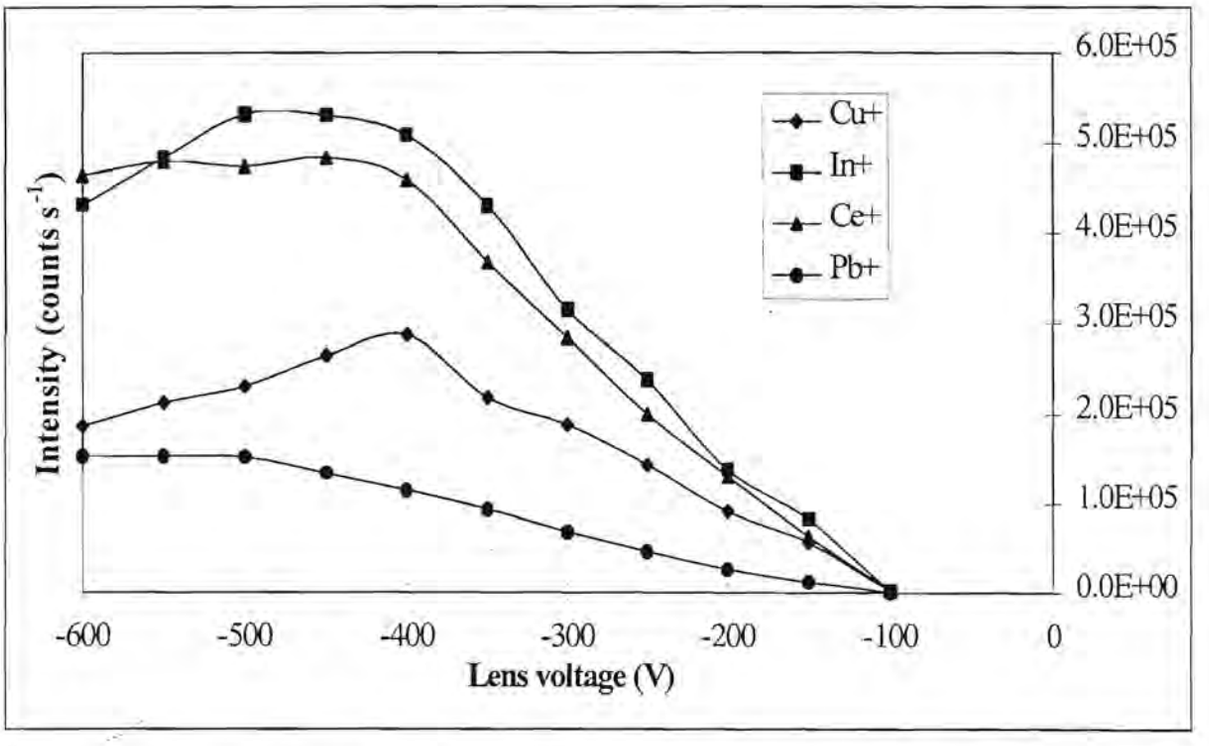

Figure 2.41(a): Effect of the lens parameter LO on the response curves of the heavier elements.

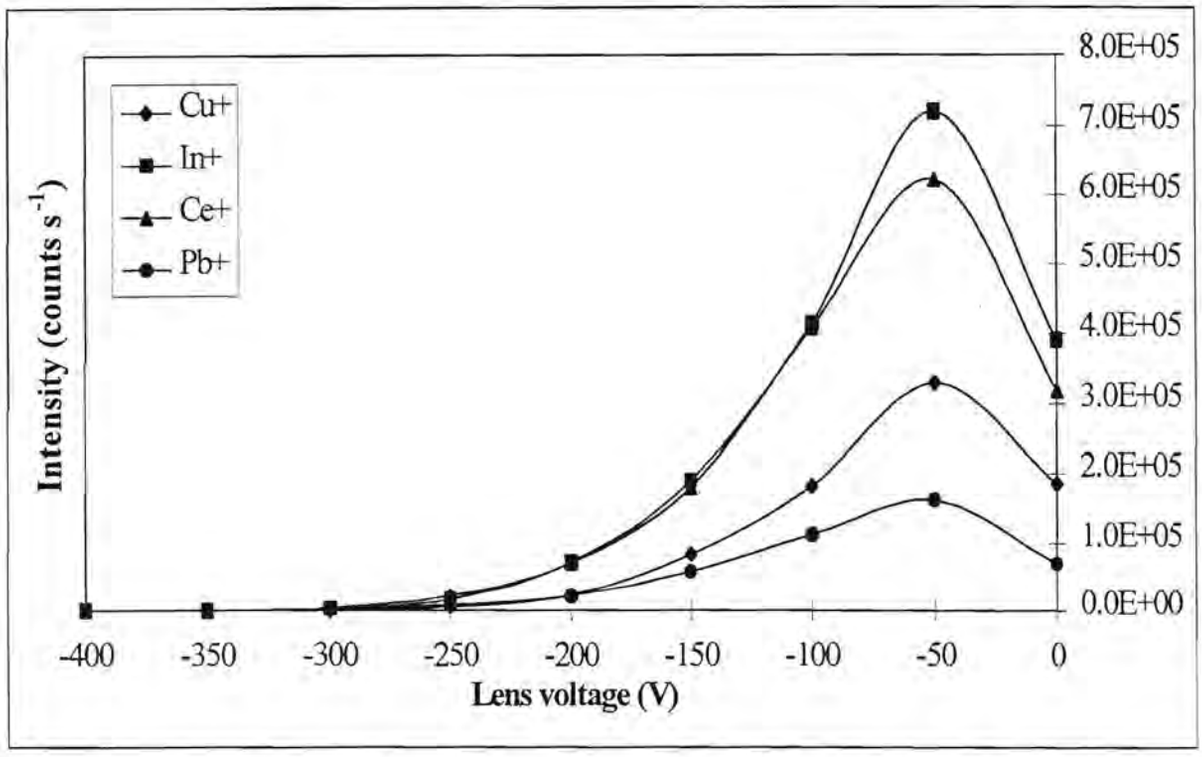

Figure 2.41(b): Effect of the lens parameter LA on the response curves of the heavier elements.

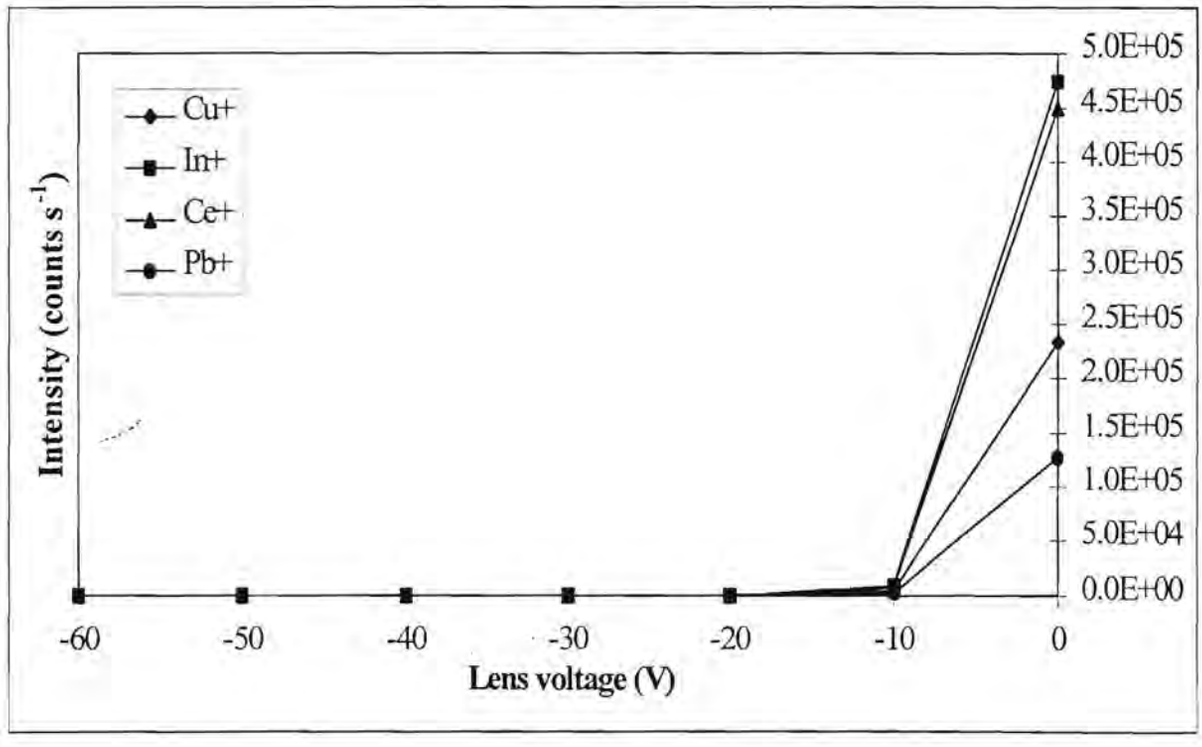

Figure 2.41(c): Effect of the lens parameter LB on the response curves of the heavier elements.

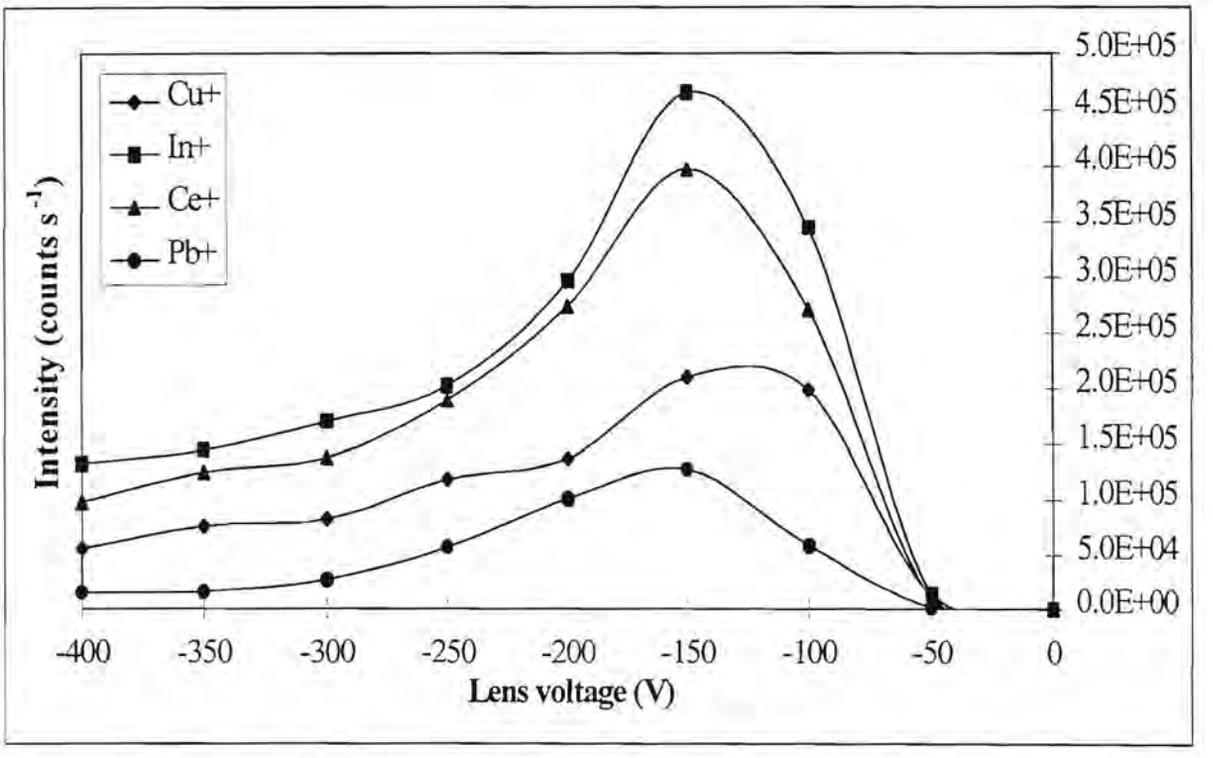

Figure 2.41(d): Effect of the lens parameter LC on the response curves of the heavier elements.

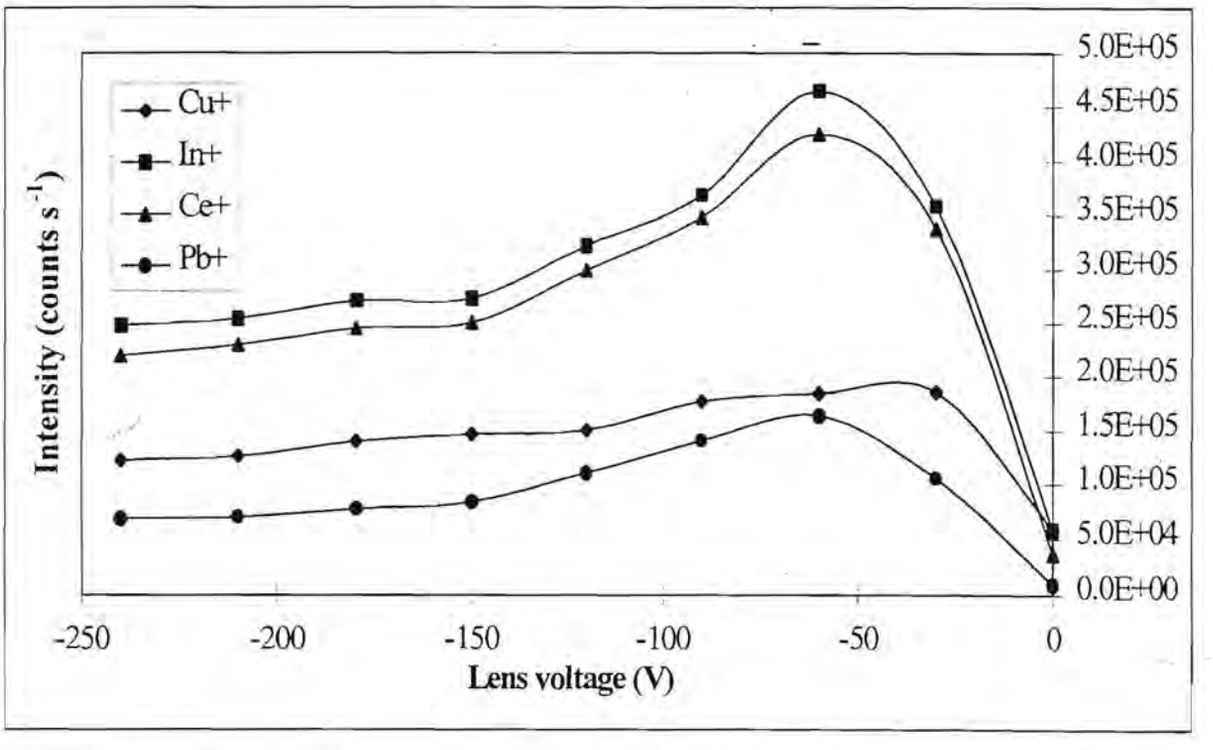

Figure 2.41(e): Effect of the lens parameter LD on the response curves of the heavier elements.

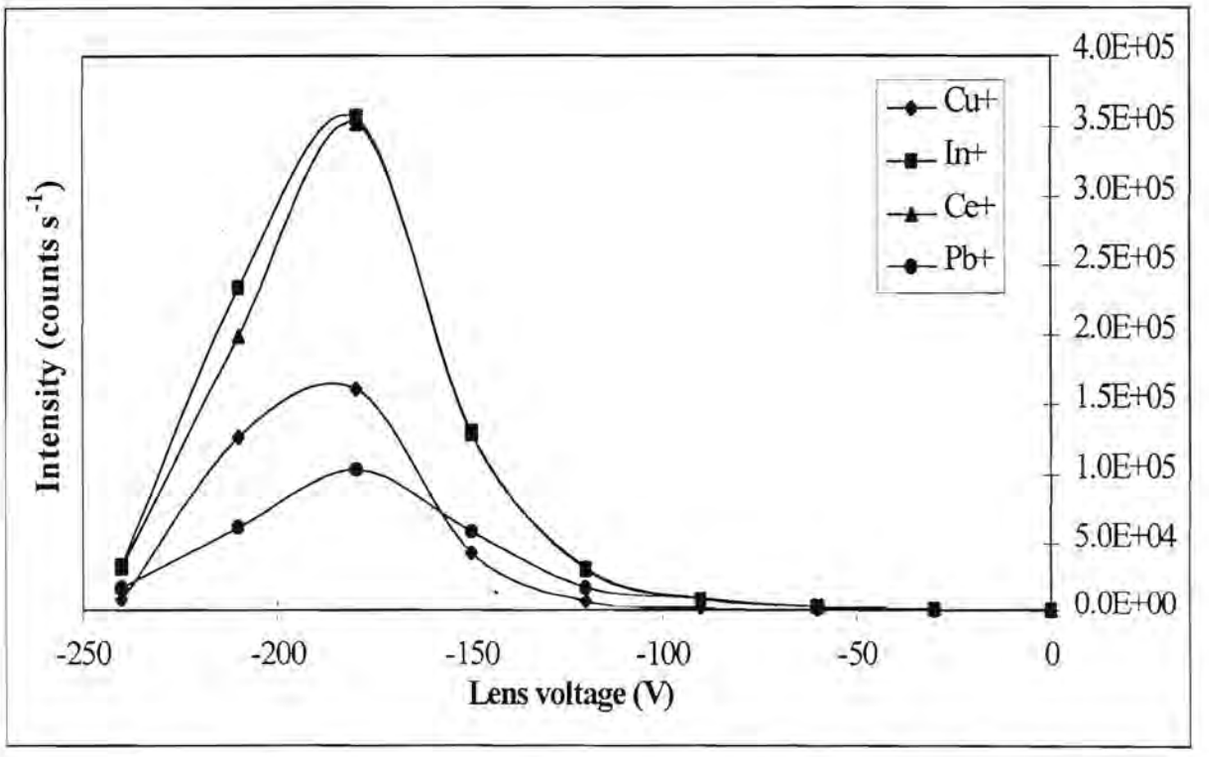

Figure 2.41(h): Effect of the detector outer diameter voltage OD on the response curves of the heavier elements.

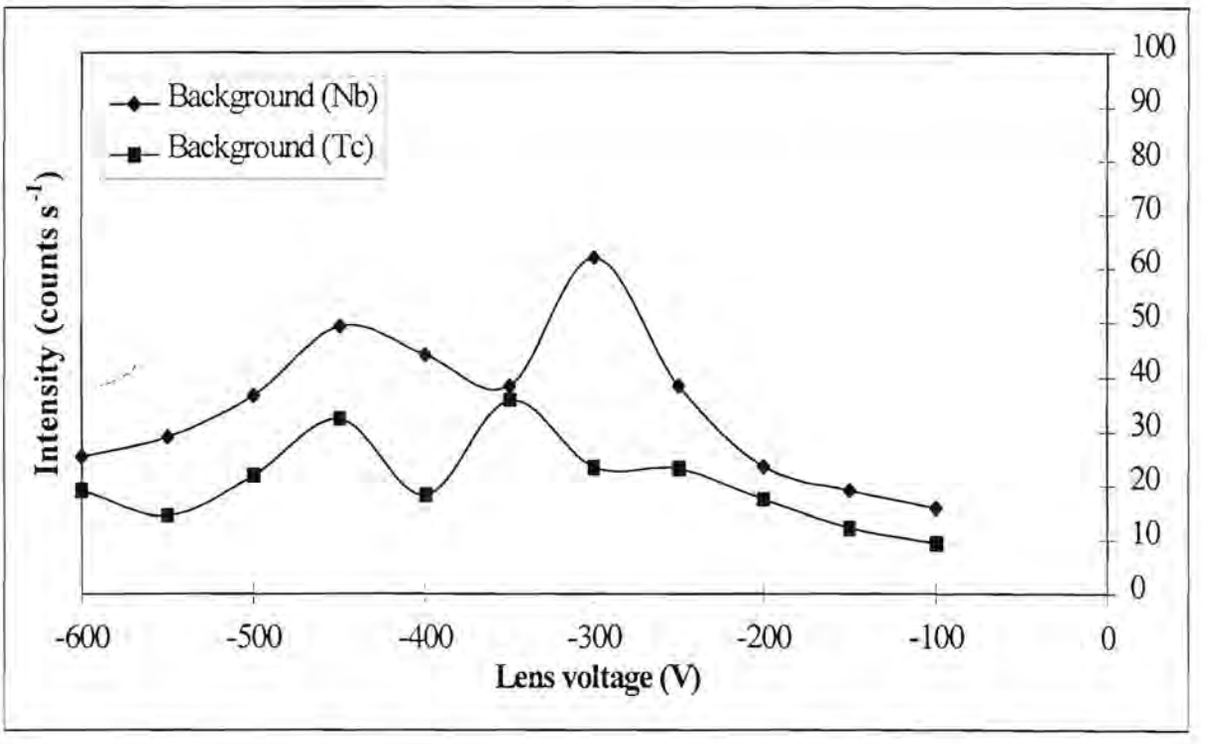

Figure 2.42(a): Effect of the lens parameter LO on the background intensities.

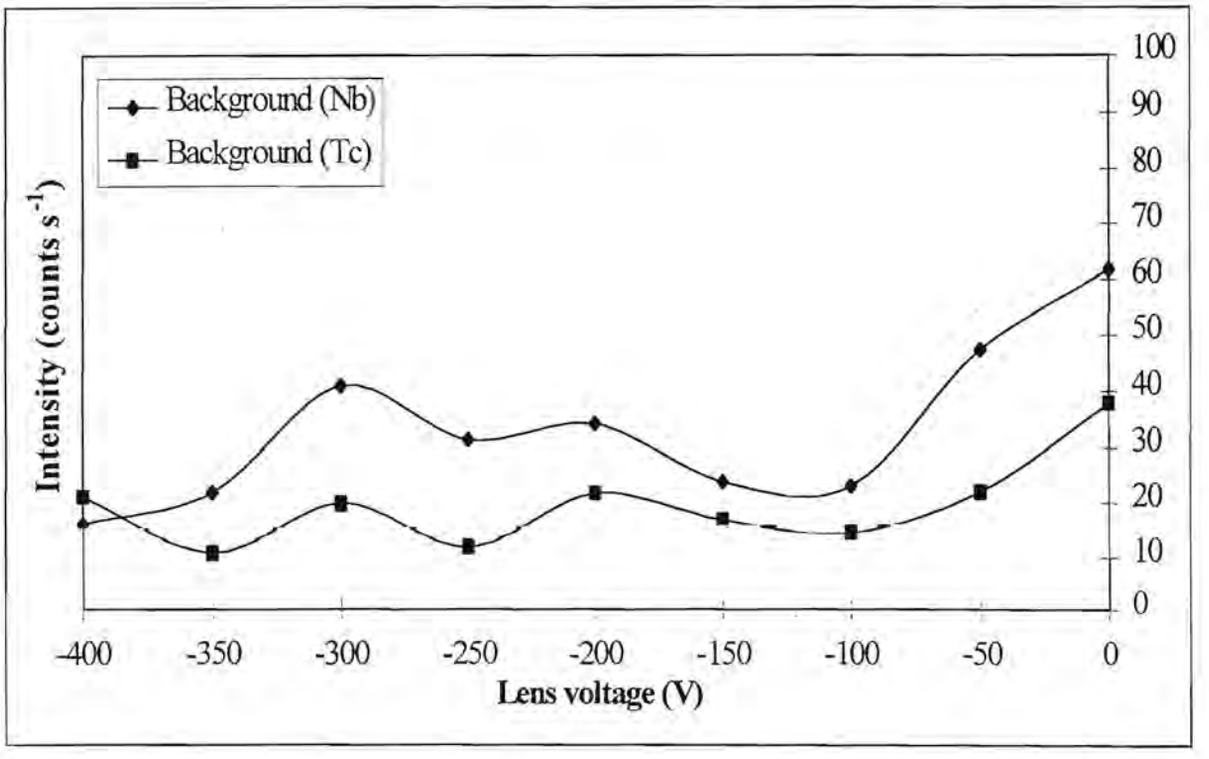

Figure 2.42(b): Effect of the lens parameter LA on the background intensities.

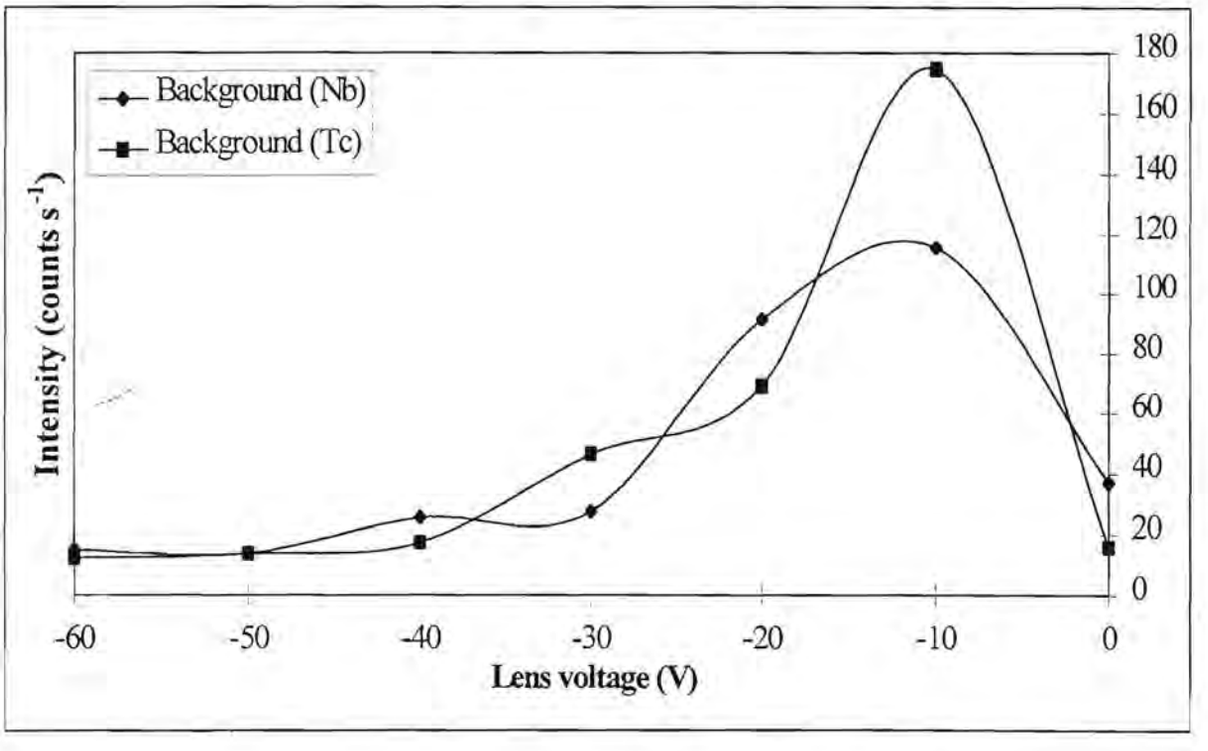

Figure 2.42(c): Effect of the lens parameter LB on the background.

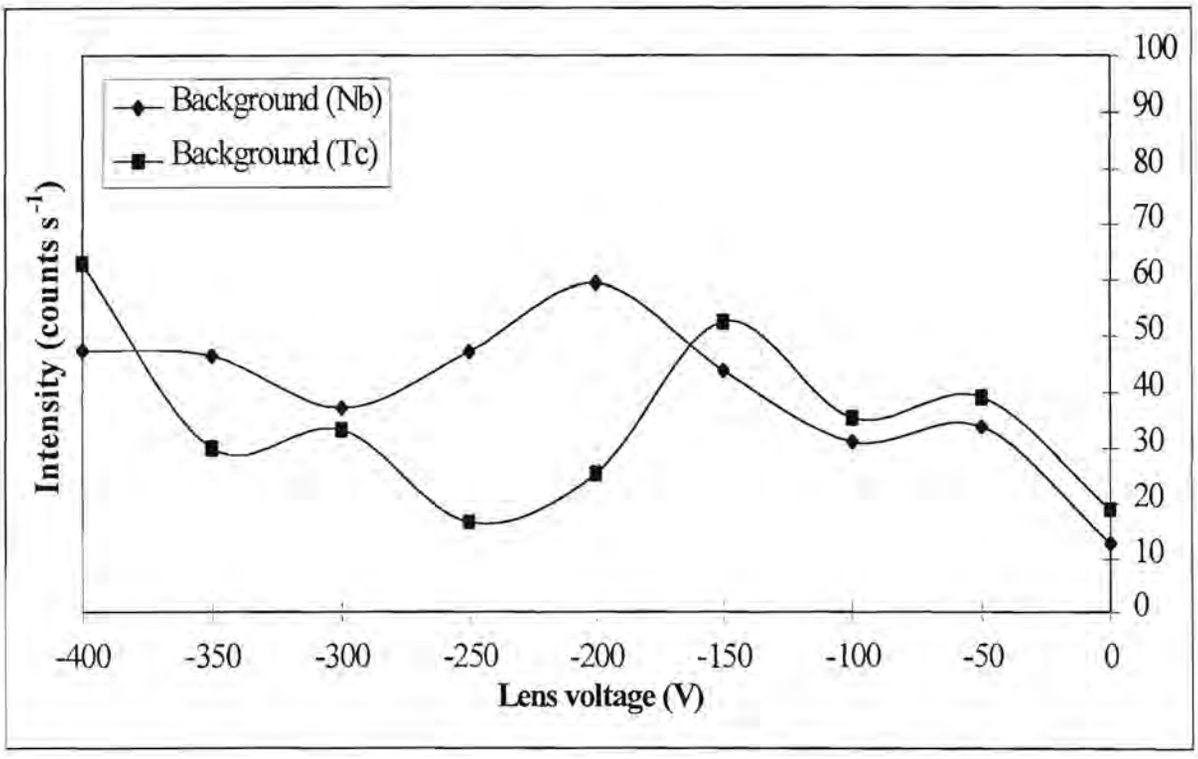

Figure 2.42(d): Effect of the lens parameter LC on the background intensities.

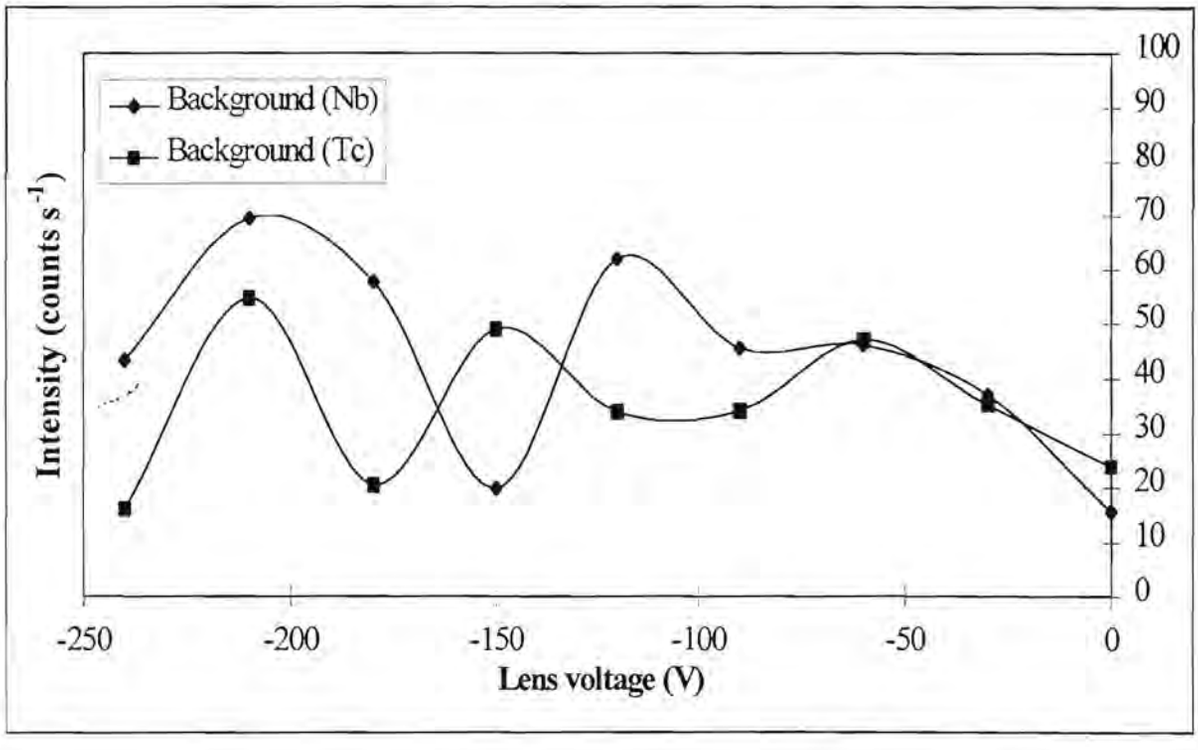

Figure 2.42(e): Effect of the lens parameter LD on the background intensities.

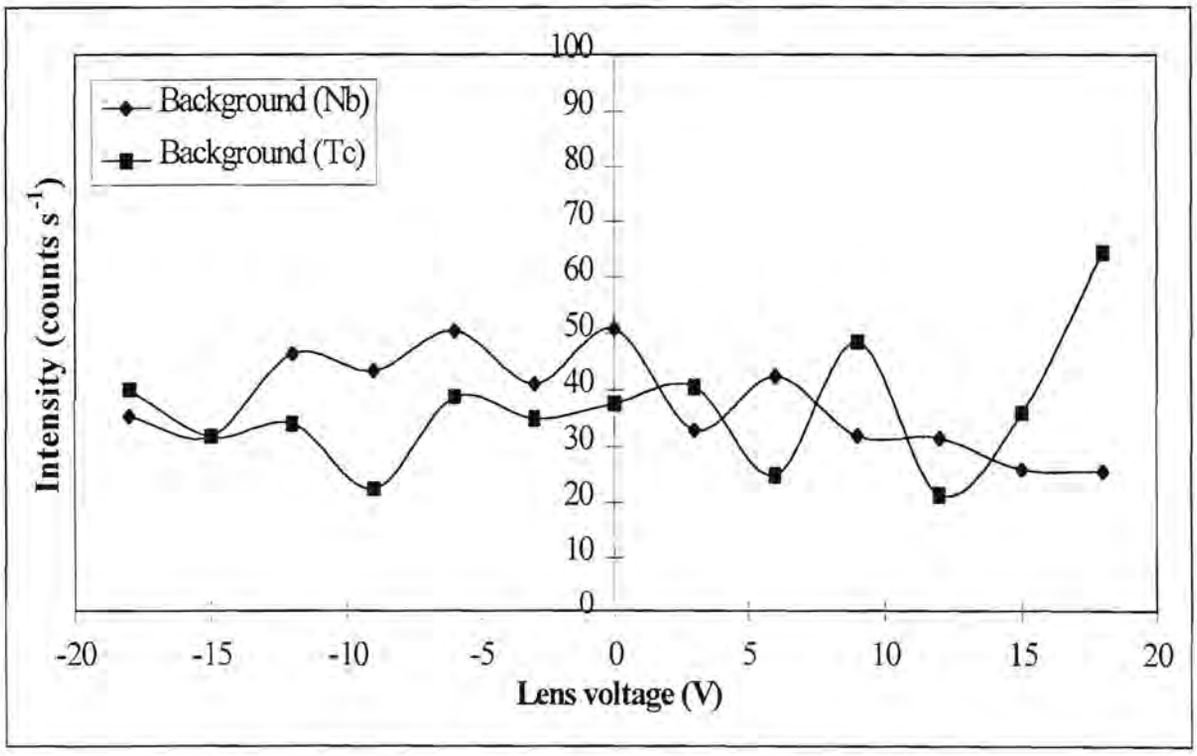

Figure 2.42(f): Effect of the field axis voltage FA on the background intensities.

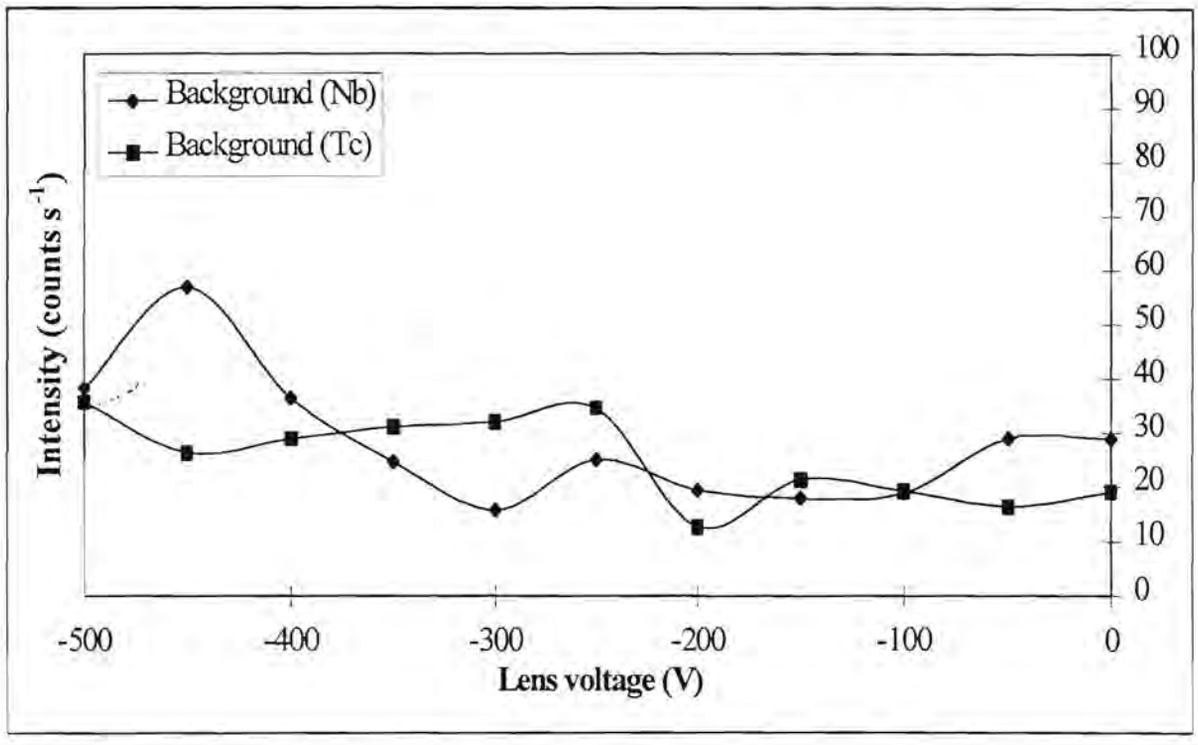

Figure 2.42(g): Effect of the detector inner diameter voltage ID on the background intensities.

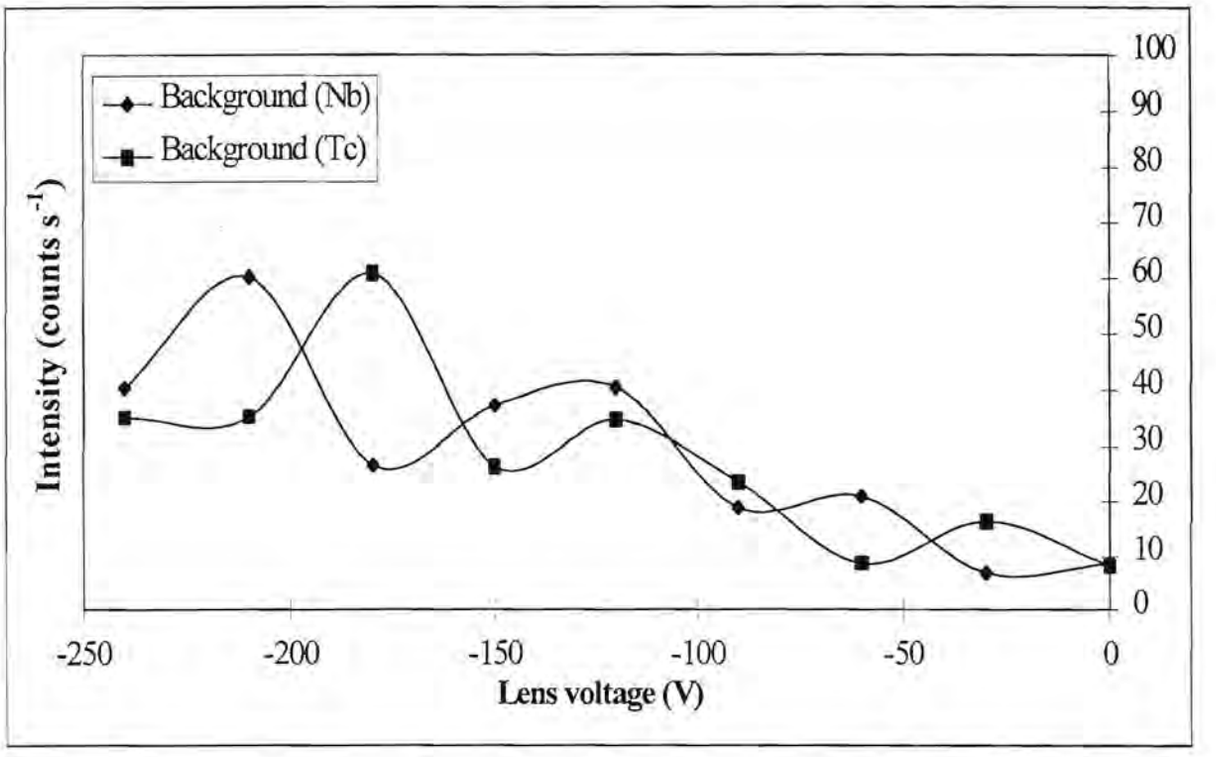

Figure 2.42(h): Effect of the detector outer diameter voltage OD on the background intensities.

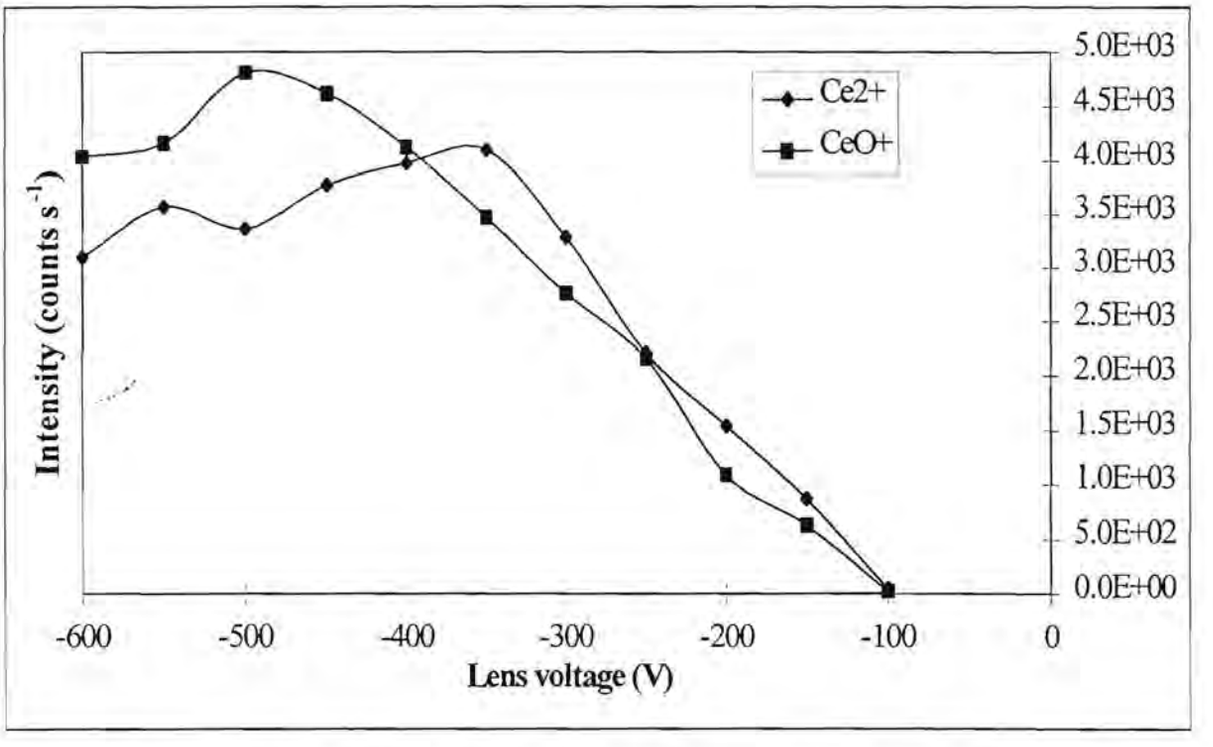

Figure 2.43(a): Effect of the lens parameter LO on the response curves of the doubly ionised and oxide ions.

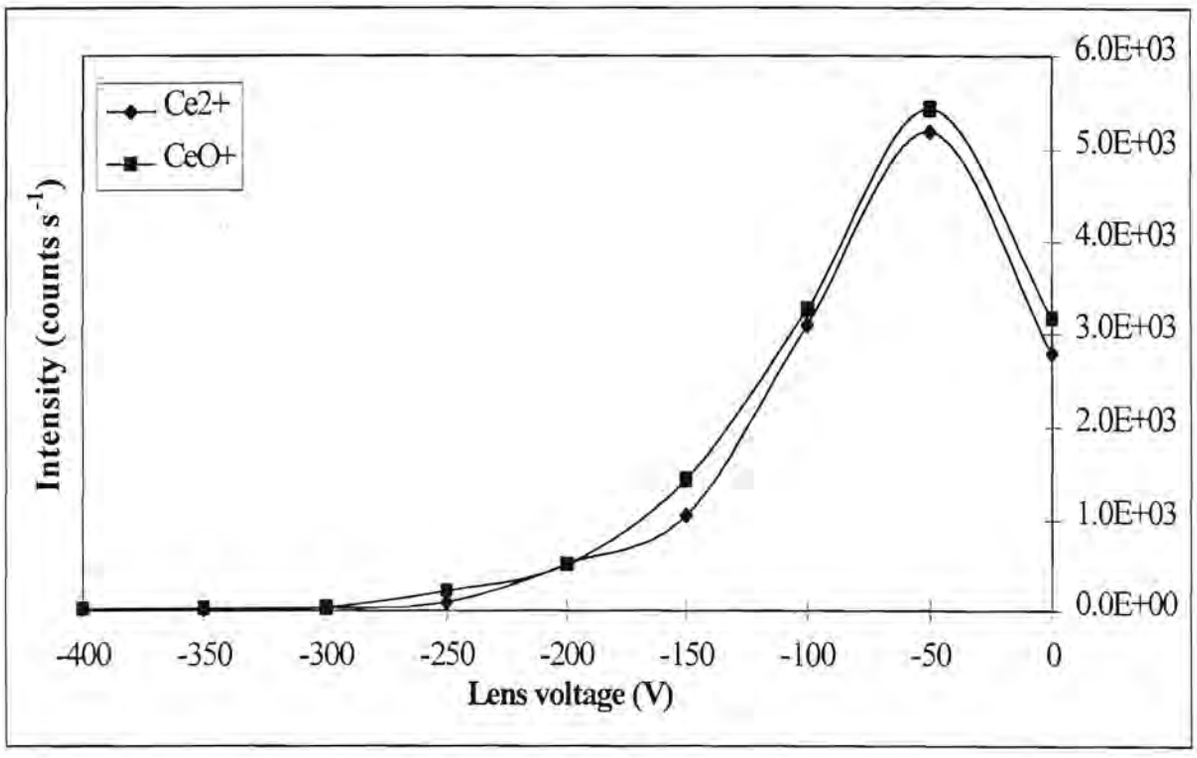

Figure 2.43(b): Effect of the lens parameter LA on the response curves of the doubly ionised and oxide ions.

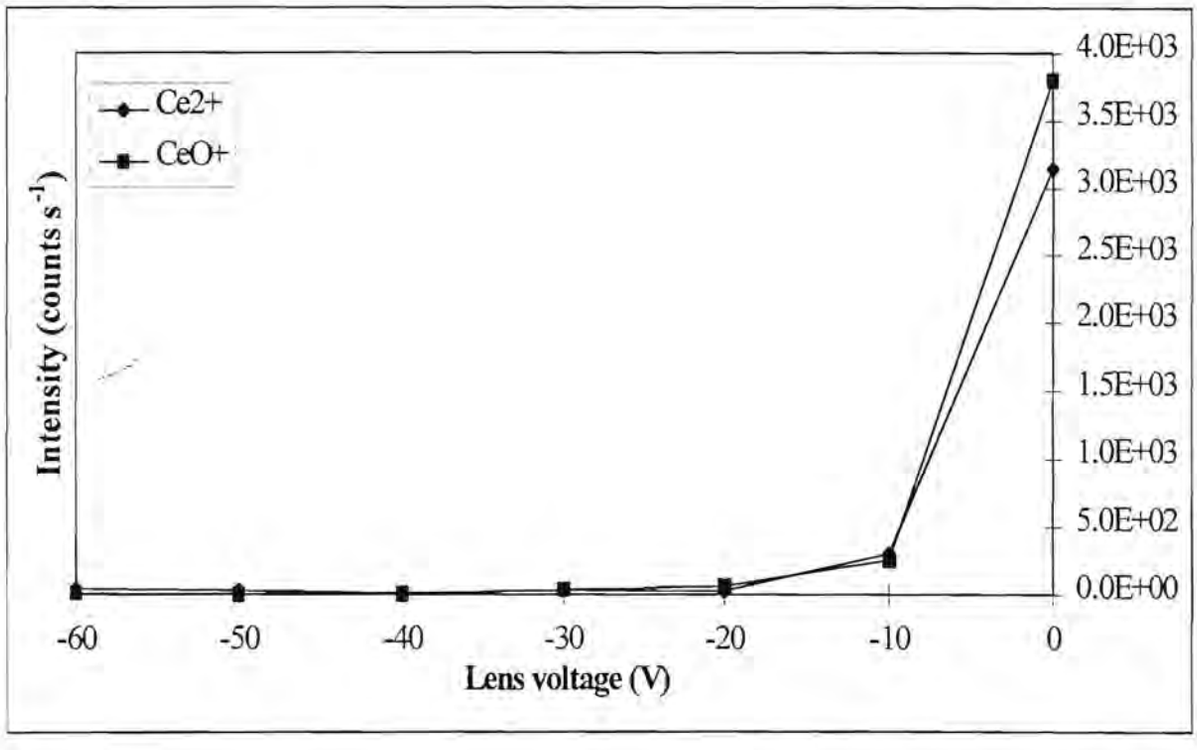

Figure 2.43(c): Effect of the lens parameter LB on the response curves of the doubly ionised and oxide ions.

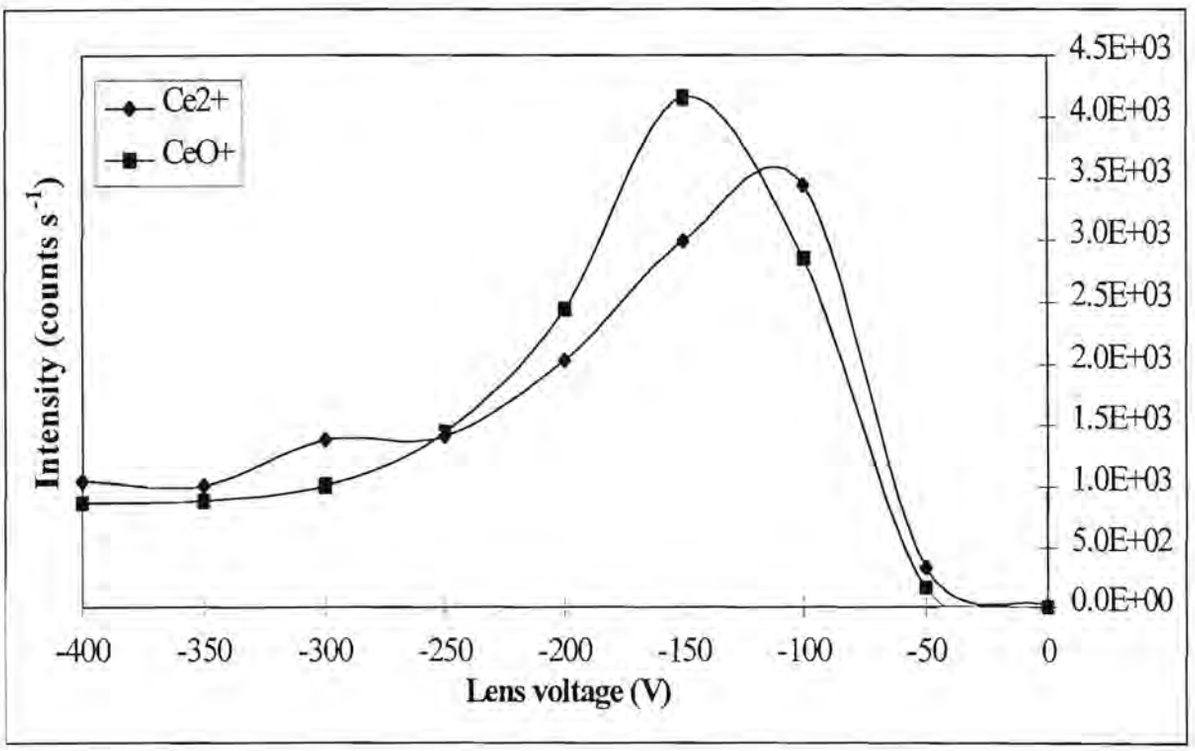

Figure 2.43(d): Effect of the lens parameter LC on the response curves of the doubly ionised and oxide ions.

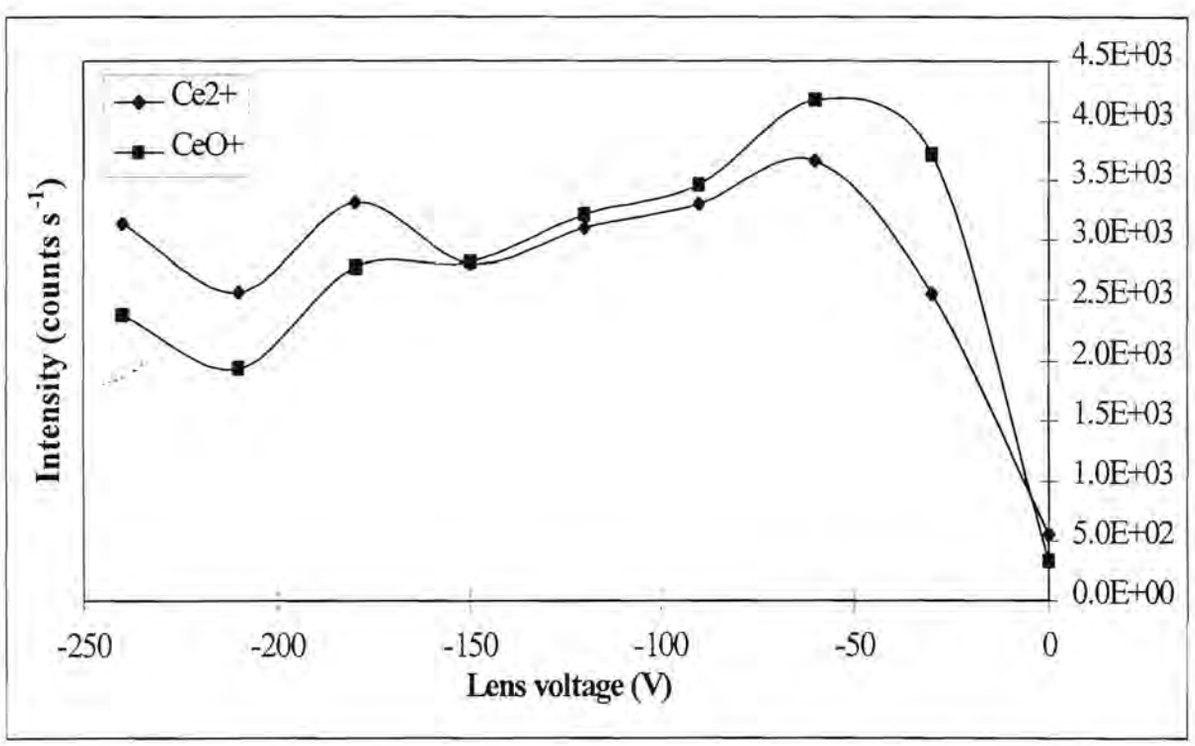

Figure 2.43(e): Effect of the lens parameter LD on the response curves of the doubly ionised and oxide ions.

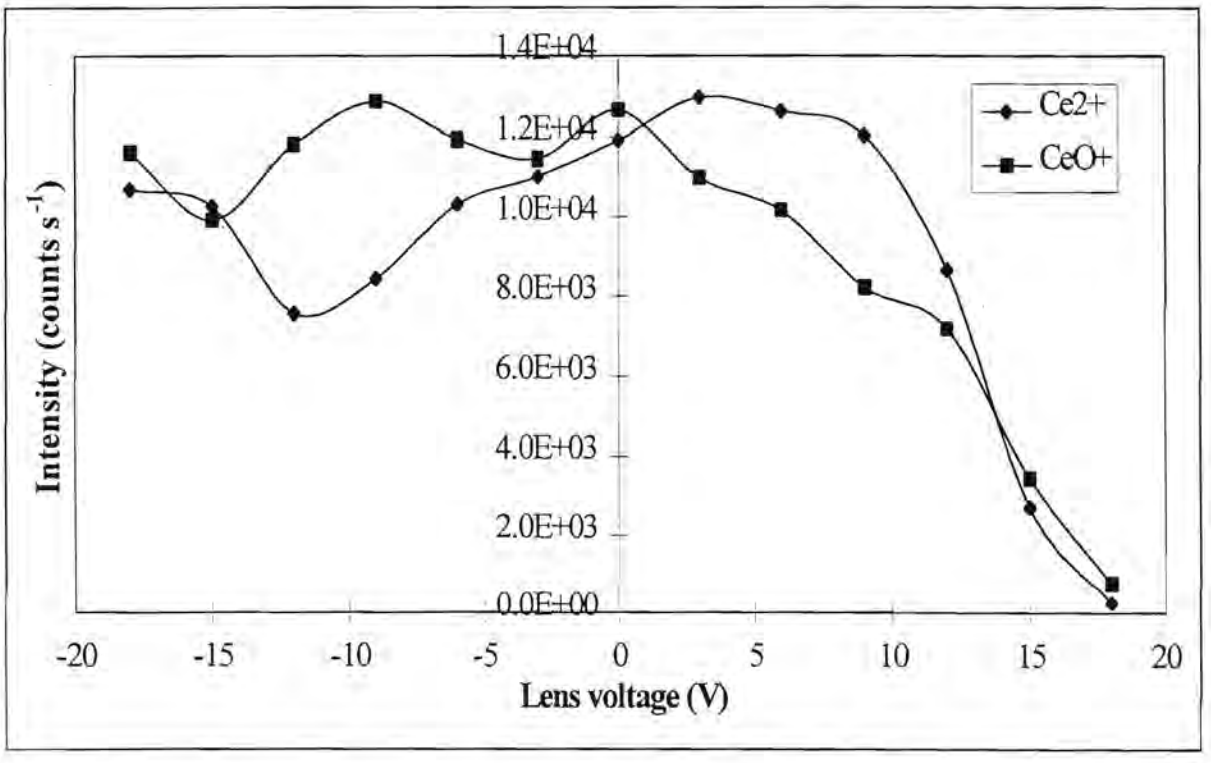

Figure 2.43(f): Effect of the field axis voltage FA on the response curves of the doubly ionised and oxide ions.

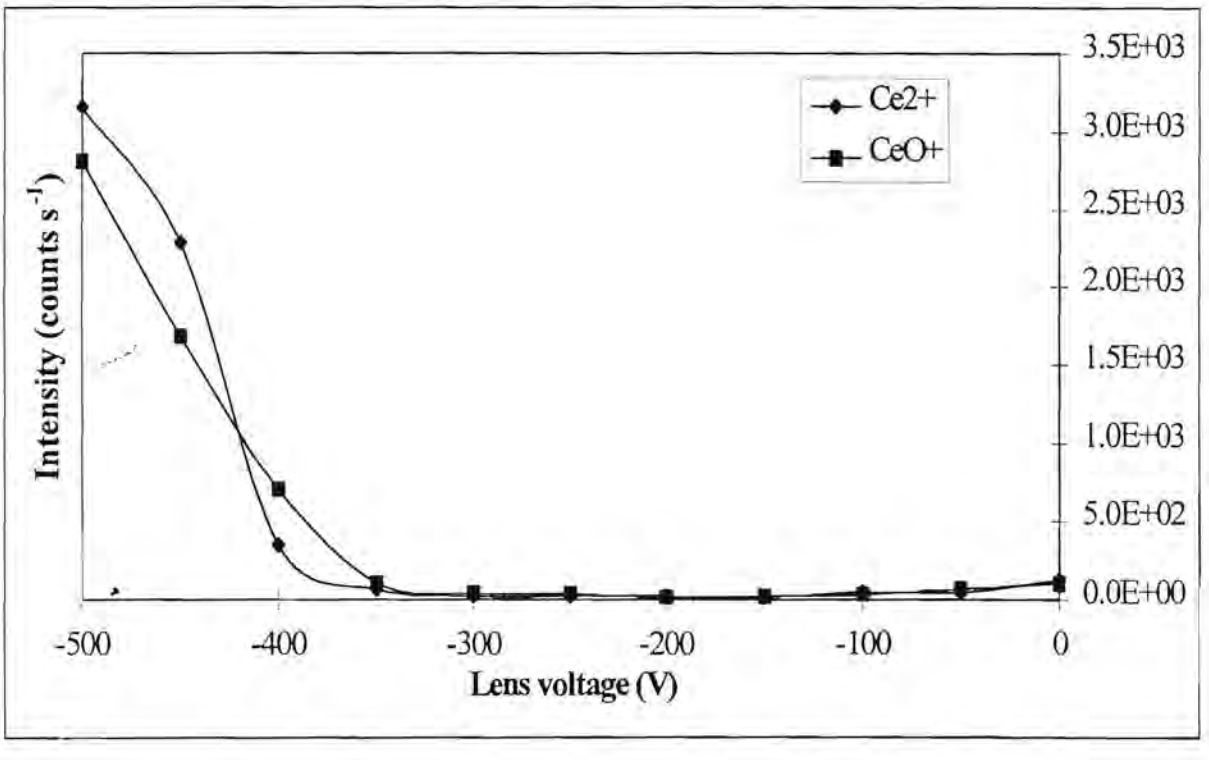

Figure 2.43(g): Effect of the detector inner diameter voltage ID on the response curves of the doubly ionised and oxide ions.

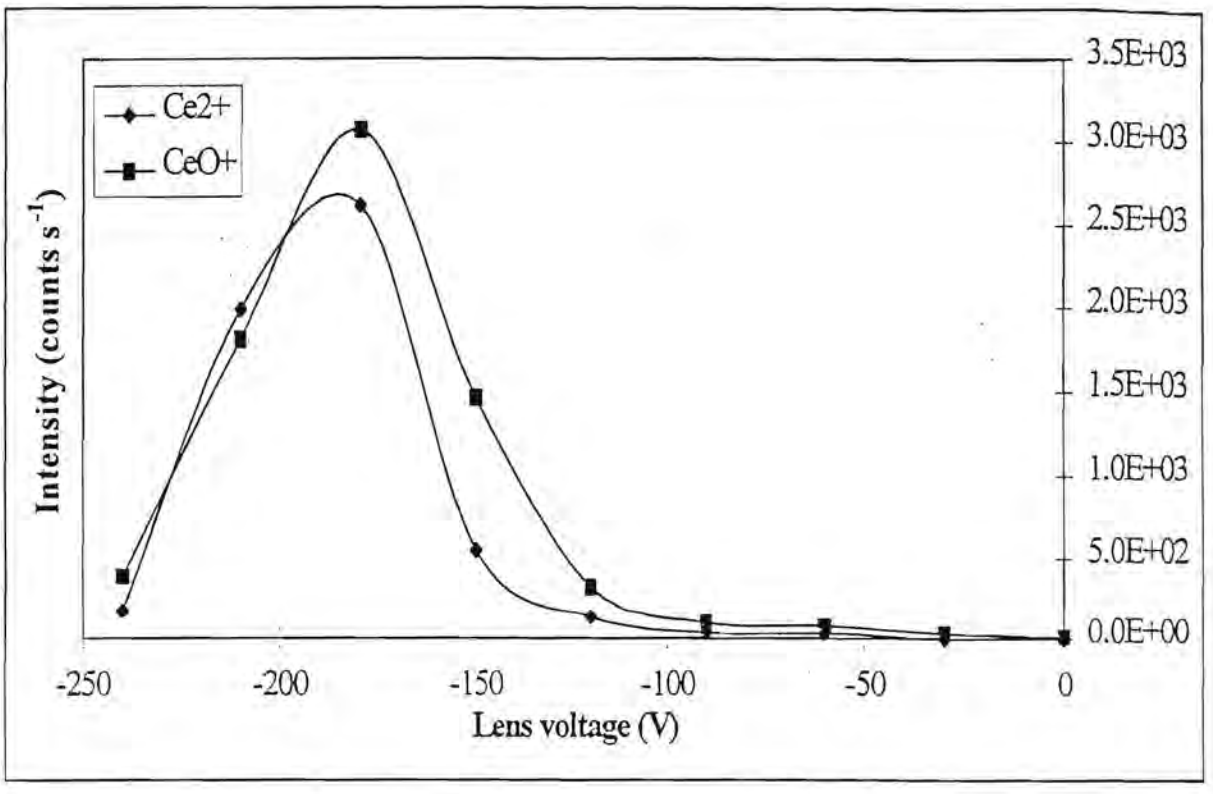

Figure 2.43(h): Effect of the detector outer diameter voltage OD on the response curves of the doubly ionised and oxide ions.

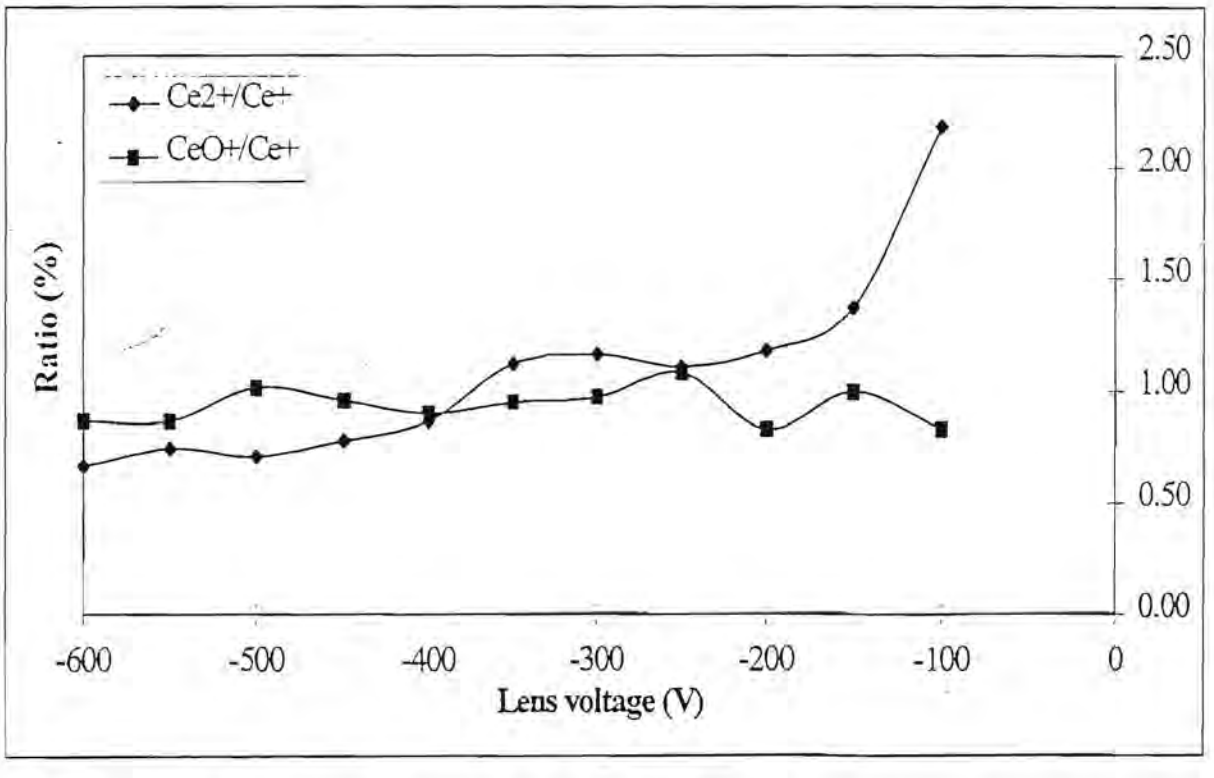

Figure 2.44(a): Effect of the lens parameter LO on the response curves of the Ce^{2+}/Ce^{+} and CeO^{+}/Ce^{+} ratios.

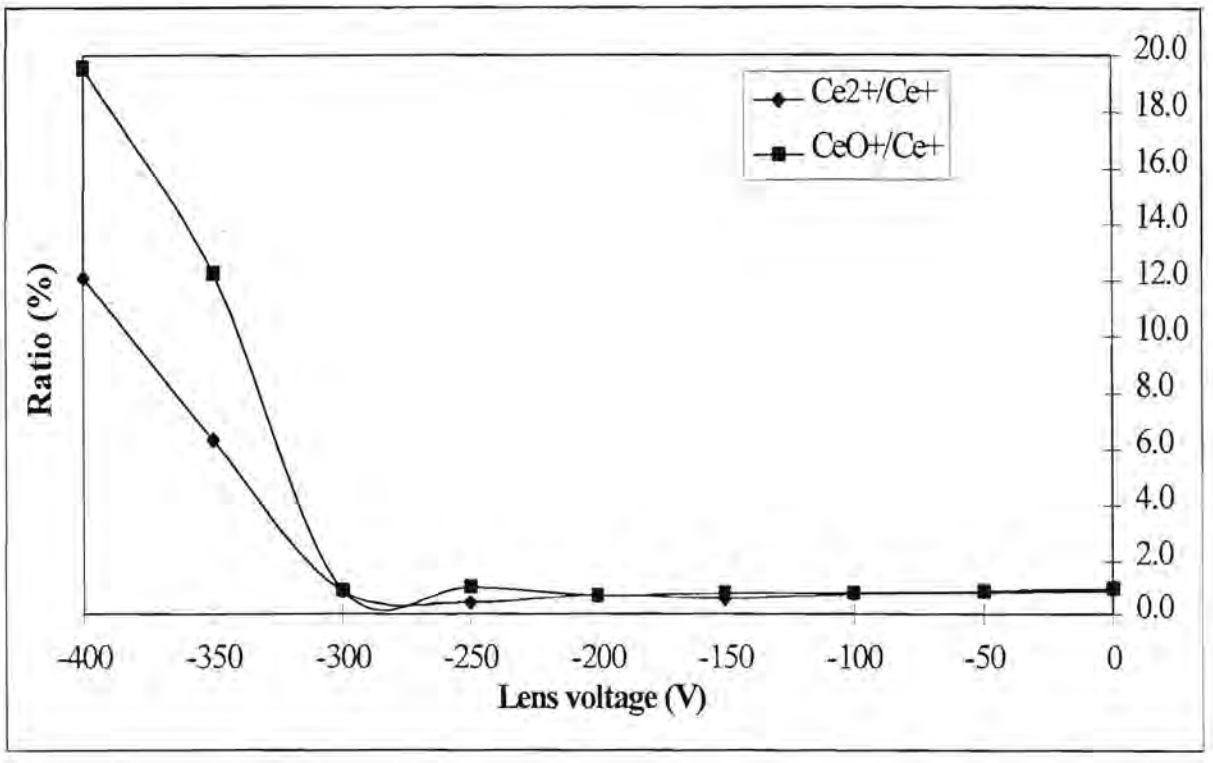

Figure 2.44(b): Effect of the lens parameter LA on the response curves of the Ce^{2+}/Ce^{+} and CeO^{+}/Ce^{+} ratios.

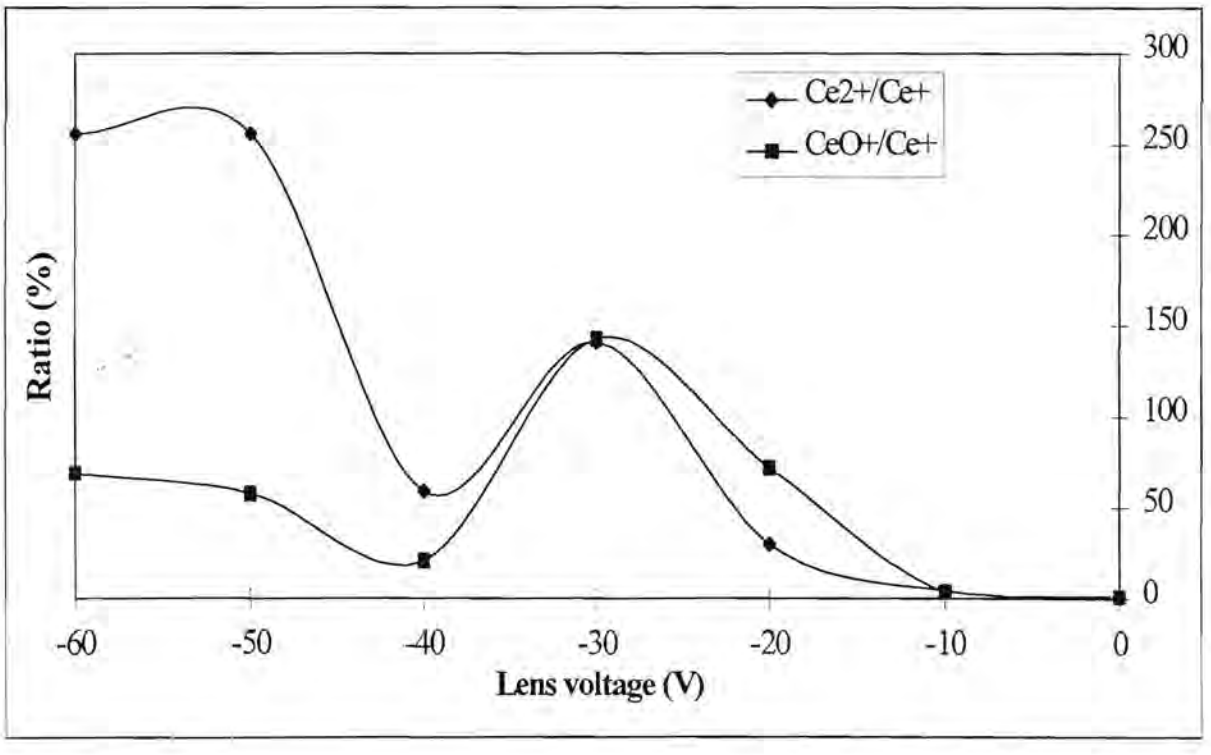

Figure 2.44(c): Effect of the lens parameter LB on the response curves of the Ce^{2+}/Ce^{+} and CeO^{+}/Ce^{+} ratios.

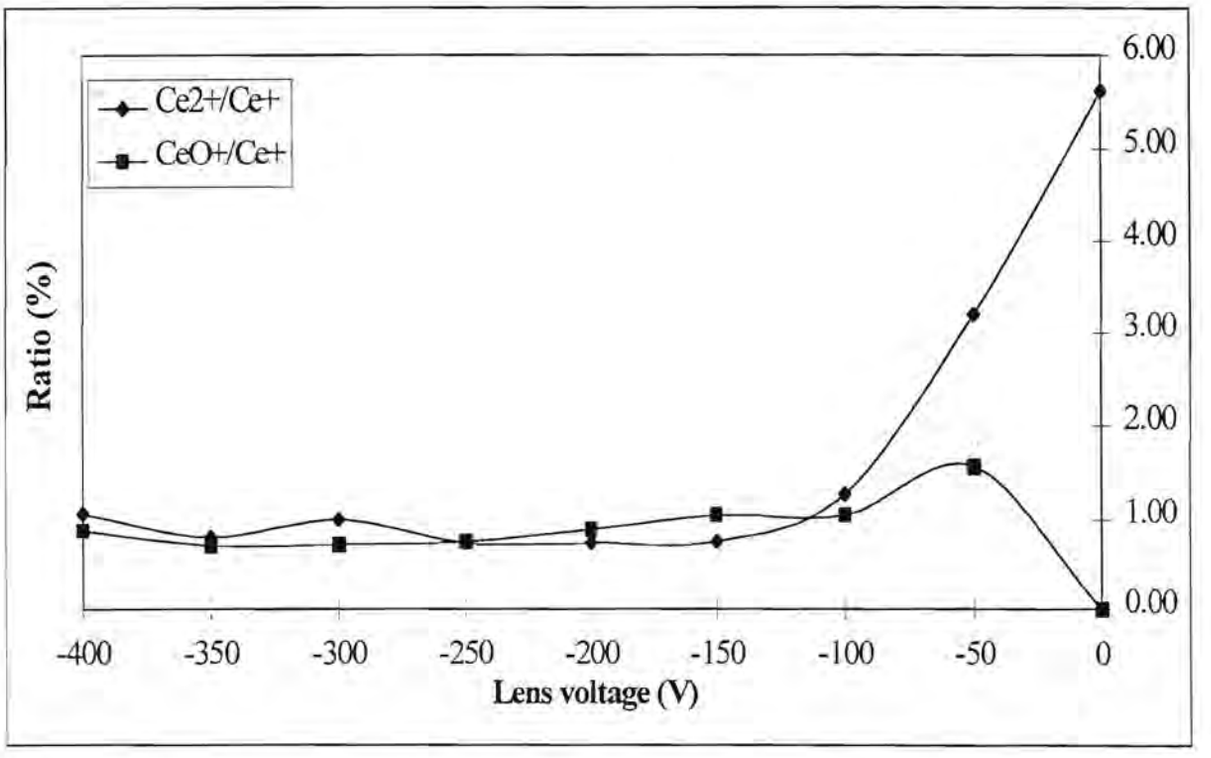

Figure 2.44(d): Effect of the lens parameter LC on the response curves of the Ce^{2+}/Ce^{+} and CeO^{+}/Ce^{+} ratios.

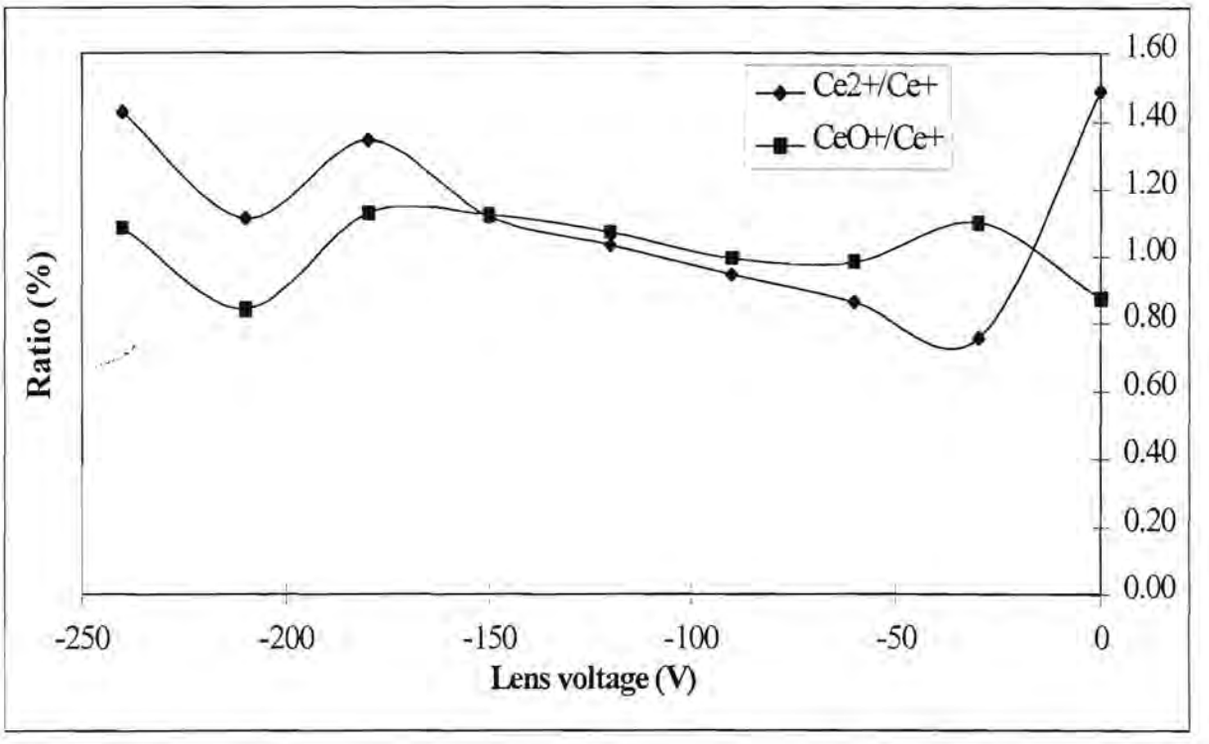

Figure 2.44(e): Effect of the lens parameter LD on the response curves of the Ce^{2+}/Ce^{+} and CeO^{+}/Ce^{+} ratios.

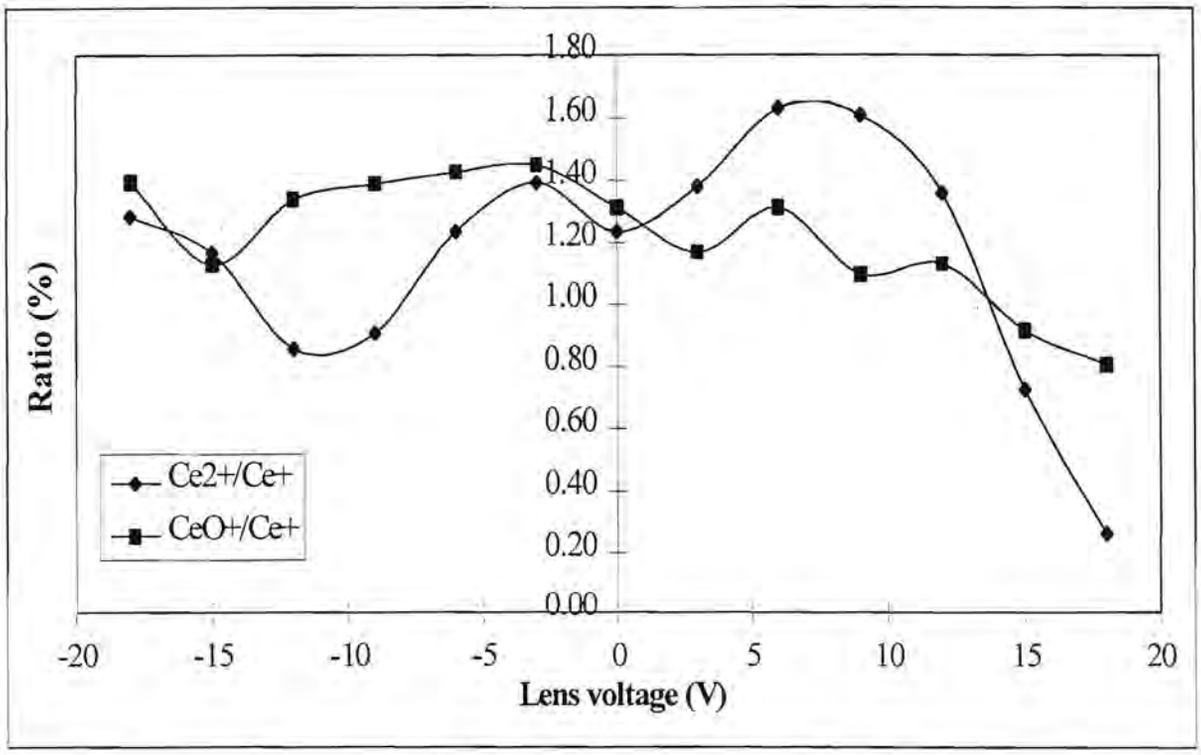

Figure 2.44(f): Effect of the field axis voltage FA on the response curves of the Ce^{2+}/Ce^{+} and CeO^{+}/Ce^{+} ratios.

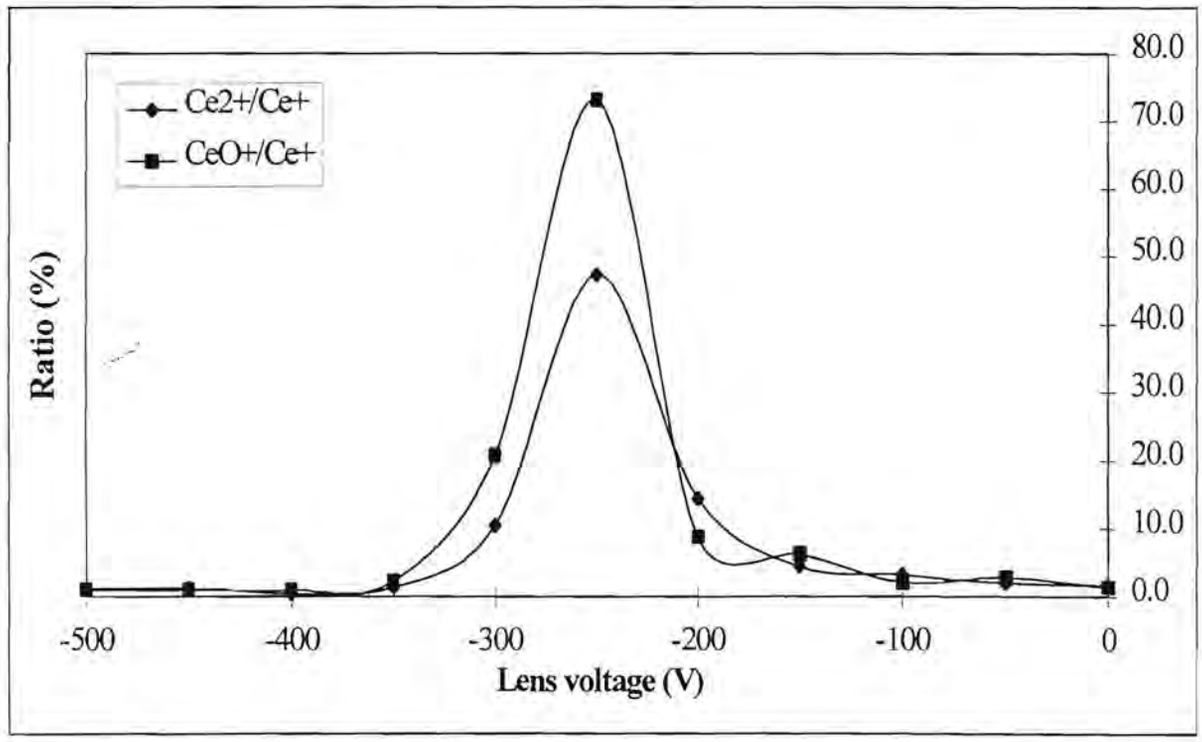

Figure 2.44(g): Effect of the detector inner diameter voltage ID on the response curves of the Ce^{2+}/Ce^{+} and CeO^{+}/Ce^{+} ratios.

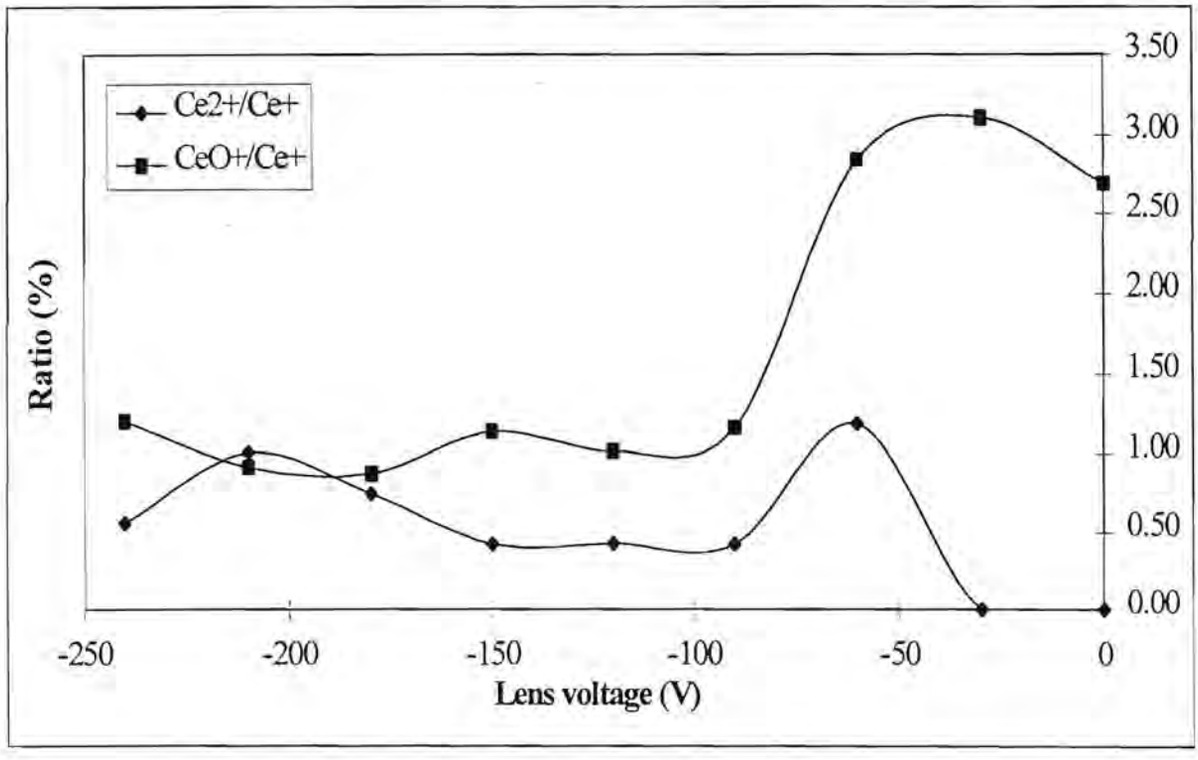

Figure 2.44(h): Effect of the detector outer diameter voltage OD on the response curves of the Ce^{2+}/Ce^{+} and CeO^{+}/Ce^{+} ratios.

Effect of ion lens settings on doubly ionised ions and oxides

Figures 2.43(a) - (h) and 2.44(a) - (h) give the effects of ion lens settings on the response curves of Ce^{2+} and CeO^{+} ions, as well as for the Ce^{2+}/Ce^{+} and CeO^{+}/Ce^{+} ratios. According to figures 2.43(a) - (h) the interference ions follow more or less the same trends as the light and heavier elements. Figures 2.44(a) - (h) show that the optimum lens settings for the analyte signals would not cause the Ce^{2+}/Ce^{+} and CeO^{+}/Ce^{+} ratios to exceed the acceptable values of 2.5% and 1%.

2.4 Conclusion

Table 2.4: Optimum values for parameters. Gas flow rates in arbitrary scales as used by the instrument manufacturer.

Parameter	Light elements and argon	Heavier elements	Background	Ratio of doubly charged to mono-charged ions	Ratio of oxide ions to mono-charged ions
Horizontal displacement of torch	"-2500" units	"-2500" units	Acceptable at all settings	"-2500" units	"-2500" units
Vertical displacement of torch	"-6500" units	"-6500" units	Acceptable at all settings	Acceptable at all settings except "500" to "3000" units	Acceptable at all settings
Axial displacement of torch	"-3000" to "-6000" units	"-3000" to "-6000" units	Acceptable at all settings	Acceptable at all settings except at values closer than "-3000" units to sampling aperture	Acceptable at all settings excepts at values closer than "-3000" units to sampling aperture
Coolant gas flow rate	40	40	Acceptable at all settings	26	Acceptable at all settings
Auxiliary gas flow rate	30	30	Acceptable at all settings	30	Acceptable at all settings
Aerosol carrier gas flow rate at a power setting of 1350 W	31	31	Acceptable at all settings	Maximum value of 29	Maximum value of 29
Lens setting: LO	-350 V	-450 V	Acceptable at all settings	-600 V	-550 V
Lens setting: LA	-50 V	-50 V	Acceptable at all settings	0 to -200 V	0 to -200 V

Parameter	Light elements and argon	Heavier elements	Background	Ratio of doubly charged to mono-charged ions	Ratio of oxide ions to mono-charged ions
Lens setting: LB	0 V	0 V	Acceptable at all settings	0 V	0 V
Lens setting: LC	-120 V	-150 V	Acceptable at all settings	-300 to -150 V	-350 to -250 V
Lens setting: LD	-25 V	-60 V	Acceptable at all settings	-30 V	-210 V
Lens setting: FA	0 V	0 V	Acceptable at all settings	18 V	18 V
Lens setting: ID	-500 V	-500 V	Acceptable at all settings	-500 to -400 V	-500 to -400 V
Lens setting: OD	-190 V	-180 V	Acceptable at all settings	0 to -30 V	-200 V

A final set of conditions that may seen as the optimised parameters can be taken from table 2.4 and can be listed as set out in table 2.5.

Table 2.5: Optimised set of parameters for the ICP-MS.

Parameter	Setting
Horizontal displacement of torch	"-2500" units
Vertical displacement of torch	"-6500" units
Axial displacement of torch	"-3000" to "-6000" units
Coolant gas flow rate	40
Auxiliary gas flow rate	30
Aerosol carrier gas flow rate at a power setting of 1350 W	29
Lens setting: LO	-500 V
Lens setting: LA	-50 V
Lens setting: LB	0 V
Lens setting: LC	-150 V

Parameter	Setting
Lens setting: LD	-60 V
Lens setting: FA	0 V
Lens setting: ID	-500 V
Lens setting: OD	-190 V

The following optimisation strategy is proposed for the instrument and setup investigated:

a) Prepare a solution containing the analytes to be investigated as well as light elements and heavier elements. The concentration of the elements in the solution should be approximately 1 mg dm^{-3} in 1% HNO_3.

b) Set the parameters of the instrument to the values as set out in table 2.5.

c) Scan the prepared solution while monitoring the magnitudes of the signals of the analytes to be investigated, light elements, heavier elements, background masses, oxide interferences and doubly charged interferences.

d) While keeping the other parameters constant, adjust the first parameter as listed in table 2.5. Monitor the magnitudes of the signals as listed in c). Optimise the parameter value, i.e. adjust in order to increase element signals and decrease background and interference signals.

e) Continue with the above mentioned for the other parameters as listed in table 2.5.

Optimised instrument settings are valid for a specific torch - load coil arrangement. This implies that as soon as the torch is replaced or is put in the load coil in a different manner, the parameters have to be optimised again.

Analyte signals in ICP-MS depend in a complex manner on instrument parameters. Parameters such as torch position, coolant and auxiliary gas flow rates and ion lens settings are important and should be optimised. However, aerosol carrier gas flow rate and power settings proved to be of critical importance for the optimisation of analyte signals and the minimisation of doubly ionised and oxide interferences.

The main conclusion drawn from this optimisation study is that similar optimum conditions are valid for most elements. The optimal parameters for minimal potential interferences correspond very closely to the optimal set of conditions for mono-ionised analyte ions.